A CONFORMATIONAL STUDY OF 5-FLUOROURACIL LABELED *ESCHERICHIA COLI* 5SrRNA

by

JAMES LEWIS SMITH

B.Sc. University of Puget Sound, 1971
M.Sc. University of Puget Sound, 1974

A THESIS SUBMITTED IN PARTIAL
FULFILMENT OF THE REQUIREMENTS
FOR THE DEGREE OF DOCTOR OF
PHILOSOPHY
in
THE FACULTY OF GRADUATE STUDIES

in the department
of
CHEMISTRY

We accept this thesis as conforming to the
required standard

THE UNIVERSITY OF BRITISH COLUMBIA

January, 1980

In presenting this thesis in partial fulfilment of the requirements for an advanced degree at the University of British Columbia, I agree that the Library shall make it freely available for reference and study. I further agree that permission for extensive copying of this thesis for scholarly purposes may be granted by the Head of my Department or by his representatives. It is understood that copying or publication of this thesis for financial gain shall not be allowed without my written permission.

Department of Chemistry

The University of British Columbia
2075 Wesbrook Place
Vancouver, Canada
V6T 1W5

Date December 5, 1979

Supervisor: Dr. Alan G. Marshall

ABSTRACT

^{19}F-nmr spectroscopy and laser Raman spectroscopy are used to interpret conformational properties of 5SrRNA. When 5-fluorouracil is added to a medium containing actively growing E. coli cells it is incorporated into the 5SrRNA (FU-5SrRNA) of the bacteria. The ^{19}F-nmr spectra of FU-5SrRNA, at 94.1 MHz and 254 MHz, are presented. They cover a chemical shift range of approximately 8 p.p.m.. At 254 MHz the spectrum consists of 8 peaks and 2 shoulders, representing fluorine resonances from approximately twenty 5-fluorouracil residues in FU-5SrRNA. The most exposed residues have been assigned by comparison of the resonance frequency of the 5-fluoro-2'-deoxyuridine monophosphate monomer with that of the heat denatured FU-5SrRNA. The remainder of the fluorine resonances (about 70% of the total) are believed to be due to buried 5-fluorouracil residues. All the T_1 values of the individual peaks were approximately the same (between 0.3 and 0.4 seconds). This is in contrast to the T_1 value of the 5-fluoro-2'-deoxyuridine monomer which is approximately 5 seconds. A nuclear Overhauser enhancement experiment confirms that these residues are rigidly situated within the FU-5SrRNA molecule and that their molecular correlation time (τ) must be the same as the overall correlation time of the macromolecule.

Two important results are obtained from laser Raman spectroscopic studies presented in this work. First, 5-fluoro-substitution affects certain vibrational properties of the uracil base. Second, from the comparison of N-5SrRNA spectra with FU-5SrRNA spectra, it appears evident that 5-fluorouracil substitution in 5SrRNA causes only minimal perturbation of the structure; thus, conclusions resulting from a study of FU-5SrRNA structure should be applicable to N-5SrRNA.

TABLE OF CONTENTS

Page

LIST OF TABLES

LIST OF FIGURES

ACKNOWLEDGEMENTS

First of all I would like to thank my research supervisor, Alan Marshall, for his guidance and direction during my five years of association with his biophysical chemistry research group. I would also like to thank the other members of his group which includes Chris Roe, Greg Luoma, Bob Bruce, Junko Crothers and K.M. Lee.

During various stages of this work equipment from other departments was employed. In particular I would like to thank the University of British Columbia Microbiology and Food Science departments, and the University of Washington Biochemistry Department for the use of their fermentation devices.

Last of all, I would like to thank certain individuals who have been of assistance during various stages of this work. They include, Ivan Kaiser (University of Wyoming), Brian Sykes (University of Alberta), and Gordon Tener (University of British Columbia).

CHAPTER 1

GENERAL INTRODUCTION

Biophysical chemistry uses physical and chemical laws to interpret structural and functional properties of biological molecules. During the last two decades X-ray crystallography has provided the atomic spatial arrangement of numerous molecules with specific biological functions. X-ray structural analysis has two major limitations. First, highly ordered single crystals of biological molecules are often difficult or impossible to obtain. Secondly, the severe constraints on molecular motion in a rigid crystal lattice are unlike the native aqueous environment where biological molecules function. These two limitations have prompted investigators to employ physical methods able to provide dynamical information about biological molecules in an aqueous environment. This thesis uses two methods, nuclear magnetic resonance (nmr) spectroscopy and laser Raman spectroscopy to investigate the conformation of a specific ribonucleic acid (RNA) molecule in solution.

Hydrogen, phosphorus, and fluorine all have spin ½ nuclei which are 100% naturally abundant. Their relative sensitivities and approximate chemical shift ranges are given in Table 1. Both hydrogen and fluorine have substantial signal sensitivity. Phosphorus has much reduced sensitivity but like fluorine its

Nucleus	Relative signal sensitivity at constant field	Approximate chemical shift range in parts per million (p.p.m.)
Hydrogen	100	12
Fluorine	83.3	500
Phosphorus	6.63	700

Table 1.1. The approximate chemical shift range and relative signal sensitivity, at constant field, of hydrogen, fluorine and phosphorus nuclei (1).

chemical shift range is large compared to the proton. An RNA molecule contains many phosphorus and hydrogen nuclei. However, phosphorus-nmr (^{31}P-nmr) and proton-nmr (^{1}H-nmr) are of limited utility. This is due mostly to the large numbers of these nuclei (i.e. 5SrRNA has 1301 hydrogen atoms and 120 phosphorus atoms). In aqueous solution most of the proton resonances are masked by the large number of proton resonances from the water. Even in deuterium oxide the small chemical shift range of the proton resonances combined with the large number of resonances, due exclusively to RNA, result in a spectral envelope of unresolvable peaks. There are two small proton populations in RNA molecules whose chemical shifts are far enough from the majority of the proton resonances that they are able to provide conformational information about these molecules. They can be resolved through the application of Fourier Transform nmr (FT nmr) and correlative ^{1}H-nmr techniques. One group, the exchangeable ring NH protons, elicit hydrogen bonding between RNA base pairs (see Figure 1.7).

These resonances are shifted downfield, relative to the proton resonances of water, due to ring current effects from the heterocyclic bases involved in the base pair. The same hydrogen bonded proton resonances are in turn sensitive to ring current effects from the base pairs which are stacked above and below them in helical regions of the RNA molecules (2). The magnitudes of these latter effects are of sufficient variety that well resolved ring NH hydrogen bonded proton resonances are spread out over a range of about 7 p.p.m.. A low field ^{1}H-nmr spectrum of a valine accepting transfer RNA ($tRNA_1^{Val}$) from Escherichia coli (E. coli) is shown in Figure 1.1. The helical regions of RNA molecules are essentially hydrophobic. Within these regions the exchangeable NH protons are not accessible to the external aqueous environment. At elevated temperatures RNA molecules unravel exposing the hydrogen bonded protons. The resulting fast exchange of these protons with the aqueous environment causes broadening and eventual disappearance of the resonances. This technique has been used to evaluate the stability of helical stem regions in specific tRNA molecules (4). It is also applicable to other types of experiments where conformational change affects base stacking interactions (3). The second group of proton resonances, the nonexchangeable methyl protons of modified nucleosides, are also resolvable using high resolution ^{1}H-nmr techniques. The proton resonances,

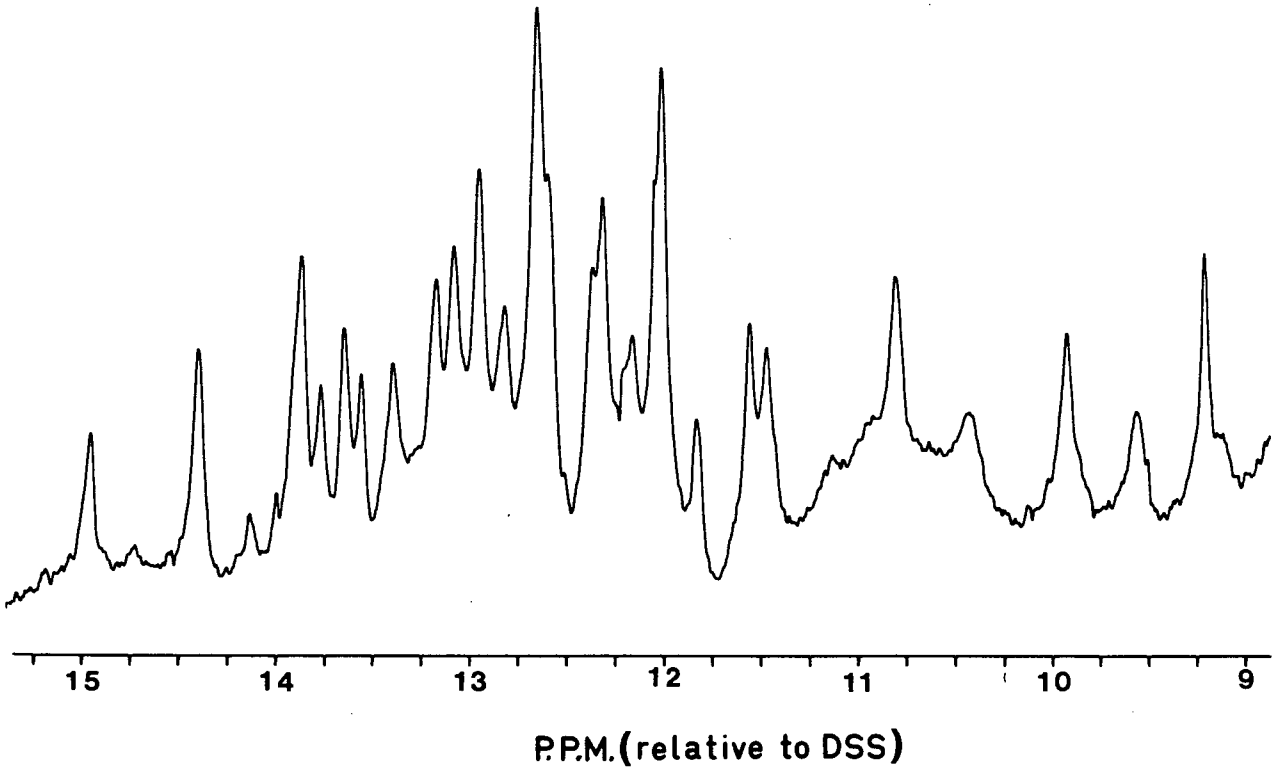

Figure 1.1. The 400 megahertz low field ^{1}H-nmr spectrum of $tRNA_1^{Val}$ was obtained on the departmental Brüker HW 400 FT nmr spectrometer by G. Luoma and A. Marshall of this laboratory. The RNA sample was kindly provided by B. Reid (3). It consisted of 1 millimolar tRNA dissolved in an aqueous 10 millimolar cacodylate buffer (pH 7) containing 5 millimolar magnesium chloride and 1 millimolar EDTA. The spectrum was obtained on single pulse correlation mode at zero dB. It consists of 1000 transients at an acquisition time of 0.82 seconds. The total accumulation times was approximately 11 minutes.

shown in Figure 1.2, are shifted upfield relative to most. The temperature dependence of their chemical shifts has been used to ascertain the order in which the local regions containing the modified bases unfold (5-7). The determination of line widths

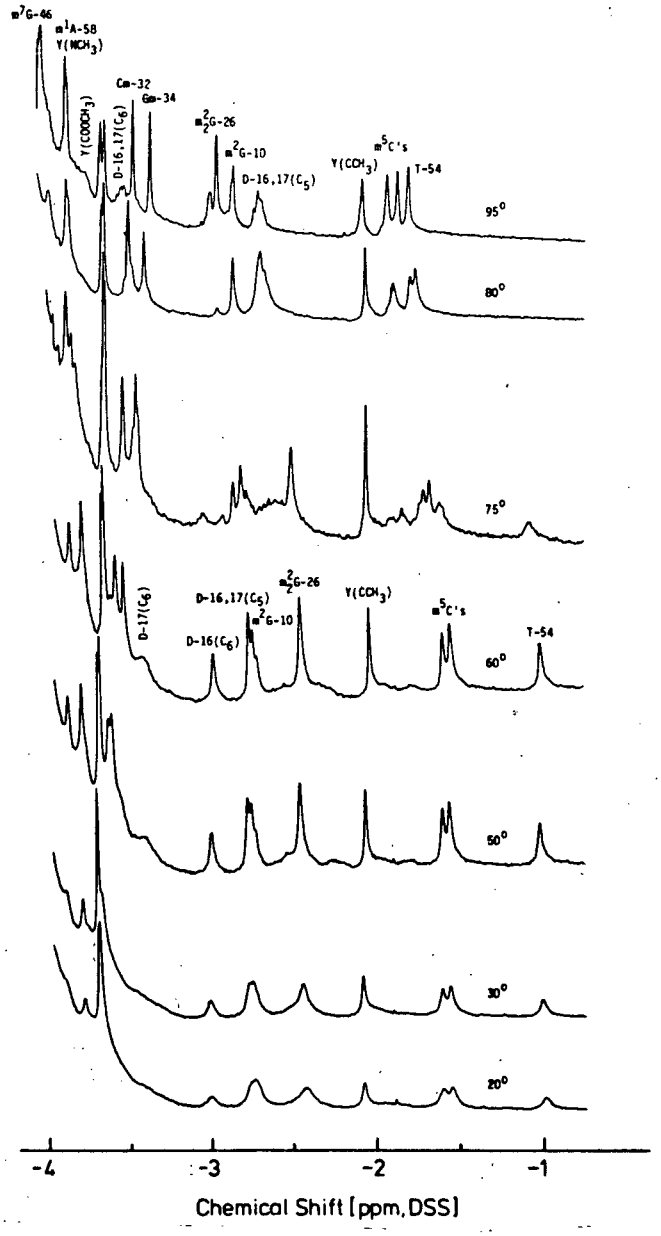

Figure 1.2. The high-field proton resonances of yeast $tRNA^{Phe}$ were obtained at several temperatures on a 270 megahertz ^1H-FT nmr spectrometer. The sample concentration was approximately 0.55 millimolar. The deuterium oxide buffer was 0.01 molar potassium phosphate (pH 6.6) and contained 0.1 molar KCl and 0.01 molar $MgCl_2$.

and direct measurement of spin-lattice relaxation times are also potentially useful for the interpretation of their motional freedom in various parts of the RNA molecule (8). Phosphorus, unlike the proton, has a potentially large chemical shift range, but in RNA molecules most of these resonances appear to experience comparable environmental effects (9-11). This is apparent from Figure 1.3. Those resonances which are displaced from the majority are unassignable even though they do appear to be affected by temperature and ionic strength (12).

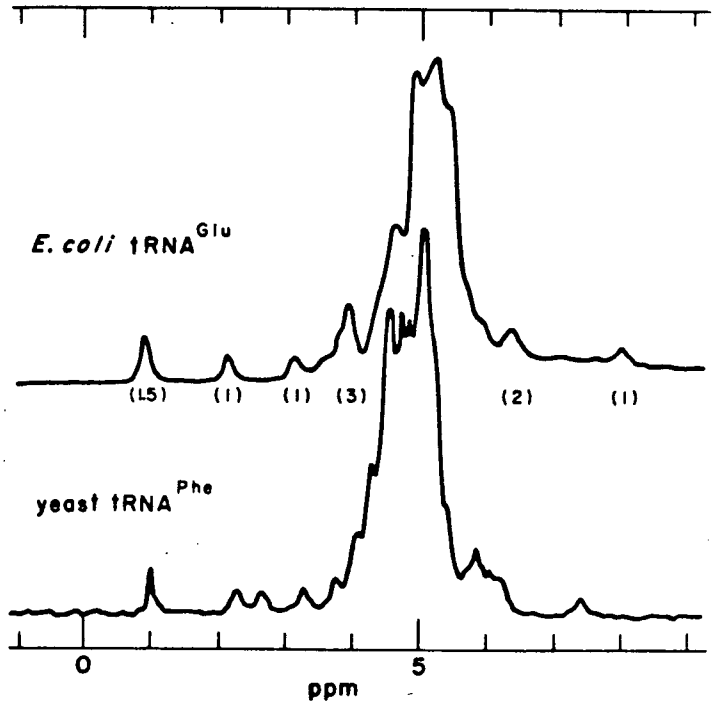

Figure 1.3. A ^{31}P-FT nmr spectrum of yeast tRNA^{Phe} and E. coli tRNA^{Glu} at 109 megahertz. The water buffer consisted of 0.01 molar sodium cacodylate (pH 7) plus 0.1 molar sodium chloride. The tRNA^{Glu} sample also contained 15 millimolar magnesium while the tRNA^{Phe} sample contained about 3.5 millimolar magnesium. There was about 25 milligrams of RNA in 0.7 milliliters of buffer which corresponds to approximately a 1.4 millimolar RNA solution. The accumulation time for each spectrum was about 10 hours (9).

The major disadvantage of both ^{1}H-nmr and ^{31}P-nmr spectroscopy is the presence of a large population of unassignable resonances. The extremely useful aspect of ^{1}H-nmr is the consideration of a relatively small population of potentially assignable and interpretable resonances. This observation led to the formulation of the first technique employed in this thesis, fluorine-nmr (^{19}F-nmr) spectroscopy. The *in vivo* incorporation of a small number of fluorine atoms at specific sites along the sequence of an RNA molecule provides a small population of spin ½ nuclei in different parts of the molecule. Fluorine has only slightly less sensitivity than the proton (83%) and a much larger chemical shift range (about 41.5 times the proton's). Therefore, extensive resolution of individual resonances was expected. The interpretation of these resonances would provide information about the local environment surrounding the individual fluorine atoms located in different parts of the RNA molecule.

The *in vivo* incorporation of fluorine into a biological molecule and subsequent ^{19}F-nmr spectroscopy was achieved in 1974 (13). Experimentors succeeded in incorporating m-fluorotyrosine into the tyrosine sites of the dimeric zinc containing metalloprotein, *alkaline phosphatase*, from *E. coli*. This was accomplished by growing a tyrosine auxotroph of *E. coli* on a medium containing m-fluorotyrosine. The resulting ^{19}F-nmr spectra, at 94 megahertz and 235 megahertz, are shown in Figure 1.4. Denaturation of this enzyme with 6 molar guanidine·HCl

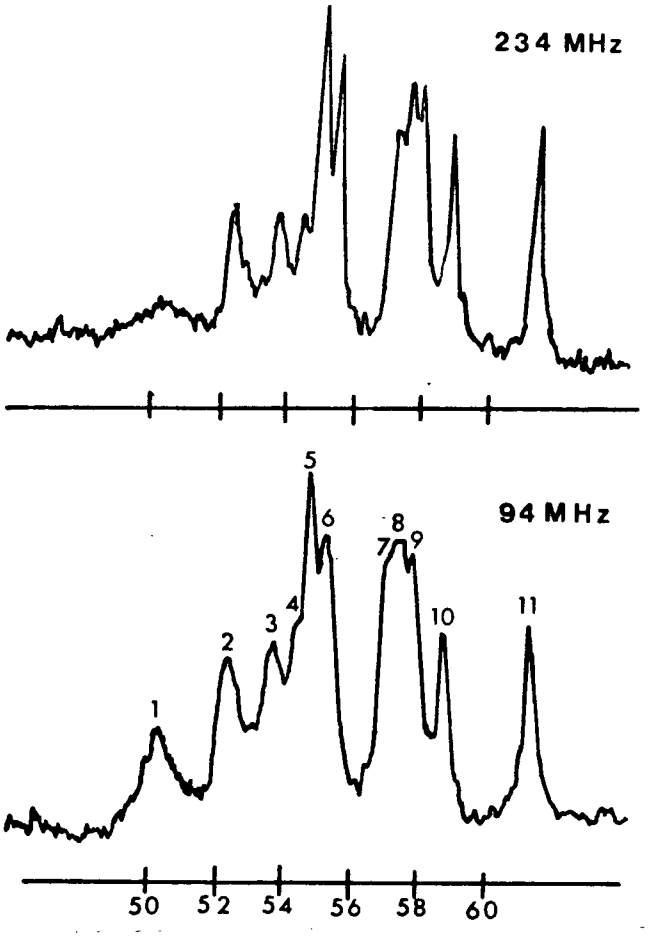

Figure 1.4. The ^{19}F-FT nmr spectra of fluorotyrosine labeled alkaline phosphatase at 94 megahertz and 235 megahertz. The aqueous buffer consisted of 0.1 molar Tris (pH 7.9) and the protein concentration was 0.30 millimolar. The accumulation time for these spectra was about 30 minutes (14).

yielded a single fluorine resonance at approximately 58.8 p.p.m. (15). Comparison of this spectrum with those of the native enzyme, shown above, suggest that resonances 7-10 are the most nearly exposed to the surface environment of the protein. Resonances 1-6 show monotonic increases in line-width with increased chemical shift to lower field. This is due to the buried m-fluorotyrosines which experience tertiary interactions with the surrounding protein environment. The data from this ^{19}F-nmr study was compared with theoretical models in an effort to determine the effect of the protein environment upon these fluorine probes. For example, calculations of spin-lattice relaxation times (T_1), at 94 megahertz, assuming only dipole-dipole relaxation via the tryosine ring proton nearest the fluorine atom provided an absolute minimum value of 0.45 seconds (16). Comparison with experimental values of T_1, for each resonance, indicated that all except resonance 10 are substantially less than the theoretical minimum value. This implied that an intermolecular dipolar relaxation mechanism existed that involved the fluorine atom and the protons of the surrounding protein environment. Their distances from the fluorine atom must be comparable to that of the vicinal proton on the tyrosine ring. Using a similar strategy experimental results were combined with theoretical considerations to provide definitive information about the molecular dynamics of m-fluorotyrosine alkaline phosphatase from E. coli. They have examined the effects of increasing magnetic field strength on

chemical shift anisotropy, the degree of internal mobility for individual m-fluorotyrosines and a molecular correlation time for the enzyme which is consistent with fluorescence depolarization data (15). Also considered were induced conformational changes in the enzyme through zinc or phosphate binding and their effects on the ^{19}F-nmr spectrum (17). One of the major goals of this thesis was to consider the applicability of the same type of study to a specific RNA molecule of biological interest. These considerations will be dealt with extensively in Chapter 3.

The action of the anticarcinogen 5-fluorouracil (5-FU) on E. coli suggested that an experiment analogous to the m-fluorotyrosine labeled alkaline phosphatase study was feasible (18-19). The drug, shown in Figure 1.5, will incorporate into the bacterial RNA if it is added during early exponential growth. The incorporation is specific for sites normally containing uridine or uridine-derived bases. The only known study concerning the functionality of a specific 5-FU containing tRNA (FU-tRNA^{Val}) indicates that replacement of 95% of the uridine and uridine-derived bases by 5-FU did not appreciably alter its ability to become amino acylated (20).

An important consideration for this study of fluorine containing nucleic acids with ^{19}F-nmr was the necessity for sufficiently large sample quantities to overcome the inherent low sensitivity of nmr spectroscopy. The study of a specific FU-tRNA would have had distinct advantages. It is relatively

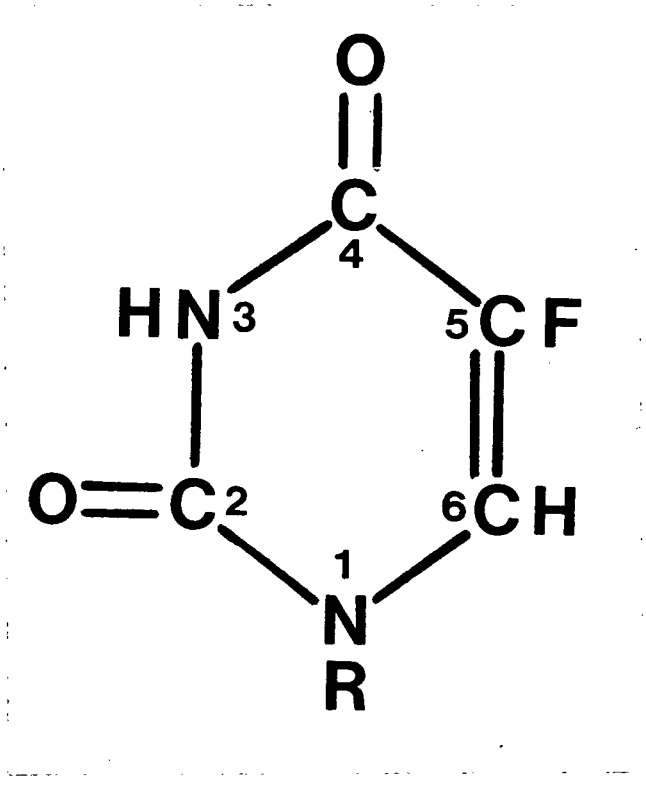

Figure 1.5. The chemical structure of 5-fluorouracil (R=H) and 5-fluorouridine (R=ribose sugar).

small in size, has a known secondary structure, and a rather well understood function in the cell. However, the requirement of large sample amounts for a sufficient signal to noise ratio on the department Varian FT-XL100 led to the selection of 5S ribosomal RNA (5SrRNA) for this study. It represents about 3% of the total cellular RNA of E. coli while a specific tRNA accounts for only about 0.8% of the total (21).

The primary objective of this ^{19}F-nmr study of 5-FU containing 5SrRNA (FU-5SrRNA) from E. coli was to observe the

individual fluorine resonances and interpret the effects of a nucleic acid environment upon them. Then to induce conformational changes in the molecule and observe the effects on the fluorine resonances as the immediate chemical environment about each of the molecular probes changed with alterations in macromolecular conformation. A major disadvantage of any study of this type is that the molecular probe is not native to the biological system. The covalently bound fluorine atom is small (about the size of an OH group) and normally unreactive. However, some fluorinated pyrimidines are highly toxic and known to markedly inhibit the growth of actively dividing cells (19). The introduction of a highly electronegative fluorine atom at a position normally occupied by a proton alters certain physicochemical properties of the vicinal atoms (i.e. pK_a of the N-3 proton of uracil and the extinction coefficient at 260 nanometers). Therefore the presence of fluorine could possibly alter base pairing and base stacking interactions involving 5-FU.

The concern over the possible effects of 5-FU on RNA conformation led to the formulation of the second physical method employed in this thesis, laser Raman spectroscopy. Spectra of native 5SrRNA and FU-5SrRNA were obtained in order to determine the effects of 5-FU incorporation on macromolecular conformation. The Raman spectrum of a polynucleotide is the sum of ring vibrations from the individual nitrogenous bases plus vibrational contributions due to the phosphate backbone which

links the nucleotides together. This meant that Raman spectra of uridine and 5-fluorouridine monomers also had to be compared before it was possible to infer similarities or differences in the macromolecular conformation of 5SrRNA due to fluorine incorporation. The utility of laser Raman spectroscopy as applied to nucleic acids is that intensities of Raman lines are sensitive to conformation. This will be discussed extensively in Chapter 4.

RNA molecules are ribonucleotide polymers of the heterocyclic bases adenine (A), guanine (G), uracil (U), cytosine (C), and a small number of modified bases. The primary structure consists of specific sequences of these bases that are interconnected through phosphodiester linkages between 3' and 5' hydroxyls of the ribose moieties. This is illustrated in Figure 1.6. Molecules of tRNA are approximately 75-80 nucleotides long while 23S ribosomal RNA (23SrRNA), 16SrRNA, and 5SrRNA are about 3700, 1700, and 120 nucleotides respectively. These molecules fold into specific secondary structures in accordance with the directional hydrogen bonding properties of the individual bases. The most stable base pairs in RNA molecules are G-C, A-U, and G-U pairs which are shown in Figure 1.7. The strongest base pair, G-C, consists of three hydrogen bonds while the A-U and G-U pairs have only two hydrogen bonds.

All of the over 87 sequenced tRNA molecules appear to have a comparable secondary structure (23). This so-called

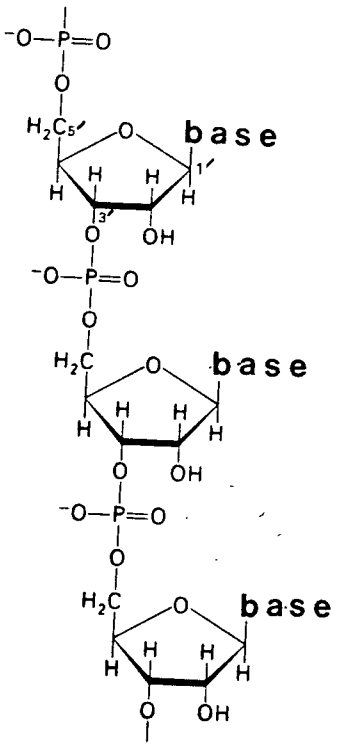

Figure 1.6. The ribose-phosphate backbone structure of an RNA molecule.

cloverleaf structure is shown in Figure 1.8. It consists of five distinct regions. The major function of two of these regions, the acceptor stem and the anticodon loop, are well established. The 3' terminus of the acceptor stem is the site of attachment of the amino acid, while the anticodon loop is the region where tRNA recognizes the mRNA codon, at the ribosome, during protein synthesis. The functional roles of the

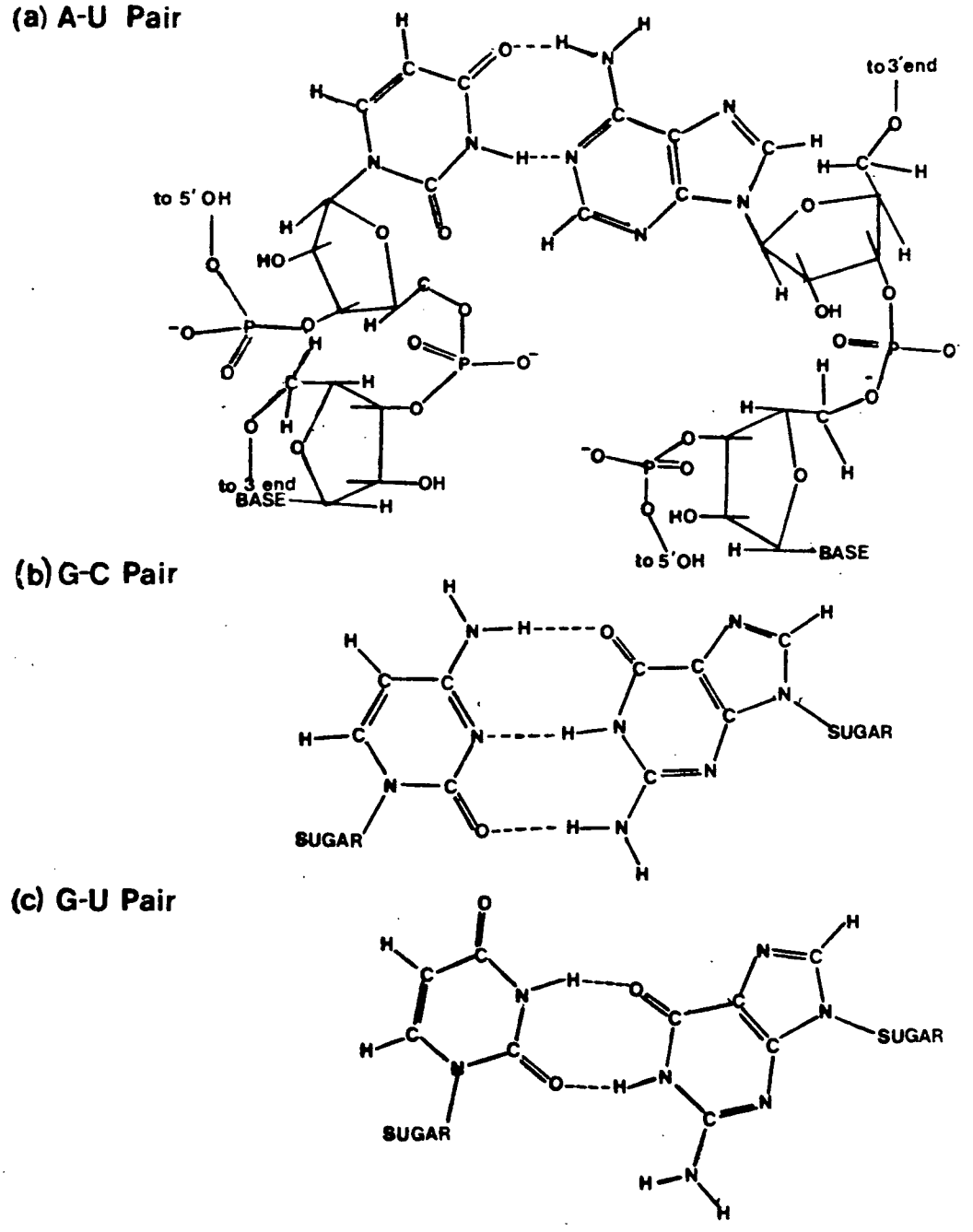

Figure 1.7. The directional hydrogen bonding properties of the three most stable base pairs found in RNA molecules (22).

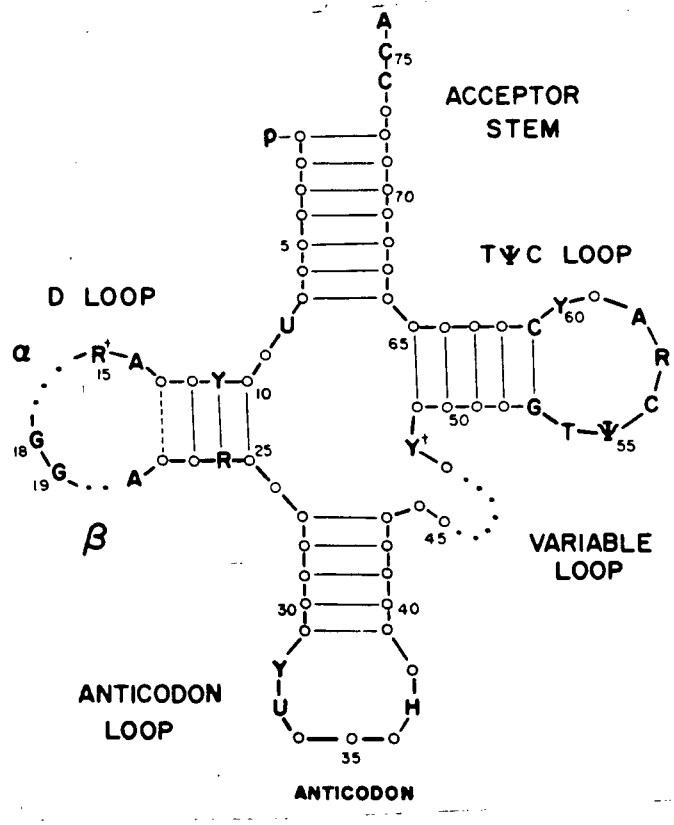

Figure 1.8. The generalized cloverleaf secondary structure of all sequenced tRNA molecules except for initiator tRNAs (24).

other three regions, the D loop, the variable loop, and the TΨC loop, are less well understood. The TΨC region may bind to 5SrRNA during the binding of tRNA to the ribosome. This will be discussed in some detail subsequently.

A complete tertiary structure is available for only one specific RNA molecule, yeast $tRNA^{Phe}$ (25-26). X-ray crystallography, to a resolution of 2.5 angstroms, has verified the cloverleaf secondary structure. The secondary hydrogen bonds

are responsible for most of the structural integrity of this RNA molecule. All secondary base pairs are of the G-C and A-U type except for a single G-U pair in the acceptor stem. The stem regions form RNA-A type right handed antiparallel double helices of about 10-12 bases per turn and have a diameter of approximately 20 angstroms. These helical regions consist of closely stacked base pairs. The secondary hydrogen bonds within these regions are virtually inaccessible to the surrounding aqueous environment. In fact about 90% of the bases in yeast $tRNA^{Phe}$ could be classified as internal hydrophobic (27). The acceptor stem consists of 7 base pairs and the D stem has 4 base pairs. Both the TΨC stem and the anticodon stem have 5 base pairs. Besides these secondary hydrogen bonds there are 11 tertiary base pairs which fold the D arm toward the TΨC arm. A schematic diagram of the crystal structure of $tRNA^{Phe}$ is shown in Figure 1.9. The molecule is L-shaped with the anticodon region at one end and the 3' terminus at the other end. The two perpendicular axes are each about 60 angstroms in length and the site of amino acid attachment (the 3' terminus) is separated from the anticodon by approximately 80 angstroms. The 7 bases in the acceptor stem and the 5 bases of the TΨC stem form a continuous helix, with one gap, along the horizontal axis. The vertical axis is a continuous helix, with two gaps, that consists of the 4 base pairs in the D stem and the 5 base pairs of the anticodon stem.

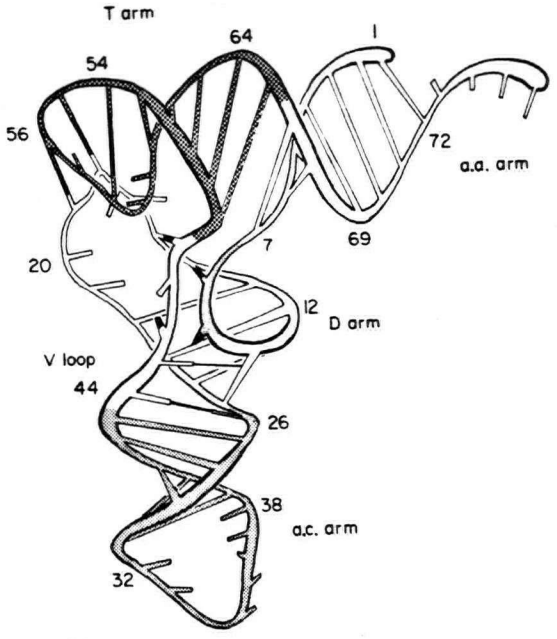

Figure 1.9 A schematic diagram of the crystal structure of yeast $tRNA^{Phe}$. The base paired regions are represented as long bars while single bases are short bars. The tertiary base pairs are indicated by solid dark rods (28).

Besides secondary and tertiary base pairs there are other factors which contribute to the molecular stability of $tRNA^{Phe}$. They include divalent cations, tertiary hydrogen bonds involving riboses and phosphates and the ionic strength of the aqueous environment. The most important divalent cation is magnesium. Both tRNA and 5SrRNA molecules assume functional conformations in the presence of magnesium and can exist in nonfunctional conformations in its absence (29-31). The number of magnesium binding sites in $tRNA^{Phe}$ has not been agreed upon;

even X-ray crystallography leaves some doubts (32). The second factor, hydrogen bonding of the riboses and the phosphates, involves the 2'-oxygens of the riboses and some bases as hydrogen donors or acceptors and a phosphate oxygen as a hydrogen acceptor (33). These interactions are much less stereospecific and not as isolated as secondary and tertiary base pairs. Therefore, they are much harder to assign. The final contributor to RNA stability, the ionic strength of the aqueous environment, is important for stabilization of the ribose phosphate backbone. The backbone is polyanionic at physiological pH due to a negative charge on one of the free phosphate oxygens. The presence of positive monovalent cations, such as sodium and potassium, neutralize like charge coulombic repulsion between the negatively charged phosphate oxygens.

The three dimensional picture provided by the X-ray structural analysis of yeast $tRNA^{Phe}$ serves as a model for structural interpretations of all RNA molecules. The same types of interactions mentioned above contribute to the molecular stability of all RNA molecules. A single crystal of $tRNA^{Phe}$ used to obtain electron density maps for structural analysis is about 75% water (34). Still these $tRNA^{Phe}$ molecules are immobile and the picture provided from X-ray studies is a static one. Numerous studies in a more native aqueous environment tend to substantiate similarities between the crystal structure and the solution structure of $tRNA^{Phe}$. These include low field ^{1}H-nmr (35-36), high field ^{1}H-nmr (37), base specific chemical

modification (38), small angle X-ray scattering (39), fluorescence studies (40), complementary oligonucleotide binding (41), ultraviolet induced cross linking experiments (42), tritium labeling studies (43), and enzymatic accessibility studies (44). However, tRNA molecules are known to have many interactions with proteins and other nucleic acids. A specific tRNA can be considered as a substrate for more than a dozen proteins (45). Many of these interactions are believed to cause (induce) conformational changes in tRNA molecules which cannot be monitored with X-ray crystallographic techniques.

The universal cloverleaf secondary structure is corroborated by the X-ray structure of $tRNA^{Phe}$. The secondary structures of 5SrRNA and other larger RNA molecules are the subject of much debate. This ambiguity with regard to secondary structure is in part due to the large sizes of these RNA molecules.

The RNA molecule of primary concern in this study is E. coli 5SrRNA. It was first isolated by two independent research groups in 1964 (46-47). Although it lacked methylated bases and pseudouridines, its overall base composition was similar to tRNA. This led one of the groups to the erroneous conclusion that 5SrRNA was a precursor of tRNA and that it became methylated at a later stage (46). Their inability to amino acylate 5SrRNA was a clue that it was not a tRNA precursor (46). The other group correctly concluded that 5SrRNA was attached to the bacterial ribosome and estimated its chain length to be approximately 105 nucleotides (47).

During preliminary studies of E. coli 5SrRNA there was much speculation concerning its origin. Besides being a possible precursor to tRNA, it was suspected to be a degradation product of messenger RNA (mRNA) or the other larger rRNA molecules. The likelihood that it was a random degradation product was excluded by its apparent homogeneity with respect to chain length and a unique 3' and 5' terminus (48). In 1966, it was confirmed that the two types of molecules, 5SrRNA and tRNA, did not exhibit appropriate sequence homologies and that the methyl accepting activity of 5SrRNA, observed previously, was not due to 5SrRNA but contaminating submethylated tRNA attached to the ribosome (49). This eliminated the possibility that 5SrRNA was a precursor of tRNA. At about this time it became apparent that 5SrRNA was ubiquitous. Besides its presence in E. coli, it was found to be associated with the ribosomes of yeast (50), rat livers (51), sea urchins (52) and amphibians (53). In 1968 the first sequence of E. coli 5SrRNA was published (54). This sequence is shown in Figure 1.10. It consisted of 120 nucleotides and had a molecular weight of 40,575 daltons. All of the nucleotides were A, U, G, and C; unlike tRNA no unusual bases were observed. Today the 5SrRNA sequences from a variety of organisms are available (55).

The major components of the E. coli ribosome are shown in Figure 1.11. A 5SrRNA molecule is an integral part of each bacterial ribosome. It, along with 23SrRNA and approximately 34 proteins, constitutes the 50S ribosomal subunit of E. coli

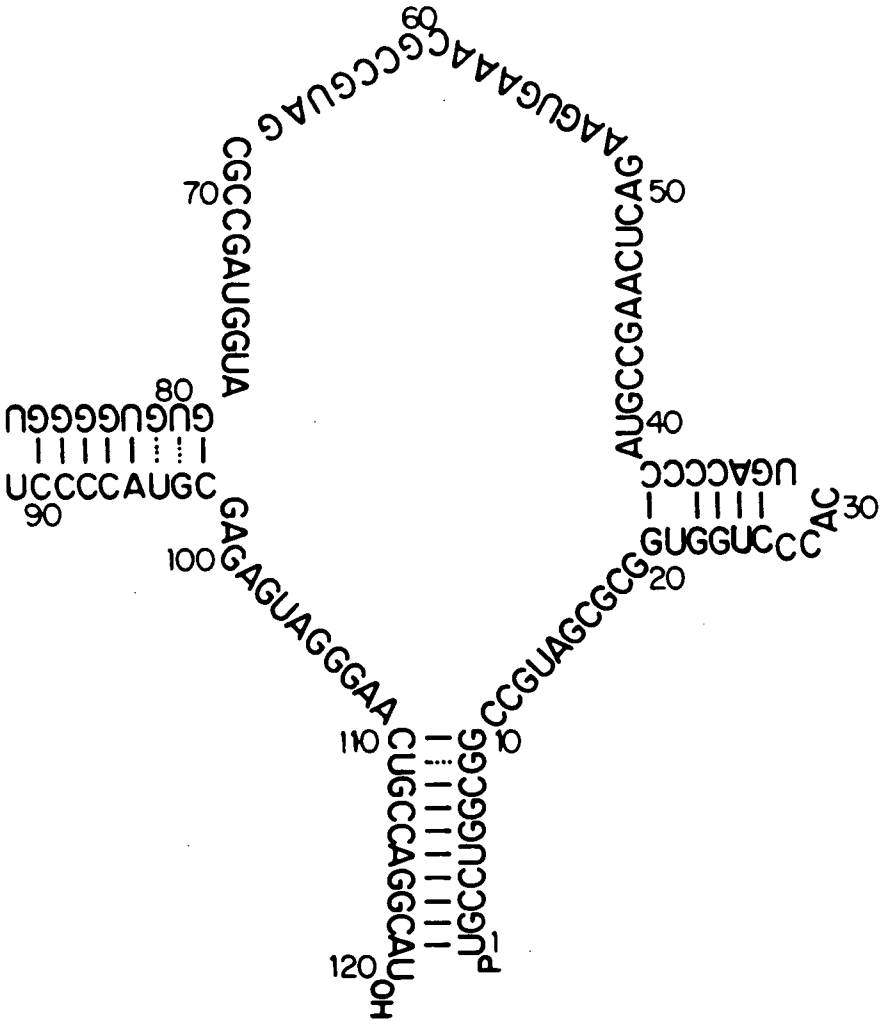

Figure 1.10. The first sequence of E. coli 5SrRNA. The sequence is drawn with an originally proposed base pairing scheme (54).

(56). The three RNA molecules combined account for approximately 63% of the ribosome's mass (56). Through cooperative interactions between these nucleic acids and proteins the ribosome functions as the protein assembly apparatus of the cell.

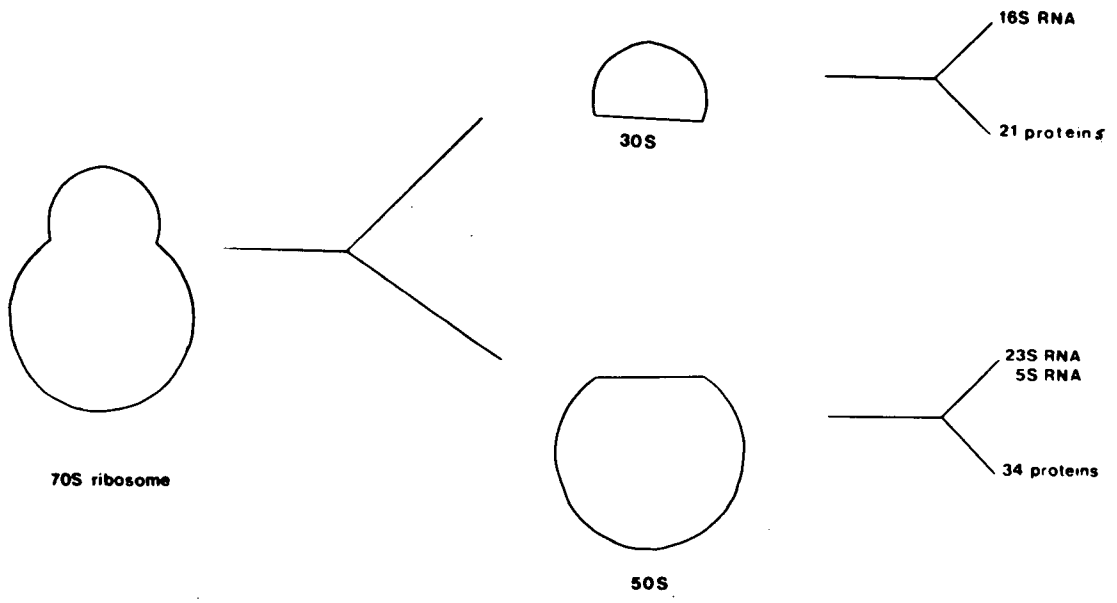

Figure 1.11. The constituent parts of an E. coli ribosome.

In E. coli, 70S ribosomes undergo continual association and dissociation into 30S and 50S subunits during protein synthesis (57-58). The fundamental steps involved in the initiation of a fully functional ribosome are outlined in Figure 1.12.

The first step is the dissociation of an inactive 70S ribosome into its two elemental subunits. Next three initiation factor proteins (IF-1, IF-2, and IF-3) bind to the 30S subunit in the order shown in Figure 1.12. The first to bind is IF-3. It is believed to actually be two proteins having

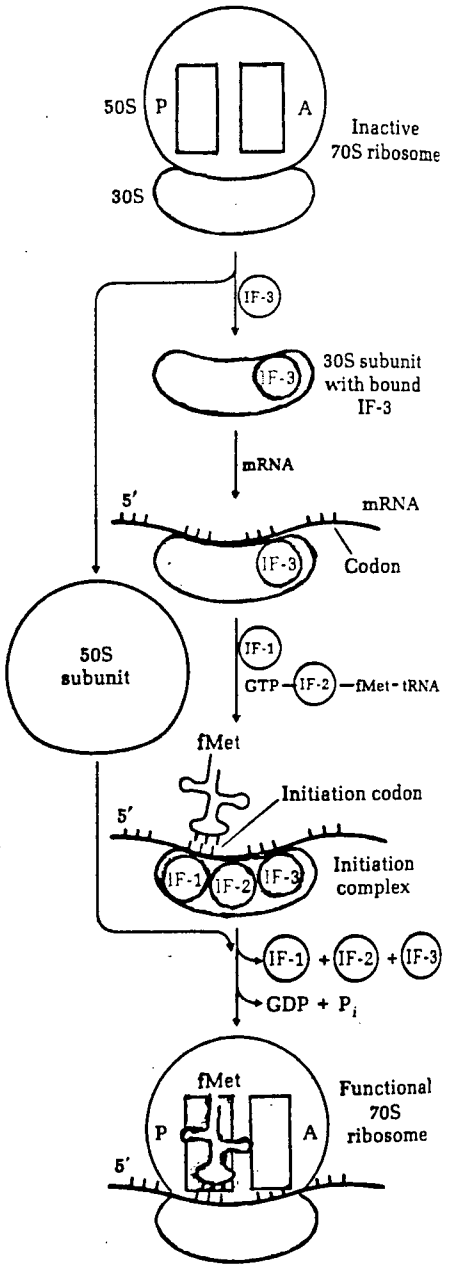

Figure 1.12. The formation of the initiation complex and the fully functional 70S ribosome of E. coli. IF-1, IF-2, and IF-3 are the initiation factor proteins (57).

molecular weights of approximately 21,500 and 23,500 daltons (59). Formation of this 30S-IF-3 complex appears to prepare

the subunit to receive mRNA, which next binds to this complex. Now IF-1 (a single protein with a molecular weight of 9,400 daltons), guanosine 5'-triphosphate (GTP), IF-2 (two proteins of 80,000 and 92,000 daltons), and initiator tRNA (N-formyl-methionyl-tRNA in E. coli) bind to the 30S x IF-3 x mRNA complex (59). The subsequent reassociation of this complex with the 50S subunit induces the release of the three initiation factors while converting a molecule of GTP to guanosine 5'-diphosphate (GDP). Accompanying this reassociation of the two ribosomal subunits is an alignment of initiator tRNA into the ribosomal P site located on the 50S subunit. The ribosomal A site, also located on the 50S subunit, is in close proximity to the P site. These two sites are implicated in protein synthesis. The first step, elongation, is shown in Figure 1.13. It consists of the alignment of an amino acyl tRNA into the A site, followed by peptide bond formation between the amino group of the amino acid attached to the tRNA in the A site and the carboxyl group of the initiator tRNA's amino acid in the P site. This is also illustrated in Figure 1.13. This peptide bond formation is accompanied by a cleavage at the ester linkage holding f-methionine to the initiator tRNA.

The next step following elongation is called translocation. It involves a transfer of the peptidyl tRNA at the A site to the P site and movement of mRNA so that the next triplet codon is in proximity to the A site. Concurrently, the tRNA previously occupying the P site is released from the

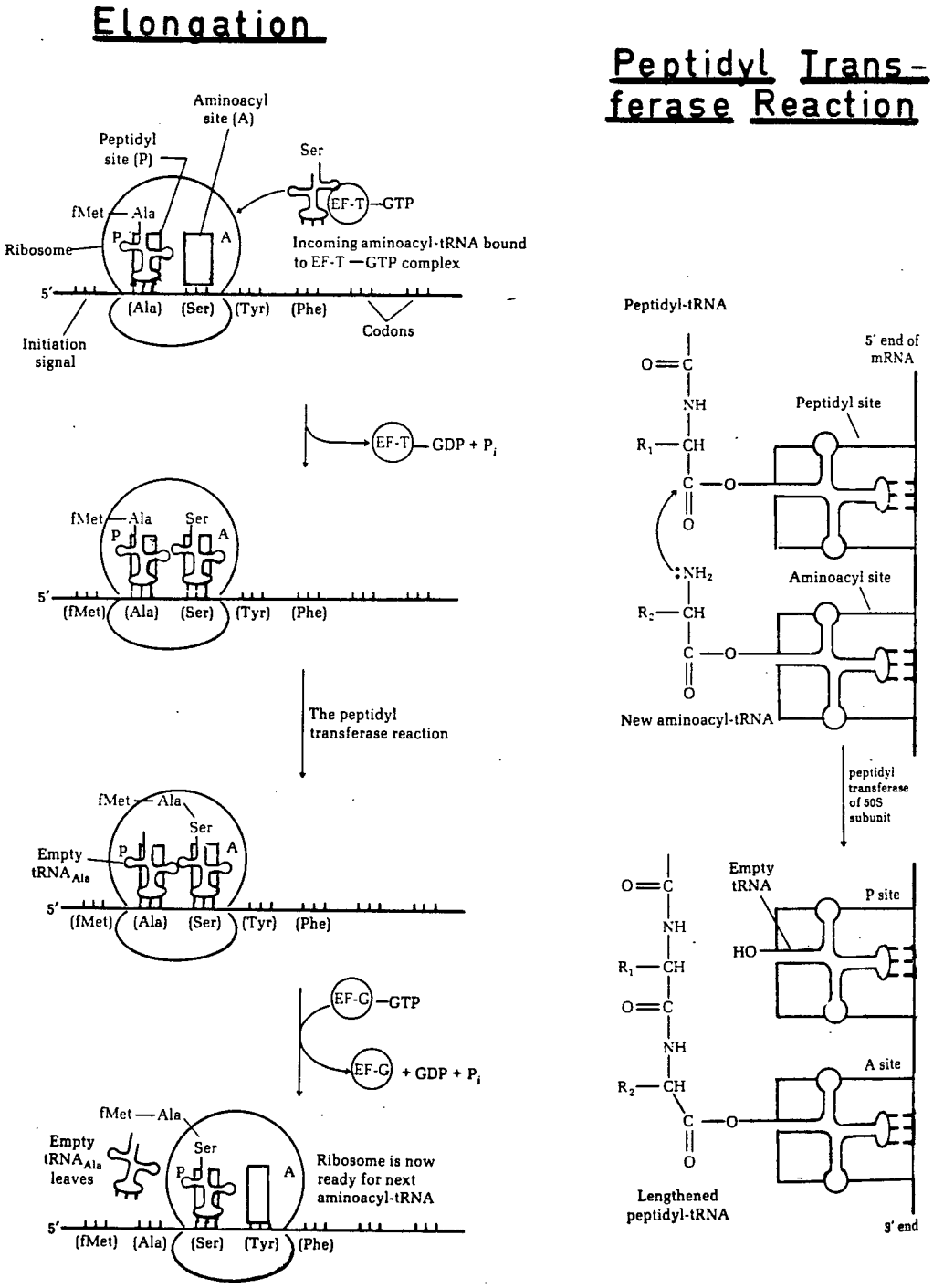

Figure 1.13. Protein elongation is shown on the left. EF-T and EF-G are the elongation factors. To the right the details of the peptidyl transferase reaction, which occurs during elongation, are shown (60).

ribosome. The A site is free to receive the next amino acylated tRNA. There is at least one specific tRNA for each amino acid. Amino acylation of the 3' terminus of tRNA is catalyzed by synthetase enzymes that are also specific for each tRNA species. The binding of an amino acylated tRNA to the ribosomal A site is preceded by the binding of one of the subunits of the dimeric cytoplasmic protein elongation factor-T (EF-T). The two subunits are called elongation factor-T_s (EF-T_s) and elongation factor-T_u (EF-T_u). EF-T first associates with GTP causing the release of the EF-T_s subunit. The GTP x EF-T_u complex then binds to the amino acylated tRNA (aa-tRNA) to form a GTP x EF-T_u x aa-tRNA complex. This complex binds to the ribosomal A site so that the anticodon loop of tRNA is situated to hydrogen bond to the complementary mRNA proximal to the A site. Complementarity is essential for the binding of tRNA to the A site. The amino group of the amino acylated tRNA in the A site is situated in close proximity to the esterified carboxyl carbon of the amino acylated tRNA in the P site. Nucleophilic attack by the amino group is facilitated by the enzyme peptidyl transferase (see Figure 1.13). Elongation and translocation require approximately 50 milliseconds (61). The polypeptide will continue to grow by repetition of these two steps until the mRNA codon for termination is signaled. In E. coli there are three termination codons, UAG, UAA, and UGA which do not have complementary tRNA anticodons. During termination, the polypeptidyl-tRNA shifts from the A site to the P site. Actual

termination is promoted by three proteins called release factors, R_1, R_2, and R_3. They are able to recognize the termination codons of mRNA (62). Hydrolysis of the ester bond between the polypeptide chain and terminal tRNA is most likely catalyzed by peptidyl transferase whose catalytic properties are changed by the releasing factors (57). Now the last tRNA and mRNA leave the 70S ribosome which in turn dissociates into 30S and 50S subunits until another initiator tRNA signals reformation of a functional ribosome to construct another protein. The amino acid sequence of a protein depends upon the order in which specific amino acylated tRNA molecules bind to the A site. This order is dependent upon the sequence of the triplet nucleotide codons of mRNA. This region of recognition is located in proximity to the A site and directly adjacent to the preceeding peptidyl tRNA which occupies the P site. Each specific tRNA has an anticodon loop containing three bases which recognizes the complementary triplet codon of mRNA. During the elongation-translocation process the mRNA also moves along so that a new three base codon is situated in the vicinity of the A site. The site is now ready to receive a new amino acyl tRNA according to the complementarity of the codon and anticodon. Codon-anticodon recognition involves the formation of Watson-Crick base pairs. According to the "wobble hypothesis" the base pairing is most stringent for the central of the three bases and one of the outer bases (63). The base pairing properties of the third base are probably less well defined.

5SrRNA is essential for protein synthesis but its specific function is not completely understood. The most widely accepted hypothesis is that it assists in the binding of tRNA to the A site of the ribosome through a mechanism comparable to codon-anticodon recognition: that is, by base pairing of a specific region of 5SrRNA to the complementary sequence of tRNA. The most likely candidates for these regions have been suggested from sequence homology studies of 5SrRNA and tRNA from different procaryotes and different strains of E. coli. Different strains of E. coli 5SrRNA exhibit variability at both the 3' and 5' ends. The middle region, bases 14-91, is highly conserved (64). Comparisons between the sequences of different procaryotes indicate a C-G-A-A segment near position 45 (55, 65). E. coli 5SrRNA also has the same segment about position 107. This latter segment is not likely to be functionally important since Bacillus stearothermophilis (B. stearothermophilis) 50S ribosomal subunits reconstituted with E. coli 5SrRNA are biologically active, but B. stearothermophilis 5SrRNA has only the central tetrameric C-G-A-A sequence (66-67). Another interesting feature of B. stearothermophilis ribosomal reconstitution experiments is that other bacterial 5SrRNA molecules which possess a central C-G-A-A sequence can be incorporated in the place of the native type with resulting biological activity (68). These observations tend to imply that a specific sequence is not entirely critical for function.

The T-Ψ-C-G segment found in almost all sequenced tRNA molecules can potentially form base pairs with the C-G-A-A region of 5SrRNA (65, 69). This has suggested that the binding of tRNA to the ribosome during protein synthesis may involve the base pairing of these two regions. However, X-ray crystallography (70-71), enzymatic accessibility studies (44), chemical modification studies (44), and oligonucleotide binding (72) all indicate that the T-Ψ-C-G segment is buried and therefore inaccessible. The binding of the C-G-A-A segment of 5SrRNA would require a conformational change in tRNA that exposes the T-Ψ-C-G region (65). Numerous experiments have been designed to test this hypothesis. Studies involving tetramers of T-Ψ-C-G or C-G-A-A tend to substantiate this proposed interaction between 5SrRNA and tRNA. The presence of the tetramer T-Ψ-C-G competitively inhibits the binding of $tRNA^{Phe}$ to E. coli ribosomes (73). The same tetramer also binds strongly to a 5SrRNA-ribosomal protein complex (74). This binding is reduced ten-fold for free 5SrRNA indicating that conformational changes in the molecule, due to ribosomal proteins, facilitate binding of the tetramer. Alternatively, the presence of tetrameric C-G-A-A inhibits poly U directed polyphenylalanine synthesis of the ribosome (75). Presumably it is competing with the C-G-A-A region of 5SrRNA for binding to the T-Ψ-C-G region of the incoming tRNA. There is also evidence that tRNA undergoes a conformational change, which exposes its T-Ψ-C-G segment, upon binding to the mRNA codon (65). Equimolar amounts

of C-G-(^{3}H)A-(^{3}H)A will bind to a 30S x phe - tRNA^{Phe} x EF-T$_u$ x GTP x polyU complex. With poly U absent only about ¼ as much tetramer binds.

It is possible to reconstitute functional 50S ribosomal subunits of E. coli where 5SrRNA is added during the last step of the assembly (76). Elimination of this final step leaves an inactive 47S ribosomal particle which lacks 5SrRNA and is partly deficient in four ribosomal proteins known to associate directly or indirectly with 5SrRNA. Experiments with these 47S pariticles have provided three important clues to the functionality of 5SrRNA. First, 5SrRNA is essential for poly U directed poly-phenylalanine synthesis. A 47S particle exhibits less than 1% of the activity of a completely reconstituted 50S subunit. Second, 5SrRNA is likely to be in proximity to the ribosomal A site and P site. Chloramphenicol, which binds to the A site and C-A-C-C-A-acLeu fragments, specific for the P site, does not bind to 47S particles. Lastly, 5SrRNA is important for the binding of Phe-tRNA^{Phe} to both the A site and the P site. No EF-T enzymatic binding of Phe-tRNA^{Phe} to the A site was observed and IF dependent binding of this amino acylated tRNA to the P site was reduced by 66% for these 47S particles. The implication is that there is direct involvement between 5SrRNA and the binding of Phe-tRNA^{Phe} to the A site. The role of 5SrRNA with the P site is apparently less direct.

The E. coli 5SrRNA molecule, at the ribosome, is surrounded by ribosomal proteins, since it is strongly protected from

degradation by ribonuclease T_1 and pancreatic ribonuclease (77). Even after trypsin digestion of the ribosomal proteins the 5SrRNA remains strongly protected from ribonuclease digestion. This inaccessibility to molecules the size of degradation enzymes suggests that the translation enzymes do not interact directly with 5SrRNA. Chemical modification with kethoxal, a small molecule that reacts with single stranded G residues indicates that G_{44} of the central C-G-A-A segment is not accessible to either ribosome bound or free 5SrRNA (78). Only G_{41} and G_{13} react readily for both free 5SrRNA and when incorporated into the 50S ribosomal subunit. For 70S ribosomes G_{13} is partially protected (79). Neither of these reactive G residues appears to be functionally significant since 5SrRNA chemically modified with kethoxal at G_{41} and G_{13} can be reconstituted into 50S ribosomal subunits without extensive loss in biological activity (78). The strong protection of 5SrRNA, at the ribosome, from ribonuclease digestion and chemical modification by smaller molecules means that the C-G-A-A segment, postulated to interact with the T-Ψ-C-G loop of tRNA, is not accessible. This suggests that there may be some requirement for conformational changes in ribosomal proteins and/or 5SrRNA in order for the postulated interaction to occur. Extensive conformational changes of the ribosomal proteins occur during mild dissociation of the ribosome into its two subunits through magnesium removal with ethylenediaminetetraacetate (EDTA) (80). This is evident from changes in the far ultraviolet circular dichroism

spectrum, an indication of alterations in the helical structure of ribosomal proteins due to subunit dissociations. The near ultraviolet circular dichroism spectrum, due exclusively to the three RNA molecules, is unchanged by such dissociation. Only under extreme conditions of ribosomal unfolding was any conformational change in the RNA observed by circular dichroism. These experiments demonstrate the strong conformational integrity of the three RNA molecules in the ribosome and postulate the possibility for extensive conformational alterations in ribosomal protein structure during protein synthesis. Ribosomal dissociation does not alter kethoxal modification (81) nor does it expose the C-G-A-A segment of 5SrRNA to enzymatic degradation (77). However, the possibility that translation enzymes or tRNA molecules can induce conformational changes in surrounding ribosomal proteins, which would expose the C-G-A-A region of 5SrRNA for binding to the T-Ψ-C-G segment of tRNA, cannot be ruled out.

Treatment of E. coli ribosomes with high concentrations of lithium chloride or ammonium chloride releases 5SrRNA and some ribosomal proteins (82-83). Dialysis to reduce the salt concentration results in 70 - 80% reattachment of 5SrRNA to the ribosome core (84). Further experiments show that only three proteins, L5; L18, and L25 are required for reattachment. This suggests that 5SrRNA and these three proteins represent a discrete unit of the ribosomal 50S subunit. The L5, L18, and L25 proteins have also been shown to have the strongest binding

affinity for free 5SrRNA (85-86). Only two other 50S subunit proteins, L20 and L3, bind very weakly to 5SrRNA (85). The affinity of L18 for 5SrRNA is the strongest. It is 16 times greater than L25 and 100 times that of L5 (86). The functions of L5 and L18 may be related since the association of L5 with 5SrRNA appears to be cooperatively stimulated by the presence of L18 while L25 does not exhibit cooperativity with either L5 or L18 (87). Ribonuclease digestion involving L18 and L25 bound 5SrRNA suggest that the most important recognition region for both L18 and L25 is the sequence 69-110 of 5SrRNA (88). Competitive binding studies involving ethidium bromide indicate that these proteins (L5, L18, and L25) are probably not binding to the same site (89). Ethidium bromide, which intercalates between A-U pairs of double stranded regions of nucleic acids has 5 or 6 binding sites on 5SrRNA. An L18 x 5SrRNA complex causes a two-fold decrease in the number of bound ethidium bromides. A complex of L5 x 5SrRNA has a slight effect while L25 x 5SrRNA has no effect on ethidium bromide binding. These observations suggest that L18 must be blocking ethidium bromide binding sites at the same double stranded regions as ethidium bromide and that the binding sites of the other two proteins, L25 and L5, are in different locations. This implies that the apparent cooperativity between L5 and L18 must be fairly indirect.

The effects of ribosomal proteins L5, L18, and L25 on the conformation of free E. coli 5SrRNA have been investigated

(90-92). The ribosomal protein with the strongest affinity for 5SrRNA, L18, causes a marked increase in the ultraviolet circular dichroism spectral intensity. This is an indication of increased secondary structure for the RNA molecule. One study indicates that an L25 x 5SrRNA complex gives a slight, but significant, decrease suggesting a small reduction in secondary structure (91). The L5 x 5SrRNA complex has no effect on the near ultraviolet circular dichroism spectrum of 5SrRNA. A 5SrRNA complexed with all three proteins gives a spectrum which is the sum of the above individual effects. A conformational change due to protein binding is also indicated from the enzymatic and chemical accessibility to the U_{87}-C_{88}-U_{89} region of 5SrRNA (88). In an L18 x L25 x 5SrRNA complex this region is accessible to both pancreatic ribonuclease and carbodiimide. Free 5SrRNA is not accessible to either of these agents in this region. The changes in molecular conformation due to the binding of ribosomal proteins suggest that free 5SrRNA in aqueous solution has a different conformation than when it is part of the ribosome.

A complex of L5, L18, and L25 plus 5SrRNA exhibits <u>in vitro</u> GTPase activity (92). Cross linking experiments using 4-mercaptobutyrimide indicate formation of disulfide bonded cross links between L5-L7 and L5-L12 (93). Proteins L7 and L12 are known to be located near the peptidyl transferase center (L16, L11, and L2) (94). This suggests a relationship between the

peptidyl transferase and GTPase centers of the 50S ribosomal subunit. It also implies that 5SrRNA is vicinal to these two catalytic sites.

A stable complex between E. coli 23SrRNA and 5SrRNA can be formed in the presence of the ribosomal proteins L18, L25, L6, and L2 (95). Only 8 50S ribosomal proteins independently bind to 23SrRNA (including L2 and L6). L18 and L25, which bind strongly to 5SrRNA, have no affinity for 23SrRNA. This indicates a cooperative interaction between 5SrRNA, 23SrRNA and the four ribosomal proteins. When the 50S subunit is split with high salt concentration under conditions of controlled pancreatic ribonuclease digestion fragments of 23SrRNA result; an 18S (3' end) and a 13S fragment (96). An 18SrRNA:5SrRNA complex can be formed with the above mentioned proteins indicating that the overall integrity of the 23SrRNA is not required for association with 5SrRNA. No association of 5SrRNA with either the 13S fragment of 23SrRNA or with the 16SrRNA (from the 30S subunit) has been observed. A proposed site of interaction between 5SrRNA and 23SrRNA is the 72-83 sequence of 5SrRNA which is highly conserved in procaryotes. A fragment of 23SrRNA, accessible to kethoxal modification, is complementary to this 5SrRNA segment (96).

The above remarks represent current understanding of 5SrRNA function at the ribosome. Based on sequence homology studies and oligonucleotide experiments a likely functional role for 5SrRNA is shown in Figure 1.14; namely, the recognition of the

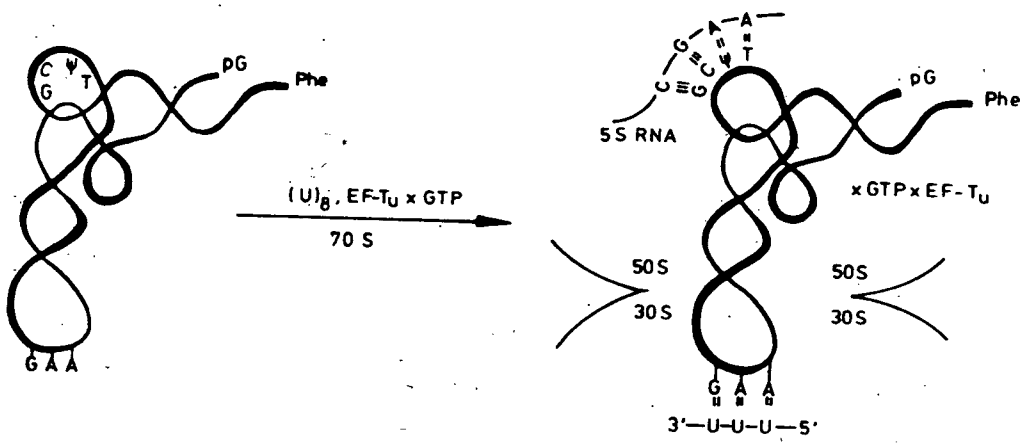

Figure 1.14. A proposed model for the function of 5SrRNA. The model requires that there be an induced conformational change of the G-C-Ψ-T region of tRNA which allows it to hydrogen bond to the C-G-A-A segment of 5SrRNA (69).

T-Ψ-C-G region of tRNA during its binding to the ribosomal A site. 5SrRNA and three ribosomal proteins (L5, L18, and L25) apparently form a discrete unit within the ribosome strongly protecting it from enzymatic degradation. Besides protein-RNA interactions there is also evidence for an RNA-RNA interaction between 5SrRNA and 23SrRNA. Multiple functions for E. coli 5SrRNA cannot be ruled out as evident from the apparent proximity of 5SrRNA to the peptidyl transferase and GTPase catalytic centers of the 50S subunit.

The work which will be presented in this thesis is concerned exclusively with the use of ^{19}F-nmr and laser Raman spectroscopy to interpret conformational properties of free E. coli 5SrRNA in aqueous solution. Much information about the macromolecular conformation of free 5SrRNA is available in the

literature. It has a sedimentation coefficient ($S_{20,w}$) of approximately 4.5S-4.8S which is fairly insensitive to counter-ions (97). This is indicative of a fairly rigid structure. According to the most recent small angle X-ray scattering studies 5SrRNA probably assumes the shape of a prolate elipsoid with an axial ratio of 5:1 in solution (98). Its radius of gyration (R_g) has been estimated to be 34±1.5 angstroms. This compares with a theoretical R_g value of 48 angstroms for a straight rigid double helix of 120 bases. 5SrRNA in solution also appears to be more asymmetric than tRNA and probably bulges at one end (98-99). Free 5SrRNA is known to exist in two stable forms under denaturing conditions (7 molar Urea and 0.01 molar EDTA) (100-101). Both forms are stable and can be separated by Sephadex G-100 or methylated bovine serum albumin-coated kieselguhr (MAK) chromatography. The B form will not reincorporate during reconstitution of 50S ribosomal subunits while the A form behaves like native 5SrRNA. Under renaturing conditions, in the presence of magnesium, the B form can be converted to the A form. Such multiple conformations for RNA molecules are not uncommon. Numerous examples of biologically inactive forms of tRNA have been presented in the literature (102).

Ultraviolet spectroscopy and ^{1}H-nmr spectroscopy have been used to obtain generalized base pairing properties of E. coli 5SrRNA. Optical melting curves at 260 millimicrons indicate that 5SrRNA has a relatively high melting temperature

compared to tRNA and the presence of magnesium and monovalent cations increases the melting temperature by about 10 degrees centigrade (103). It is also possible to estimate the total number of base pairs, the number which are G-C pairs, and the number of A-U pairs under a variety of buffer conditions. This data is compiled in Table 1.2. The large number of G-C base pairs (60-68% of the total) explains the high melting temperature of E. coli 5SrRNA. The ^{1}H-nmr spectra also indicate extensive G-C base pairing (24 G-C pairs) (108). However, the low number of predicted A-U pairs (only 4) and the inability to detect structural alterations between samples containing magnesium and those without is inconsistent with the available optical data.

Chemical modification studies have been used to probe the secondary structure of E. coli 5SrRNA. The most widely used chemical modifiers of RNA molecules are kethoxal, glyoxal, nitrous acid, monoperphthalic acid and methoxyamine. Both kethoxal and glyoxal react with unpaired guanines. The most reactive site in native 5SrRNA is G_{41} while the second most reactive site is G_{13} (109). After 45 minutes treatment of 5SrRNA with kethoxal 100% of G_{41} has reacted while only about 40% of G_{13} is modified. Exposures of this time duration will reduce ribosomal affinity. This is probably due to chemical modification of G_{13} since formylation of only G_{41}, with glyoxal, does not greatly affect ribosomal affinity (more than 70% retention) (110). In denatured E. coli 5SrRNA (B form)

NaCl(M)	$MgCl_2$(M)	A-U	G-C	Total B.P.	T_m (^oC)	Melt. Range (^oC)	Reference
0.1	None	13	28	41	—	—	104
0.15	None			38-39	60 (est.)	40-80 (est.)	105
2.0	None	11-14	22-25	36	70 (est.)	60-90 (est.)	106
None	0.01	18	27	45	80 (est.)	65-90 (est.)	107
			Denatured or B Form				
None	0.01	17	26	43	80 (est.)	65-90 (est.)	107
0.15	None			31	60 (est.)	40-80 (est.)	105

Accurate T_m determination from derivative curve:

1) low salt (0.01M KCl, 0.001M Tris-HCl, pH7) 103
$T_m=56^oC$

2) physiological salt (0.13M KCl, 0.09M NaCl, 0.06M $MgCl_2$, 0.001M Tris-HCl, pH7) 103
$T_m=66^oC$

Table 1.2. Shown above are estimates of the base pairing in E. coli 5SrRNA obtained by optical spectroscopy. As indicated they are at various concentrations of NaCl and $MgCl_2$ for both the native and denatured forms. The accurate melting temperature, T_m, at physiological salt concentrations and at low salt concentrations is also shown. The most significant features of this table are the extensive G-C base pairing and the apparent increase in T_m due to the presence of monovalent and divalent cations.

G_{41} is not accessible to these two chemical modifiers while G_{61} becomes exposed (110). It has been suggested that during the renaturation-denaturation process G_{41} and G_{61} play an important role. Nitrous acid is a less specific chemical modifier. It deaminates exposed adenines, guanines, and cytosines. The most reactive regions of 5SrRNA are bases 34-41 and 44-55 (109). These modifications result in loss of affinity for ribosomal proteins but the lack of specificity makes interpretation difficult. Methoxyamine is specific for accessible cytosines in RNA. The most exposed region in E. coli 5SrRNA is around positions 35-39 (109). The reaction of E. coli 5SrRNA with methoxyamine causes rapid loss of affinity for ribosomal proteins, but again interpretation is difficult due to the large number of reactive sites. Oxidation with monoperphthalic acid indicates that 10 of the 23 adenines of 5SrRNA are unpaired (111). This also causes a rapid loss in ribosomal affinity. It has been postulated that two of the adenines which react are those associated with the G-C-A-A segment. The basis for this argument is the inability to bind T-Ψ-C-G to 5SrRNA after oxidation of the adenines (111). Another more recently developed chemical modifier is 1,4-phenyldiglyoxal (PDG). Unlike kethoxal and other aliphatic dicarbonyls which only react with unstacked guanines, PDG can react with base paired guanines (112). Its aromatic character allows it to intercalate into double helical RNA regions producing cross linkages between neighboring guanines.

This modifier gives evidence for a helical stem formed by the two ends of E. coli 5SrRNA by showing that G_2 and G_{112} become cross linked with PDG. This is only possible if these two bases are in the direct neighborhood across the large groove of the double helix and are about 5 base pairs apart. It does however require that the two bases unstack and protrude slightly from the helix upon linkage with PDG. The major sites of chemical reactivity in E. coli 5SrRNA mentioned above are summarized in Figure 1.15. Clearly the most reactive regions are segments 34-41 and 44-51 which suggest single stranded loops in these regions.

Various ribonuclease enzymes are also sensitive to RNA secondary structure. Sheep kidney ribonuclease, which has no preferential specificity for purines or pyrimidines, will not hydrolyze double stranded helices and is even retarded by stacked single stranded loops (113). This enzyme is particularly reactive in the vicinity of G_{41} (113). The G_{41} residue is also most accessible for ribonuclease IV and ribonuclease T_1 (114-116). These and other major enzymatic cleavage sites (117) are summarized in Figure 1.15. Another method, which has identified single stranded regions about 39-50 in E. coli 5SrRNA, consistent with chemical modification and ribonuclease studies, is the binding of complementary oligomers (118). This is also shown in Figure 1.15.

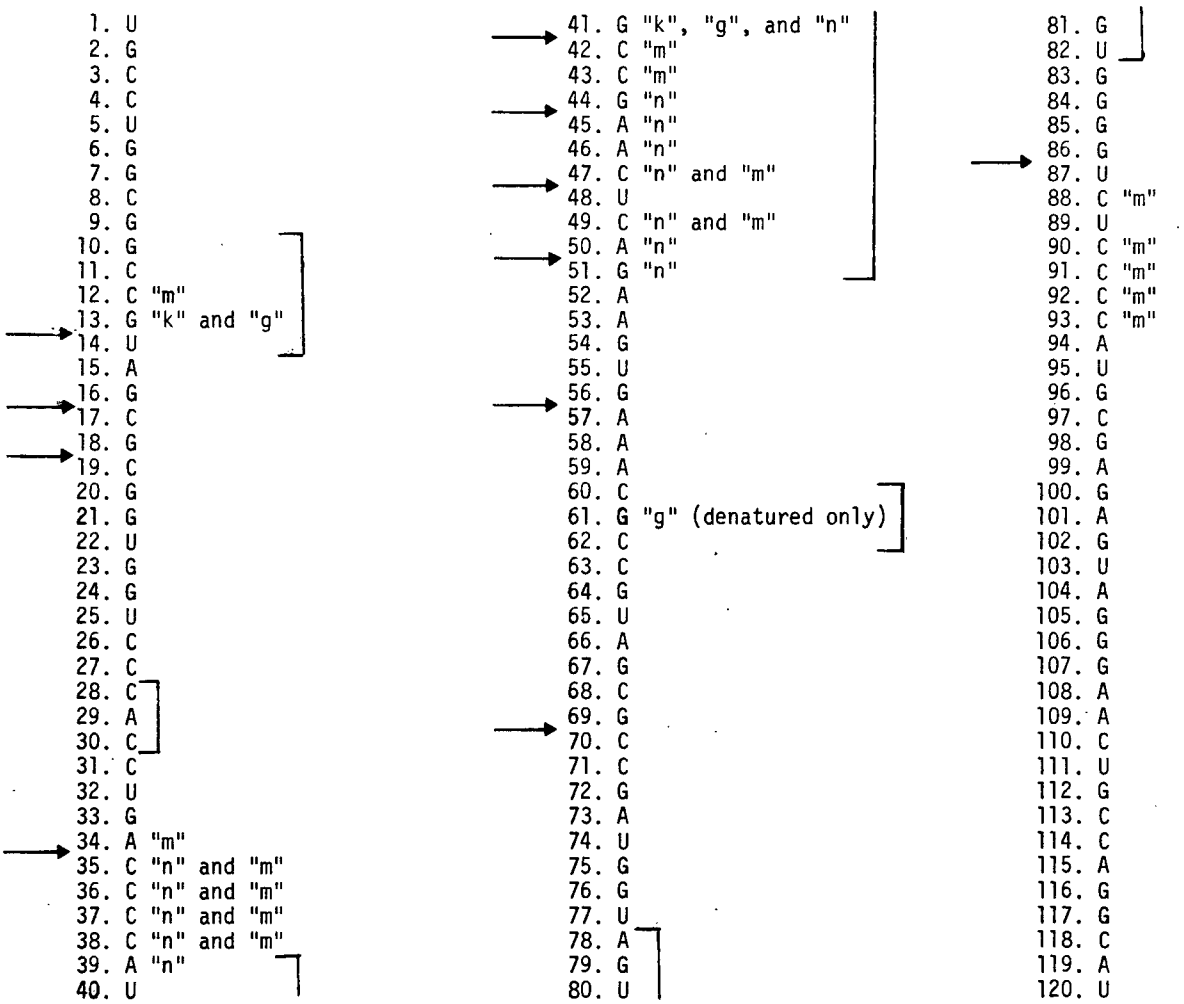

Figure 1.15. A summary of the regions of 5SrRNA which are most accessible to enzymes and chemical modifying agents. The chemical modifiers considered are kethoxal ("k"), glyoxal ("g"), nitrous acid ("n"), and methoxyamine ("m"). The arrows indicate the sites of enzymatic cleavage. The enzyme responsible for cleavage in each specific region of 5SrRNA is not indicated (see text). The bracketed regions indicate sites of oligonucleotide binding.

Unlike tRNA no unique secondary structure for E. coli 5SrRNA can be ascertained. The difficulty with inferring a secondary structure for this molecule is mostly due to three factors. First, 5SrRNA is about half again larger than tRNA. Computer studies have shown that the number of possible structures increase exponentially with size of the molecule (117). Secondly, the function of 5SrRNA is still not well understood. Any proposed secondary structure is therefore debatable on grounds of functional uncertainty. Lastly, it is not clear that free 5SrRNA has the same conformation as in its native ribosomal environment. As previously mentioned ultraviolet circular dichroism studies involving the dissociation of intact E. coli ribosomes into 30S and 50S subunits indicate conformational integrity of the three RNA molecules is retained (80). However, binding studies involving free 5SrRNA and the ribosomal protein L18, shows changes in the spectrum indicative of substantial alterations in conformation (90-92).

A number of secondary structures for E. coli 5SrRNA have been proposed but none are entirely consistent with all the available physical, chemical, and biochemical data (119-122, 108). Two models which are most consistent with the experimental results are shown in Figure 1.16. The formulation of the first model (Figure 1.16A) involved a comparative study of sequences from known procaryotic 5SrRNA molecules (120). It assumes that functionally equivalent 5SrRNA molecules from different procarotes will have similar structures. Based upon this

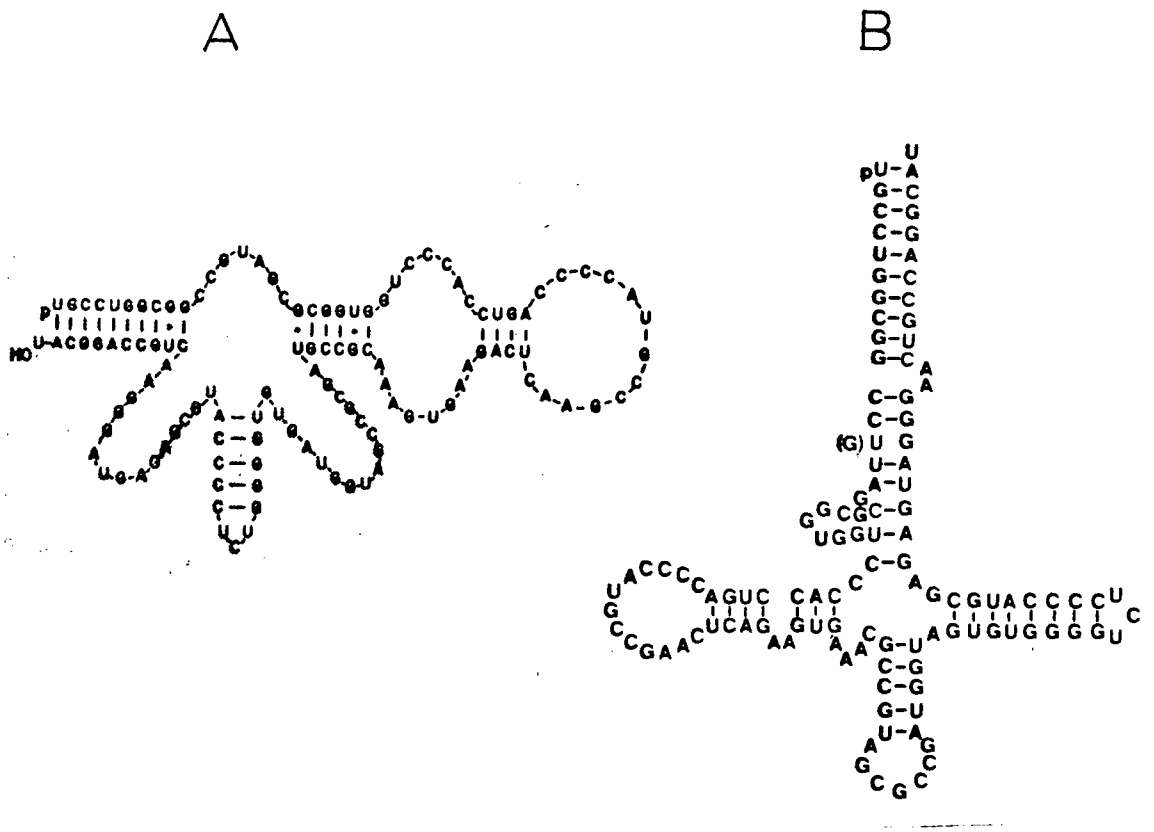

Figure 1.16. Two proposed models of the secondary structure of E. coli 5SrRNA which best fit the experimental data. The model proposed by Fox and Woese (1.16A) (120) has only 25 base pairs which is a low value compared to the optical data. The model proposed by Luoma and Marshall (1.16B) is remarkably similar to the cloverleaf secondary structure of tRNA (121).

study the model postulates the existence of four conserved helical regions; a molecular stalk (1-10 base paired to 119-110), a tuned helix (18-23 base paired to 65-60), a common arm (31-34

base paired to 51-48) and a procaryotic loop (82-86 base paired to 94-90). This structure is consistent with most ribonuclease digestion and chemical modification experiments provided that allowances are made for the protection of certain residues due to tertiary interactions. The model for E. coli has a total of 25 base pairs (5 A-U, 17 G-C, and 3 G-U). This is inconsistent with optical data (see Table 1.2) which suggest more extensive base pairing. An interpretation of A and B conformational changes for 5SrRNA, based on this model, have recently been proposed (123). It postulates a disruption of the helical stem region of the procaryotic loop to form a new helical segment involving bases 88-82 paired to bases 41-47. This necessitates disruption of the tuned helix and the common arm (see Figure 1.16A).

More recently, G. Luoma and A. Marshall of this laboratory have proposed a universal secondary structure for RNA molecules of this length (121). It is remarkably similar to the cloverleaf of tRNA as shown in Figure 1.16B. The model has a total of 37 base pairs (9 A-U, 22 G-C, and 6 G-U) which is consistent with the optical data. Ribonuclease accessibility and chemical modification experiments are also consistent with single stranded or strained regions of this structure.

Besides the work presented in this thesis two other nmr studies and one laser Raman study of 5SrRNA have appeared in the literature. One study involved ^{1}H-nmr spectroscopy of the low field exchangeable ring NH protons of E. coli 5SrRNA (108).

Spectra at various temperatures are shown in Figure 1.17. They have determined that there are 4 A-U and 24 G-C base pairs. However, these spectra are poorly resolved and as previously mentioned there is no significant difference between the magnesium containing sample and the one not containing magnesium. A low value for the degree of base pairing, as compared to the optical data, may be attributed to the integration technique which is known to give low values for $tRNA^{Phe}$ (124). The only other published nmr study used ^{13}C-nmr of enriched C-4 labeled uracil. The in vivo incorporation into Salmonella typhimurium 5SrRNA, whose sequence is similar to E. coli 5SrRNA, provided the spectra shown in Figure 1.18 (125). The 37°C spectrum shows 8 well resolved peaks and indicates that at least 75% of the uracils are involved in secondary interactions. Most recently a laser Raman spectrum of E. coli 5SrRNA, in aqueous solution, has appeared in the literature. It is shown in Figure 1.19 (126). This spectrum has been compared with a number of different tRNA molecules in order to infer some specific conformational information about 5SrRNA. Their results indicate more effective stacking of G residues than in $tRNA^{Phe}$ and the fraction of G residues in the stem must be larger than expected. On the other hand the fraction of stacked A residues must be less in 5SrRNA than in $tRNA^{Phe}$.

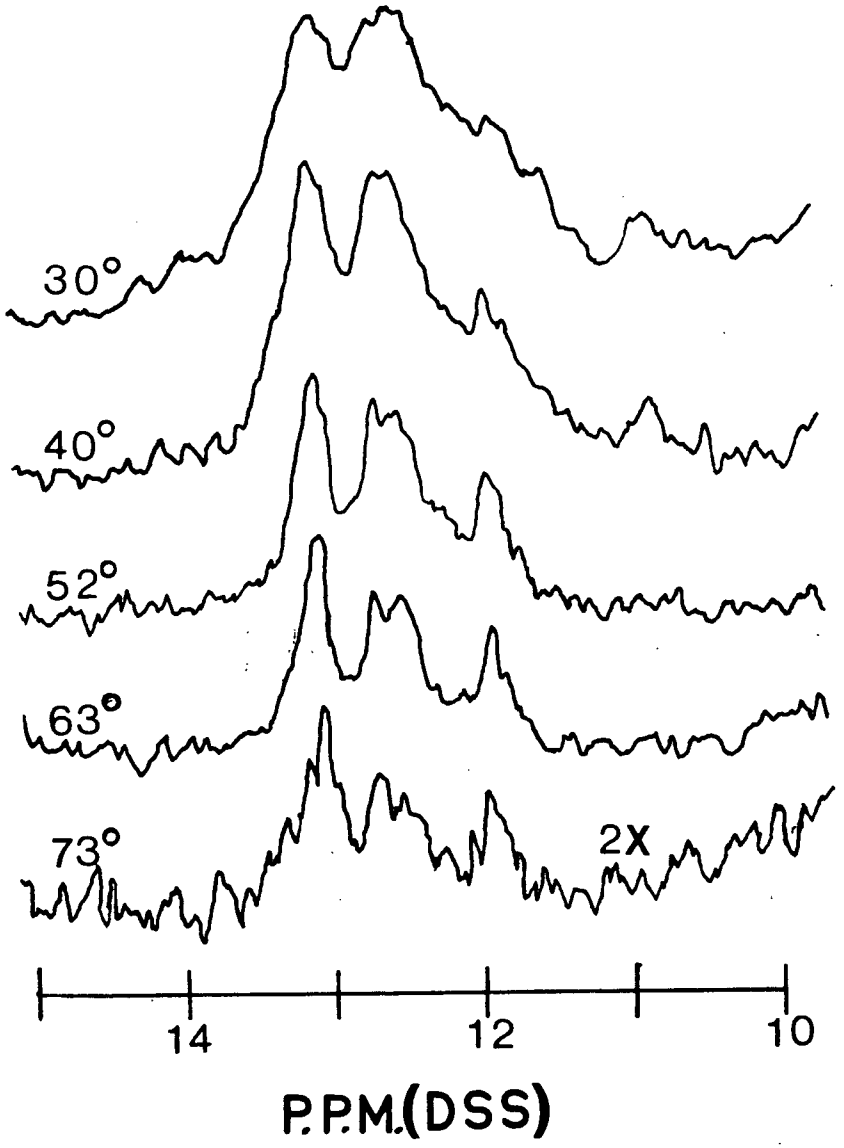

Figure 1.17. 300 megahertz low field ^{1}H-nmr spectra of E. coli 5SrRNA at various temperatures. The sample concentration was 1.4 millimolar. The aqueous buffer contained 0.01 molar cacodylate (pH 7) and 0.1 molar NaCl. The presence of magnesium had no effect on the spectra (108).

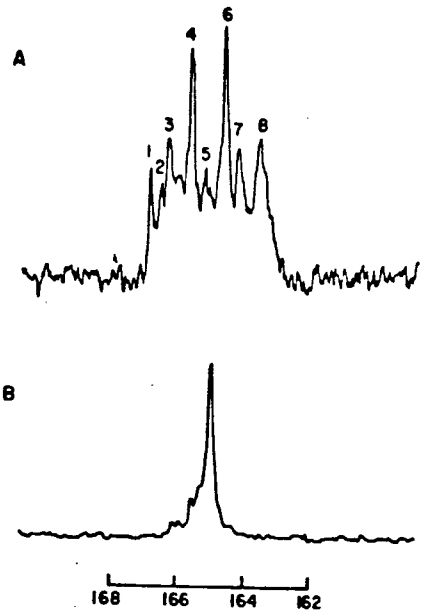

Figure 1.18. The ^{13}C-nmr spectrum of the C-4 uridine carbons of Salmonella typhimurium 5SrRNA at 37°C (A) and 75°C (B). The sample was millimolar. An aqueous buffer of 5 millimolar dithiothreitol (pH 7.4), containing 40 millimolar magnesium chloride and 2 millimolar EDTA, was used. Spectrum A required 18,000 transients while spectrum B is from 14,000 transients (125).

There were three major objectives in writing this chapter: first, to convey to the reader the reasons for formulating this study; second, to provide the reader with background information about the structure and function of E. coli 5SrRNA which is available in the literature; lastly, to acquaint the reader with physical and chemical techniques that have been applied to the elucidation of the structure and function of E. coli 5SrRNA. The remainder of this thesis will consider the utility of

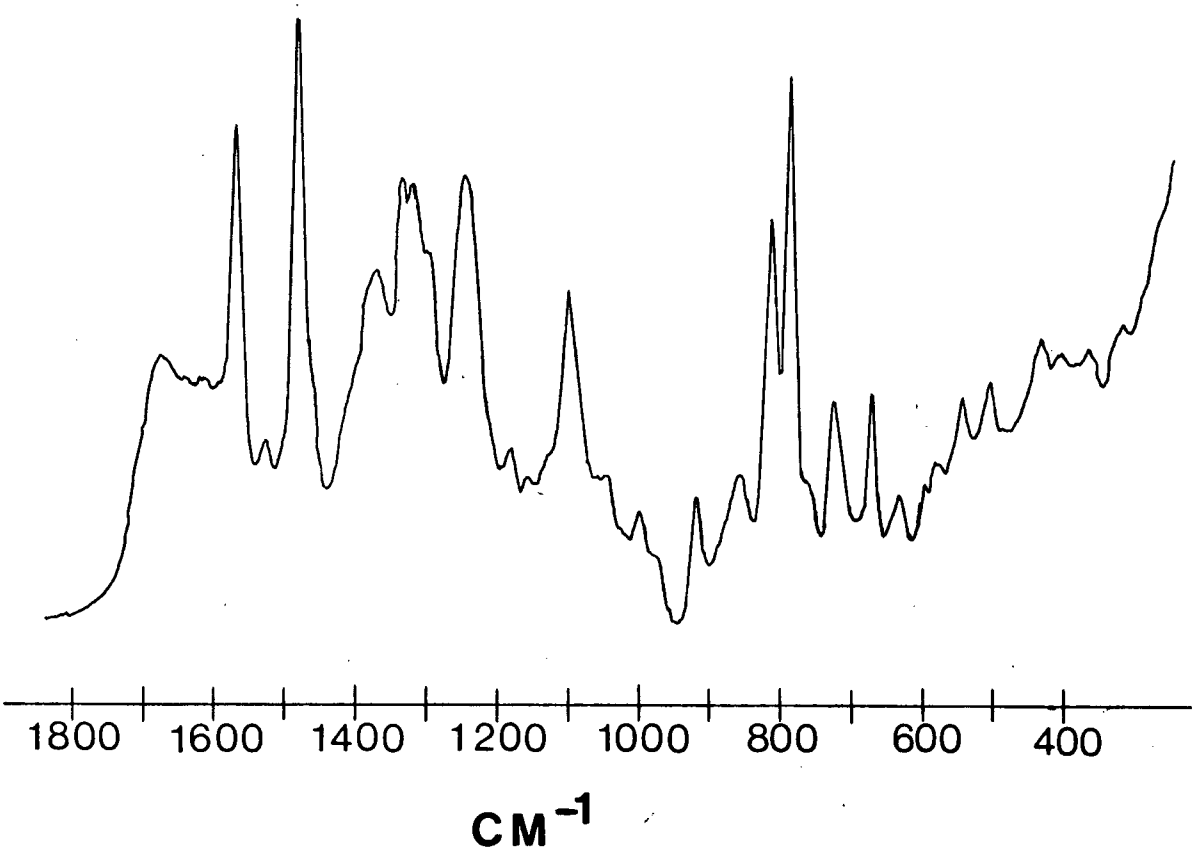

Figure 1.19. A laser Raman spectrum of a 5% aqueous solution of E. coli 5SrRNA (126).

^{19}F-nmr spectroscopy and laser Raman spectroscopy for interpreting conformation properties of E. coli 5SrRNA.

REFERENCES: CHAPTER 1

1. R.A. Dwek, in Nuclear Magnetic Resonance in Biochemistry, Oxford University Press, London, 1973; pages 2 and 30.

2. D.B. Arter and P.G. Schmidt, Nucl. Acid Res. 3, 1437 (1976).

3. B.R. Reid, N.S. Ribeiro, L. McCollum, J. Abbate, and R.E. Hurd, Biochemistry 16, 2086 (1977).

4. C.W. Hilbers and R.G. Shulman, Proc. Nat. Acad. Sci. USA 71, 3239 (1974).

5. L.S. Kan, P.O.P. Ts'o, F. von der Haar, M. Sprinzl, and F. Cramer, Biochemistry 14, 3278 (1975).

6. L.S. Kan, P.O.P. Ts'o, F. von der Haar, M. Sprinzl, and F. Cramer, Biochem. Biophys. Res. Commun. 59, 22 (1974).

7. P. Davanloo, M. Sprinzl, and F. Cramer, Biochemistry 18, 3189 (1979).

8. D.M. Crothers and P.E. Cole, in Transfer RNA, S. Altman, ed., The MIT Press, Cambridge, 1978; page 217.

9. M. Gueron and R.G. Schulman, Proc. Nat. Acad. Sci. USA 72, 3482 (1975).

10. L.M. Weiner, J.M. Backer, and A.I. Rezuukhin, FEBS Letters 41, 40 (1974).

11. F. Hayashi, K. Akasaka, and H. Hatano, Biopolymers 16, 655 (1977).

12. Reference 8; page 218.

13. B.D. Sykes, H.I. Weingarten, and M.J. Schlesinger, Proc. Nat. Acad. Sci. USA 71, 469 (1974).

14. W.E. Hull and B.D. Sykes, J. Mol. Biol. 98, 121 (1975).

15. Reference 13; page 472.

16. W.E. Hull and B.D. Sykes, Biochemistry 13, 3431 (1974).

17. W.E. Hull and B.D. Sykes, Biochemistry 15, 1535 (1976).

18. J. Horowitz and E. Chargaff, Nature 814, 1213 (1959).

19. C. Heidelberger, Prog. Nuc. Acid Res. 4, 1 (1965).

20. J. Horowitz, C.-N. Ou, M. Ishaq, J. Ofengand, and J. Bierbaum, J. Mol. Biol. 88, 301 (1974).

21. D.G. Comb and T. Zehavi-Willner, J. Mol. Biol. 23, 441 (1967).

22. G.A. Luoma in Laser Raman Evidence for New Universal Cloverleaf Structures for 5.8S RNA and 5S RNA, Masters Thesis, U.B.C. chemistry department, 1976; page 11.

23. B.F.C. Clark, reference 8; page 17.

24. A. Rich and U.L. Raj Bhandary, Ann. Rev. Bioc. 45, 805 (1976).

25. J.L. Sussman, S.R. Holbrook, R.W. Warrant, G.M. Church, and S.-H. Kim, J. Mol. Biol. 123, 607 (1978).

26. S.R. Holbrook, J.L. Sussman, R.W. Warrant, and S.-H. Kim, J. Mol. Biol. 123, 631 (1978).

27. B.F.C. Clark, reference 8; page 37.

28. Reference 26; page 638.

29. T. Lindahl, A. Adams, and J. Fresco, Proc. Nat. Acad. Sci. USA 55, 941 (1966).

30. J.P. Fresco, A. Adams, R. Ascione, D. Henley, and T. Lindahl, Cold Spring Harbor Symposia on Quantitative Biology 31, 527 (1966).

31. S. Holbrook, J. Sussman, R. Warrant, G. Church, and S.-H. Kim, Nucl. Acid Res. 4, 2811 (1977).

32. S.-H. Kim, Reference 8; page 262.

33. S.-H. Kim, Reference 8; page 256-257.

34. A. Rich and S.-H. Kim, Scientific American 238, 52 (1978).

35. P.H. Bolton, C.R. Jones, D. Lerner, L. Wong, and D.R. Kearns, Biochemistry 15, 4370 (1976).

36. B.R. Reid and G.T. Robbilard, Nature 257, 287 (1975).

37. L.S. Kan, P.O.P. Ts'o, F. van der Haar, M. Sprinzl, and F. Cramer, Biochem. Res. Commun. 59, 22 (1974).

38. D.M. Brown, in Basic Principles in Nucleic Acid Chemistry 2, P.O.P. Ts'o ed., Academic Press, New York, 1975; page 2.

39. S.-H. Kim, reference 8; page 266.

40. R. Langlois, S.-H. Kim, and C.R. Cantor, Biochemistry 14, 2554 (1975).

41. O. Pongs, R. Bald, and E. Reinwald, Eur. J. Biochem. 32, 117 (1973).

42. S.-H. Kim, reference 8; page 268.

43. R.C. Gamble, H.J.P. Shoemaker, E. Jekowsky, and P.R. Schimmel, Biochemistry 15, 2791 (1976).

44. D.H. Gauss, F. van der Haar, F. Maelicke, and F. Cramer, Ann. Rev. Biochem. 40, 1045 (1971).

45. S.-H. Kim, reference 8; page 275.

46. D.G. Combs and S. Katz, J. Mol. Biol. 8, 790 (1964).

47. R. Rosset, R. Monier, and J. Julien, Soc. Chim. Biol. Bull. 46, 87 (1964).

48. D.G. Comb and T. Zehavi-Willner, J. Mol. Biol. 23, 441 (1967).

49. R.S. Hayward, J. Legault-Démare, and S.B. Weiss, Fed. Proc. 25, 520 (1966).

50. J. Marcot-Queiroz, J. Julien, R. Rosset, and R. Monier, Soc. Chim. Biol. Bull. 47, 183 (1965).

51. F. Galibert, C.J. Larsen, J.C. Lelang, and M. Boiron, Nature 207, 1039 (1965).

52. D.G. Comb, S. Katz, R. Branda and C.J. Pinzino, J. Mol. Biol. 14, 196 (1965).

53. D.D. Brown and E. Littna, J. Mol Biol. 20, 95 (1966).

54. G.A. Brownlee, F. Sanger, and B.G. Barrell, J. Mol. Biol. 34, 379 (1968).

55. V.A. Erdman, Nucl. Acid. Res. 6, 29 (1979).

56. R. Brimacombe, K.H. Nierhaus, R.A. Garrett, and H.G. Wittman, Prog. Nuc. Acid. Res. 18, 1 (1976).

57. A.L. Lehninger, in Biochemistry, Worth Publishers, Inc., New York, 1975; pages 939-945.

58. P. Lengyel, in The Ribosomes, N. Nomura, A. Tissiére and and P. Lenygel, eds., Cold Spring Harbor Sym., 1974; pages 13-52.

59. Reference 57; page 940.

60. Reference 57; page 942.

61. From a seminar given by A. Rich at U.B.C..

62. Beaudet, A.L. and Caskey, C.T., in The Mechanism of Protein Synthesis, L. Bosch, ed., North-Holland, Amsterdam, 1972; page 133.

63. U. Lagerkuist, Proc. Nat. Acad. Sci. USA 75, 1759 (1978).

64. R. Monier, FEBS Symp. 23, 85 (1973).

65. U. Schwarz, R. Lührman, and H.G. Gassen, Bioc. Biophys. Res. Comm. 56, 807 (1974).

66. G. Bellemare, R. Vigne, and B.R. Jordan, Biochimie 55, 29 (1975).

67. N. Delihas, J.J. Dunn, and V.A. Erdman, FEBS Letters 58, 76 (1975).

68. P. Wrede and V.A. Erdman, FEBS Letters 33, 315 (1973).

69. U. Schwarz, H.M. Menzel, and H.G. Gassen, Biochemistry 15, 2484 (1976).

70. S.-H. Kim, G.J. Quigley, F.L. Suddath, A. McPherson, D. Sneden, J.J. Kim, J. Winzirl, and A. Rich, Science 179, 285 (1975).

71. J.D. Robertus, J.E. Ladner, J.T. Finch, D. Rhodes, R.S. Browne, B.F.C. Clark, and A. Klug, Nature 250, 546 (1974).

72. O. Pongs, R. Bald, and E. Reinwald, Eur. J. Biochem. 32, 117 (1973).

73. J. Ofengand and C. Henes, J. Biol. Chem. 244, 6241 (1969).

74. V.A. Erdman, M. Sprinzl, and O. Pongs, Bioc. Biophys. Res. Comm. 54, 942 (1973).

75. Reference 65; page 807.

76. F. Dohme and K.H. Nierhaus, Proc. Nat. Acad. Sci. USA 73, 2221 (1976).

77. J. Feunteun and R. Monier, Biochimie 53, 657 (1971).

78. N. Delihas, J.J. Dunn, and U.A. Erdman, FEBS Letters 58, 76 (1975).

79. W. Herr and H.F. Noller, J. Mol. Biol. 130, 421 (1979).

80. K.P. Wong and J.M. Dunn, FEBS Letters 44, 50 (1974).

81. H.F. Noller and W. Herr, J. Mol. Biol. 90, 181 (1974).

82. J. Marcot-Queiroz and R. Monier, Soc. Chim. Biol. Bull. 49, 477 (1967).

83. J.R. Gormley, C.-H. Yang, and J. Horowitz, Biochim. Biophys. Acta. 247, 80 (1971).

84. R.S.T. Yu and H.G. Whittman, Biochim. Biophys. Acta. 324, 375 (1973).

85. J. Horne and V.A. Erdman, Mol. Gen. Genetics 119, 337 (1972).

86. P. Spierer, A. Boydanou, and R.A. Zimmerman, Biochemistry 17, 5394 (1978).

87. P. Spierer and R.A. Zimmerman, Biochemistry 17, 2474 (1978).

88. P.N. Gray, G. Bellemare, R. Monier, R. Garrett, and G. Stoffler, J. MOl. Biol. 77, 133 (1973).

89. J. Feunteun, R. Monier, R. Garrett, M. LeBrett, and J.B. LePecq, J. Mol. Biol. 93, 535 (1975).

90. J.W. Fox and K.-P. Wong, J. Chem. 253, 18 (19).

91. D.G. Bear, T. Schleich, H.F. Noller and R.A. Garrett, Nuc. Acid. Res. 4, 2511 (1977).

92. P. Spierrer, A.A. Bodanov, A. Alexei, and R.A. Zimmerman, Biochemistry 17, 5394 (1978).

93. J.W. Kenny, A. Sommer, and R.R. Traut, J. Biol. Chem. 250, 9434 (1975).

94. Reference 8; page 95.

95. P.N. Gray and R.A. Garrett, Eur. J. Biochem. 28, 412 (1972).

96. P.N. Gray and R. Monier, Biochimie 54, 41 (1972).

97. H. Boedtker and G. Kelling, Biochem. Biophys. Res. Comm. 29, 758 (1967).

98. P.G. Connors and W.W. Beeman, J. Mol. Biol. 71, 31 (1972).

99. R. Österberg, B. Sjöberg, and A. Roger, Eur. J. Biochem. 68, 481 (1976).

100. M. Aubert, J.F. Scott, M. Reynier, and R. Monier, Proc. Nat. Acad. Sci. USA 61, 292 (1968).

101. E.G. Richards, R. Lecanidou, and M.E. Geroch, Eur. J. Bioc. 34, 262 (1973).

102. Reference 8; pages 221-222.

103. R.N. Nazar, G.D. Sprott, A.T. Matheson, and N.T. Van, Biochim. Biophys. Acta. 521, 228 (1978).

104. E.G. Richards, M.E. Geroch, H. Simpkins, and R. Lecanidou, Biopolymers 11, 1031 (1972).

105. J.F. Scott, R. Monier, M. Aubert, and M. Reynier, Biochem. Biophys. Res. Comm. 33, 794 (1968).

106. P.N. Gray and G.F. Saunders, Arch. Biochem. Biophys. 156, 104 (1973).

107. E.G. Richards, R. Lecanidou, and M.E. Geroch, Eur. J. Biochem. 34, 363 (1973).

108. D.R. Kearns and Y.P. Wong, J. Mol. Biol. 87, 744 (1974).

109. G. Bellemare, B.R. Jordan, J. Rocca-Serra, and R. Monier, Biochimie 54, 1453 (1972).

110. M. Aubert, G. Bellemare, and R. Monier, Biochimie 55, 135 (1973).

111. F. Cramer and V.A. Erdman, Nature 218, 92 (1968).

112. R. Wagner and R.A. Garrett, Nuc. Acid. Res. 5, 4065 (1978).

113. K. Kasai and M. Grunberge-Manago, Eur. J. Bioc. 1, 152 (1967).

114. P.F. Spahr and R.F. Gesteland, Proc. Nat. Acad. Sci. USA 59, 876 (1968).

115. B.R. Jordan, J. Mol. Biol. 55, 423 (1971).

116. B.R. Jordan and R. Monier, J. Mol. Biol. 59, 219 (1971).

117. R. Vigne and B.R. Jordan, J. Mol. Evol. 10, 77 (1977).

118. J.B. Lewis and P. Doty, Biochemistry 16, 5016 (1977).

119. Reference 17, page 77.

120. G.E. Fox and C.R. Woese, Nature 256, 505 (1975).

121. G.A. Luoma and A.G. Marshall, Proc. Nat. Acad. Sci. USA 75, 4901 (1978).

122. R. Osterberg, B. Sjöberg and R.A. Garrett, Eur. J. Bioc. 68, 481 (1976).

123. H. Weidner, R. Yuan, and D.M. Crothers, Nature 266, 193 (1977).

124. B.R. Reid and R.E. Hurd, Accounts of Chem. Res., 396 (1977).

125. W.D. Hamill, D.M. Grant, R.V. Cooper, and S.A. Harmon, J. Am. Chem. Soc. 100, 633 (1978).

126. M.C. Chen, R. Giege, R.C. Lord, and A. Rich, Biochemistry 17, 3134 (1978).

CHAPTER 2

EXPERIMENTAL

2.1 Introduction

The Experimentation involved in this thesis is described in sections 2.2 - 2.8. The first consideration was the growth of E. coli, in the presence or absence of 5-FU, on chemically defined minimal media (section 2.2). Next the bacterial 5SrRNA (or FU-5SrRNA) was isolated by extraction and chromatographic procedures. The initial feasibility of this study was determined by two specific experiments. The first one involved determination of the amount of radioactive 5-FU (labeled with carbon-14 at the 2-carbon position of 5-FU) incorporated into the bacterial tRNA (section 2.6). This experiment showed that the incorporation was extensive. The second feasibility experiment concerned the obtainment of an ^{19}F-nmr spectrum of heterogeneous tRNA from E. coli. After practicability was established a specific RNA molecule was selected for further study. The choice of 5SrRNA was determined largely by the relatively large sample requirement for ^{19}F-nmr spectroscopy. For an adequate signal to noise ratio in a convenient amount of time on the departmental Varian XL-100 spectrometer, 90 milligrams of sample in 3 milliliters of buffer was required. At a later stage of this study a Brüker HX-270 spectrometer (University

of Alberta biochemistry department) was employed. Then only 15 milligrams of 5SrRNA in 0.5 milliliters of buffer was required. The ^{19}F-nmr spectra are presented in section 2.7.

The concern about possible alterations in 5SrRNA conformation due to 5-FU incorporation led to the second technique employed in this thesis, laser Raman spectroscopy. The Raman spectrum of a specific RNA is the sum of the vibrational contributions from all the bases plus vibrational components from the ribophosphate backbone. Conformational change affects the intensities of many of these vibrational components. Raman spectra of native 5SrRNA and FU-5SrRNA are given in section 2.8. Also considered in the final section are the effects of 5-fluoro- substitution on the Raman spectrum of the uracil and uridine bases.

2.2 Bacterial Growth

Cultures of E. coli B cells, provided by the U.B.C. microbiology department, were grown on a chemically defined minimal media (1). The constituents for one liter of media are given in Table 2.1. These chemicals were weighed, dissolved in the

Chemical	Amount (grams)
Potassium Phosphate Dibasic	7
Potassium Phosphate Monobasic	3
Magnesium Sulfate	0.1
Ammonium Sulfate	1
Sodium Citrate	0.5
Glucose	2

Table 2.1. The chemical composition of one liter of minimal media (1).

appropriate volume of deionized water, mixed, and autoclaved. This liquid media was used for all bacteria grown in this laboratory. Solid media for slants and petri dishes contained 0.2% agar. A requirement for relatively large quantities of 5SrRNA made necessary the use of fermentation devices of various capacities. The fermentors employed during various stages of this work are listed in Table 2.2. The yield for cells treated with 5-FU was about one gram (wet weight) per liter of media while untreated cells gave yields of at least two grams per liter.

Suitable inocula were usually prepared in erlenmeyer flasks the night before a fermentation. They were allowed to grow overnight at room temperature. The size of the inoculum

Fermentation Device	Capacity (liters)
Erylenmeyer Flask	1-4
New Brunswick Batch Fermentor (Chemistry Department, University of British Columbia)	10
New Brunswick Batch Fermentor (Microbiology Department, University of British Columbia)	25
New Brunswick Batch Fermentor (Food Sciences, University of British Columbia)	60
New Brunswick Batch and Continuous Flow Fermentor (Biochemistry Department, University of Washington, Seattle, Washington)	100

Table 2.2. The fermentation devices used during various stages of this work.

represented at least 3% of the fermentor volume. Larger inocula were desirable since they markedly diminished the initial lag phase prior to exponential growth and reduced the possibility of contamination. In all cases the fermentation temperature was 37 degrees centigrade and growth was with constant agitation and aeration. Progress of bacterial growth was monitored by measurement of the media's dispersion at 686 millimicrons (A_{686}) usually on a Gilford 240 spectrometer. This involved withdrawing two milliliter aliquots at various time intervals and determining the media's turbidity from its A_{686} value. The growth curves for untreated and 5-FU treated E. coli B cells are shown in Figure 2.1. Untreated bacteria grew to an A_{686}

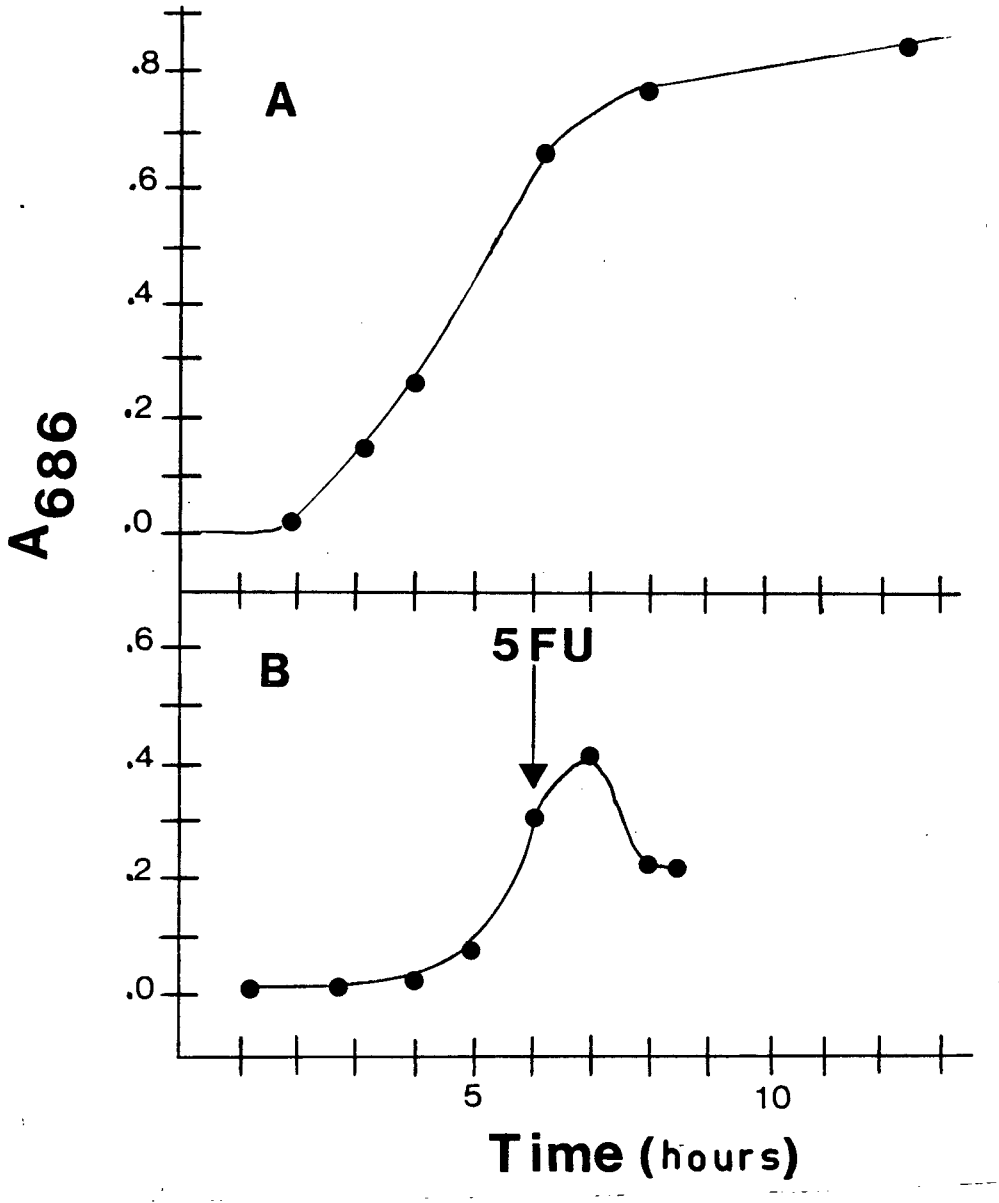

Figure 2.1. Bacterial growth curves of E. coli B grown on minimal media. Figure 2.1A shows normal exponential growth. In Figure 2.1B 25 milligrams of 5-FU was added to each liter of media during early exponential growth (A_{686} = 0.3). The reduced lag-phase, prior to exponential growth, for Figure 2.1A is due to the addition of a larger inoculum.

of about 0.85 before leveling to a stationary phase. The addition of 5-FU (25 milligrams per liter of media) during early exponential growth ($A_{686} \simeq 0.3$) caused inhibition of cell growth and apparent cell destruction. Media turbidity would continue increasing until about one hour after the addition of 5-FU. This was followed by a 50% reduction in turbidity prior to a stationary phase. This indicated cellular destruction due to the presence of 5-FU. In support of this hypothesis was the apparent increase in viscosity of the media which led to extensive foaming shortly after the addition of 5-FU. No foaming was observed in bacteria grown without 5-FU. The foaming was presumably caused by the release of highly viscous deoxyribonucleic acid and protein material due to cell lysis. After addition of 5-FU agitation and aeration was continued for three hours. The cells were usually harvested with a Sharples continuous flow centrifuge. The harvested cells were washed two times with 0.01 molar tris·HCl (pH 7.4) containing 0.01 molar magnesium acetate and stored at -20 degrees centigrade.

The reduction in the bacterial population due to the presence of 5-FU caused concern about the extent of incorporation into bacterial RNA. Evidence that the remaining bacteria were able to metabolize and incorporate 5-FU is given in sections 2.6 and 2.7.

At one stage of this work two pounds of 5-FU treated *E. coli* B cells were graciously provided by Professor Ivan Kaiser at the University of Wyoming. His kindness is greatly appreciated.

2.3 Isolation of 5SrRNA

The isolation procedures for 5SrRNA from untreated and 5-FU treated E. coli B cells were identical. The water soluble RNA (sRNA) was extracted from the bacteria with an emulsion that consisted of equal volumes of water and phenol. The phenol facilitates extraction of the sRNA by increasing the porosity of the cells through the extraction of lipids and proteins from the cell membrane. Phenol also denatures ribonucleases to prevent enzymatic degradation of the RNA. The combined effects of the phenol allow intact tRNA, 5SrRNA, and a small amount of the larger rRNA to leak out of the cells and dissolve in the aqueous phase of the water-phenol emulsion. DNA and most of the rRNA remain inside the cell membrane due to their larger size. The aqueous phase can be separated from phenol and cellular debris by centrifugation.

The sRNA isolated by the above technique consists of about 8% rRNA, 86% tRNA, and 6% 5SrRNA (see Figure 2.2). Since this mixture consists of three molecules which differ in size and shape, the 5SrRNA was conveniently separated from the other two RNA species by gel filtration chromatography using Sephadex G-100 or G-75 gels. The final step of the isolation procedure was to desalt the 5SrRNA on a Sephadex G-25 column and then lyophilize it. The resulting freeze dried powder was then stored at $-20^{o}C$.

The detailed isolation procedures are outlined below in five steps. Steps I, II, and III were designed by Dr. Gordon Tener of the University of British Columbia Biochemistry Department. Gel filtration procedures similar to step IV have been employed by others (2). It was possible to obtain between 10 and 20 milligrams of 5SrRNA per 100 grams of E. coli B cells.

Step I. Preparation of Buffers and Columns

The tris buffer referred to in steps I-IV was prepared with deionized water and contained 0.01 molar tris-(hydroxymethyl)-methylamine-hydrogen chloride (tris·HCl) adjusted to pH 7.5 using a solution of sodium hydroxide. To assure the presence of a native concentration of magnesium ions the buffer also contained 10 millimolar magnesium chloride. Fresh tris buffer was prepared every two days to prevent bacterial growth in the buffer and on the various columns.

A diethyl amino cellulose (DEAE-cellulose) column was prepared prior to the isolation of sRNA. For each 100 grams of E. coli B cells to be used in step II 40 grams of Whatman DEAE-cellulose (0.86 milliequivalents per gram) was mixed with 4 liters of deionized water. To facilitate a convenient flow rate fines were removed by allowing the DEAE-cellulose to settle for about 30 minutes. Then most of the water was decanted off and the process repeated a second time. The DEAE-cellulose was then poured into a column which was at least 2.5 centimeters in diameter. This column was washed with tris buffer

that contained 1 molar sodium chloride until the A_{260} of the eluent was less than 0.05. Then it was equilibrated with at least 3 volumes of tris buffer containing 0.3 molar sodium chloride.

Sephadex G-100 (or G-75) columns were prepared according to the manufacturer's specification (3). For the isolation of 5SrRNA used in ^{19}F-nmr experiments the gels were poured into 5 x 90 centimeter columns. Longer narrower columns (2 x 180 centimeters) were later adapted for laser Raman studies. The eluent in all cases was tris buffer containing 1 molar sodium chloride.

Step II. Extraction of sRNA from E. coli B cells

To each 100 grams of frozen E. coli B cells 300 milliliters of tris buffer and an equal volume of water saturated phenol were added. The resulting water-phenol emulsion was mixed with the bacterial cells for at least 30 minutes and then centrifuged at 10,000 g for 15 minutes on a Sorval RC2-B refrigerated centrifuge. Centrifugation facilitated the separation of the aqueous phase from the phenol and the cellular debris. The top aqueous phase was removed by suction and another 300 milliliters of tris buffer was added to the remaining phenol-cell debris mixture. After mixing and centrifugation this second aqueous phase was combined with the first and 0.1 volumes of 2 molar potassium acetate (pH 4.5) was added. The sRNA was then precipitated by the addition of 2.5 volumes of 95% ethanol

pre-cooled to -20 degrees centigrade. The precipitate was allowed to flocculate and settle overnight in the freezer. The next day most of the ethanol-water solution was decanted off and the remaining RNA precipitate-ethanol mixture was centrifuged at 10,000 g for 10 minutes. The resulting sRNA pellet was washed twice with cold 95% ethanol. After the second washing and centrifugation the RNA was thoroughly drained of the ethanol.

Step III. Attachment of sRNA to a DEAE-cellulose column and subsequent washing of the RNA

The sRNA from Step II was dissolved in a minimal amount of tris buffer containing 0.3 molar sodium chloride (approximately 50 milliliters for sRNA from 100 grams of frozen E. coli B cells). The solution was then centrifuged at 10,000 g for 15 minutes to remove a small amount of insoluble debris. The sRNA solution was applied to the DEAE-cellulose column which was equilibrating with tris buffer containing 0.3 molar sodium chloride (see step I). At this salt concentration the sRNA will attach to the DEAE anion exchanger and can be washed with tris buffer containing 0.3 molar sodium chloride. This facilitates removal of carbohydrates, phenol, mononucleotides and proteins which do not bind in the presence of 0.3 molar sodium chloride. Washing is continued until the A_{260} reduces to a minimum (about 500 milliliters). The sRNA was then eluted from the column with tris buffer containing 1 molar sodium chloride. The eluent with an A_{260} greater than 0.5 was collected and 20 milliliters of 0.1 molar magnesium chloride was added. The sRNA was then precipitated with

2.5 volumes of 95% ethanol pre-cooled to -20 degrees centigrade. The "washed" sRNA was allowed to flocculate and settle overnight at -20 degrees centigrade. Decantation and centrifugation (10,000 g for 10 minutes) was then used to obtain the sRNA pellet.

Step IV. Isolation of 5SrRNA from sRNA

The separation of 5sRNA from tRNA and rRNA was accomplished by gel filtration chromatography on Sephadex G-100 or G-75 columns. An elution profile of sRNA from a Sephadex G-75 column is shown in Figure 2.2. According to this profile sRNA from step III consists of about 86% tRNA, 6% 5SrRNA, and 8% rRNA. This is in agreement with the relative proportions obtained by others (2).

Sephadex G-75 (or G-100) was prepared according to the manufacturer's specifications and before using the columns were equilibrated with at least 2 volumes of tris buffer containing 1 molar sodium chloride. The best separation was obtained with long narrow columns. The 5SrRNA prepared for the laser Raman experiments was purified using 2 x 190 centimeter columns. The 5SrRNA for the ^{19}F-nmr experiments, where substantially larger sample amounts were required, was purified on shorter and wider columns (about 5 x 90 centimeters). The latter samples contained slightly larger traces of tRNA contamination as judged by polyacrylamide gel electrophoresis (see section 2.5).

Elution profiles were obtained with an LKB 8300 Uvicord II connected to a Fisher Recordall Series 5000 chart recorder.

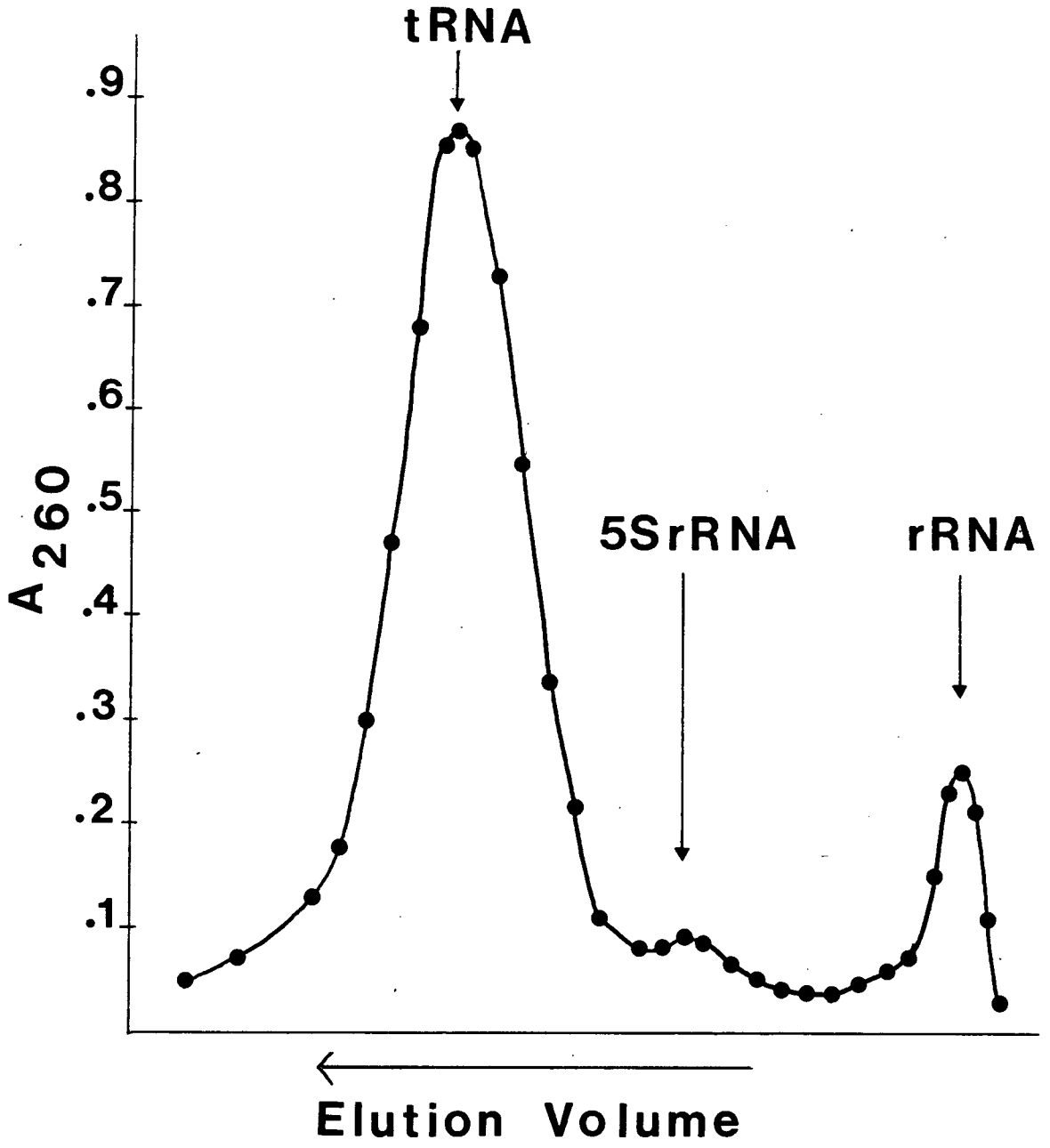

Figure 2.2. A complete elution profile of sRNA applied to a Sephadex G-100 column (5 x 90 centimeters). The largest molecular weight component, rRNA, elutes at the column's void volume. The tRNA, which is the smallest, is retained longest on the column. The 5SrRNA, which is intermediate in size, elutes just before the tRNA peak. According to this elution profile sRNA consists of about 86% tRNA, 8% rRNA, and 6% 5SrRNA.

In general the Sephadex column was overloaded with respect to tRNA and rRNA. This was done to achieve larger yields of 5SrRNA per run. A single run on a 2 x 190 centimeter column required at least 8 hours. The sRNA from about 50 grams of cells was the maximum that could be used for a single run without completely destroying peak resolution. The elution profile for sRNA from about 25 grams of cells eluted from a 2 x 190 centimeter column is shown in Figure 2.3. The eluent was collected using a Gilford microfractionator and aliquots from the center most peak, corresponding to 5SrRNA, were collected and precipitated by the addition of 0.1 volumes of 0.1 molar magnesium chloride followed by the addition of 2.5 volumes of 95% ethanol cooled to -20 degrees centigrade. After the precipitate was allowed to settle for at least one day it was collected by decantation and centrifugation at 10,000 g for 10 minutes. The resulting pellet, consisting predominantly of 5SrRNA, was dissolved in a minimal amount of tris buffer containing 1 molar sodium chloride and reapplied to the Sephadex column. An elution profile of a second run on this column is shown in Figure 2.4. The fractions corresponding to 5SrRNA were again collected and precipitated as mentioned above. After the second run the 5SrRNA sample was judged pure according to Sephadex chromatography. The elution profile of purified 5SrRNA run on the same Sephadex column is shown in Figure 2.5. Superimposed with it is an elution profile of tRNA.

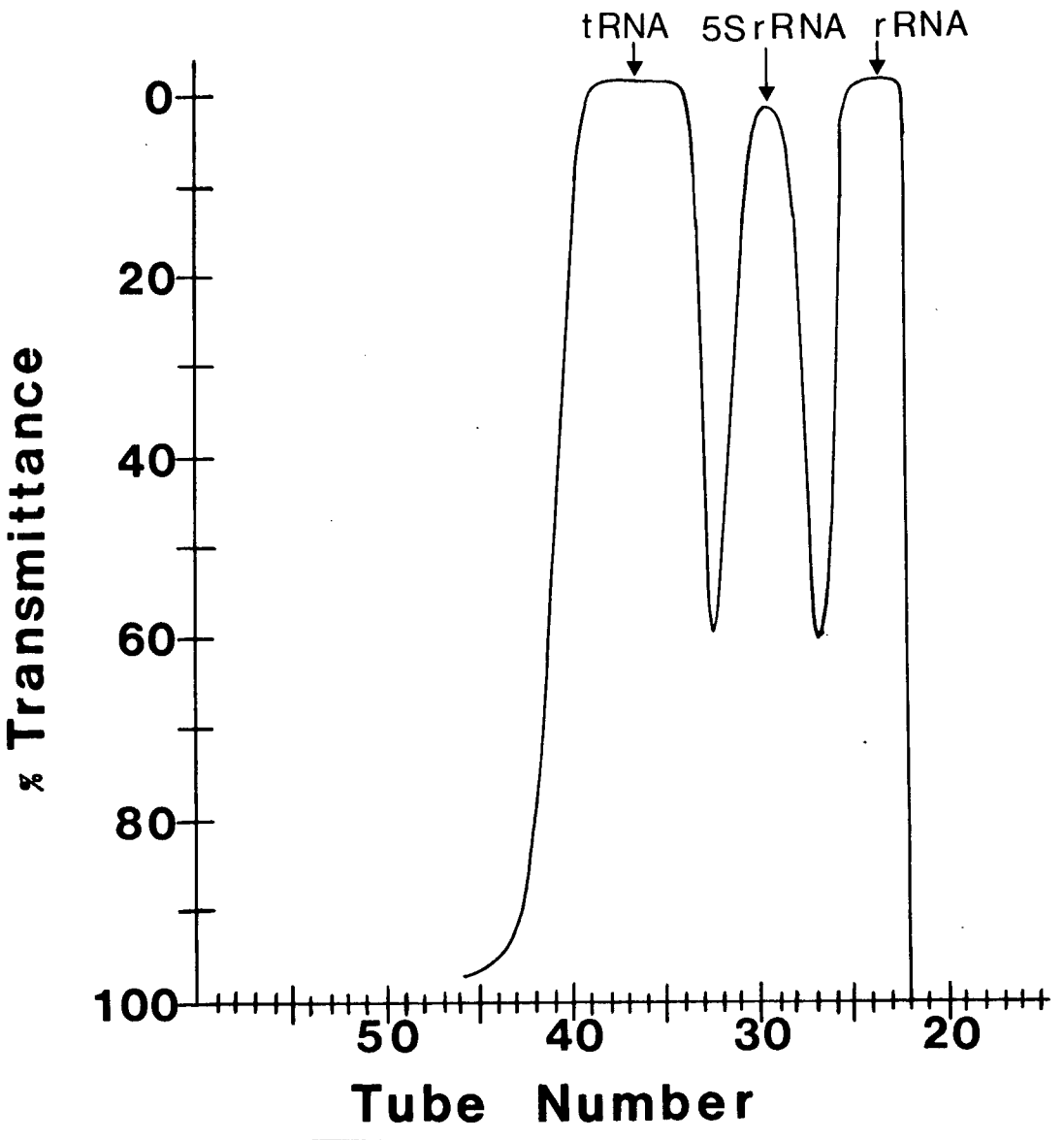

Figure 2.3. The elution profile for sRNA from approximately 25 grams of E. coli B cells. Separation is on a Sephadex G-75 column (2 x 180 centimeters). The intermediate peak, corresponding to 5SrRNA, was collected and precipitated with 95% ethanol pre-cooled to -20° C as described in the text.

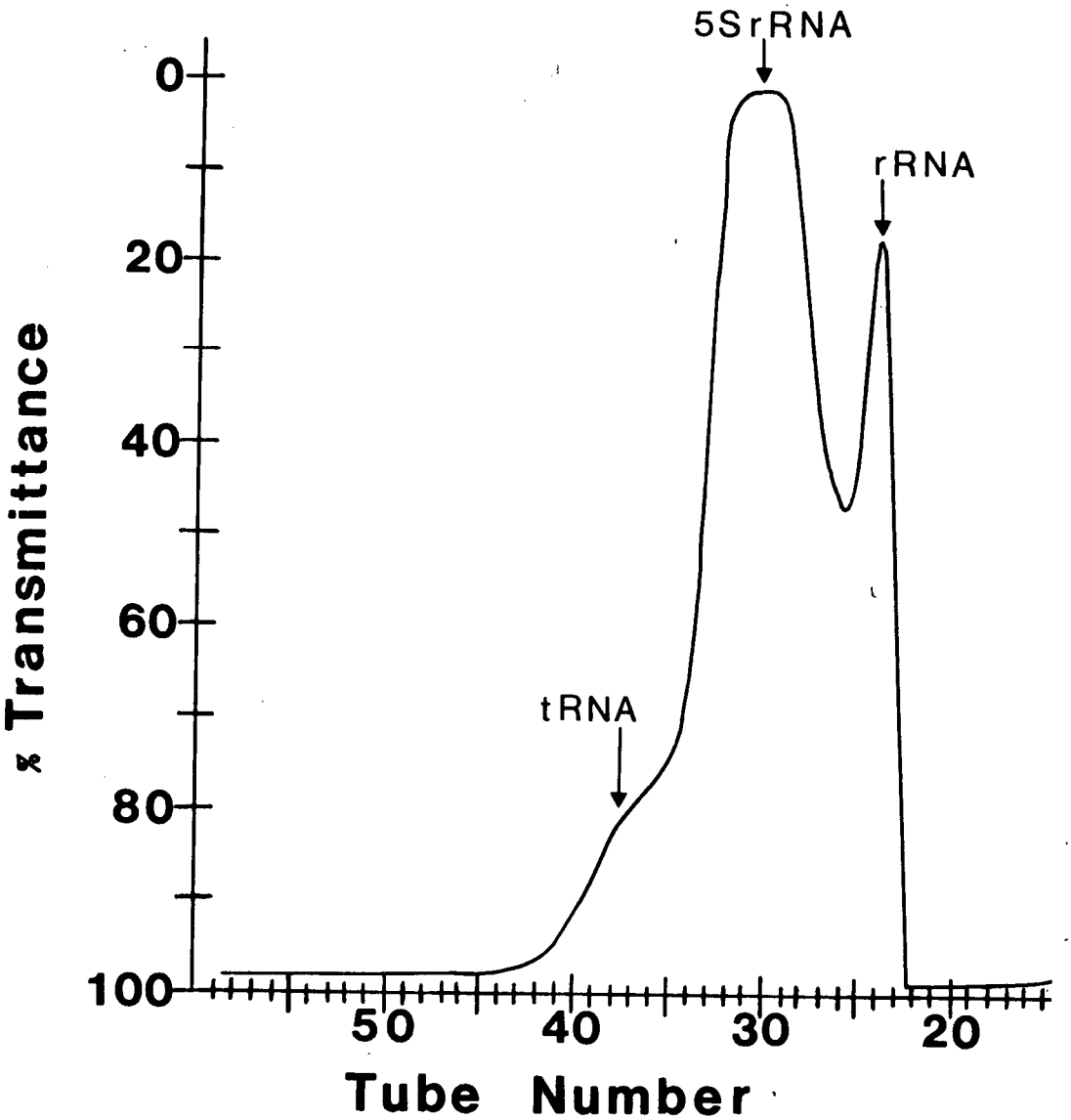

Figure 2.4. An elution profile of the 5SrRNA component obtained from Figure 2.3. After this second pass over the column the sample was judged homogeneous according to Sephadex G-75 chromatography (see Figure 2.5).

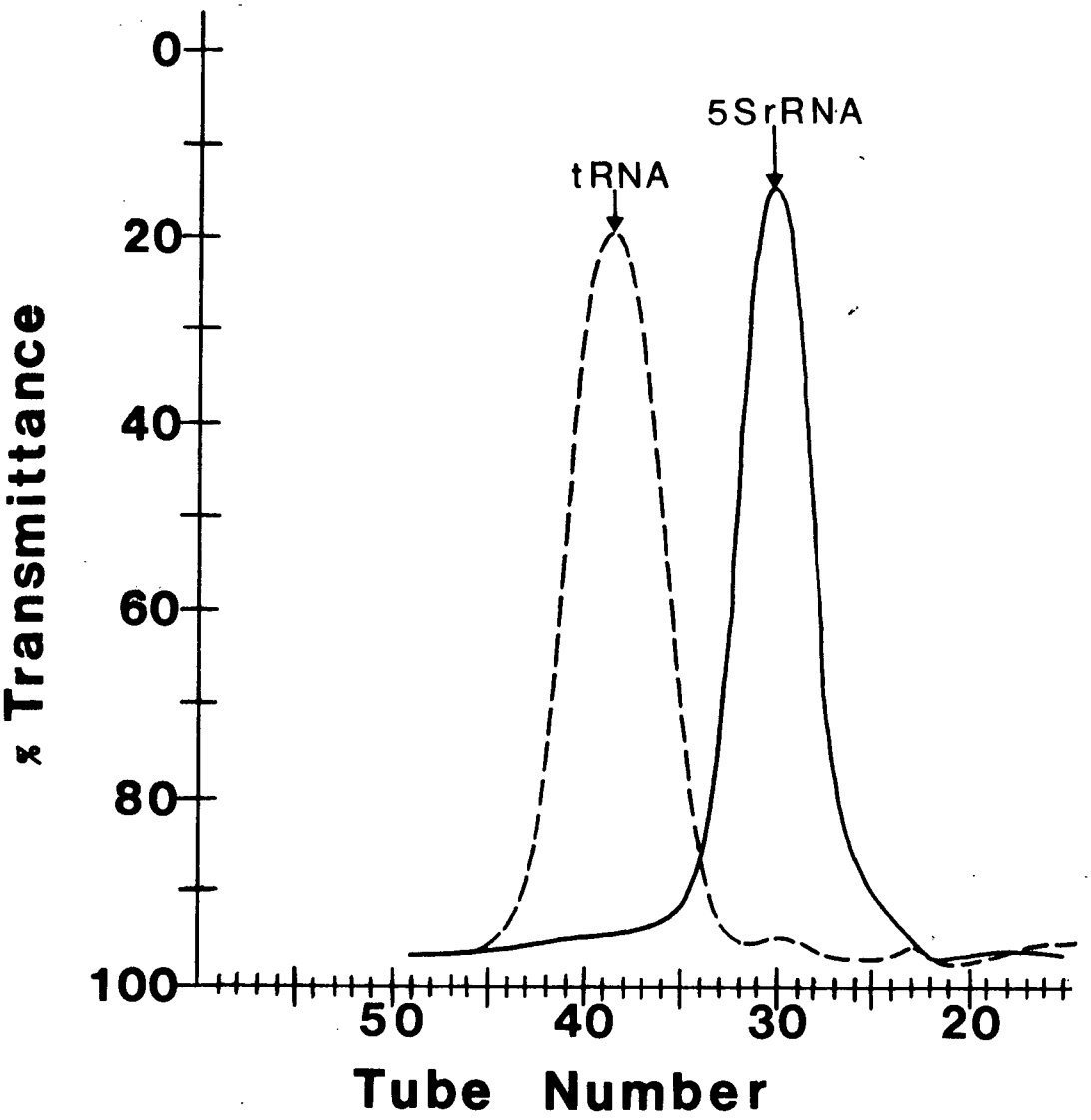

Figure 2.5. A demonstration of 5SrRNA homogeneity according to Sephadex G-75 chromatography. The solid lined profile represents a 5SrRNA sample. The dotted line represents a tRNA sample which was run independently. These profiles were both obtained on the same column used in Figures 2.3 and 2.4.

Step V. Desalting and Lyophilization of 5SrRNA

The 5SrRNA pellet from step IV was dissolved in a minimal amount of deionized water and applied to a Sephadex G-25 column (4). The eluent was monitored with the LKB Uvicord II and fractions absorbing at 260 millimicrons were collected. The eluent was poured into a lyophilization flask and frozen by immersing the spinning flask in an N-propanol-dry ice bath. After the solution was frozen the flask was attached to a Virtus Unitrap II lyophilization apparatus. The resulting pure freeze-dried 5SrRNA was weighed and stored at -20 degrees centigrade.

2.4 Separation of Normal 5SrRNA from FU-5SrRNA

The 5SrRNA isolated from E. coli B cells grown in the presence of 5-FU consisted of a mixture of normal unfluorinated 5SrRNA and FU-5SrRNA. Ivan Kaiser has shown that both unfluorinated native tRNA and 5SrRNA can be separated from the 5-FU containing molecules by DEAE-cellulose chromatography (5-6). A reduction of the pK_a for 5-FU (8.15 compared to 9.45 for normal uracil) means that at a buffer pH of 8.9 most of the 5-FU bases in 5-FU containing RNA will be deprotonated at the N-3 position of the 5-FU base. This provides a greater affinity of the FU-RNA for the DEAE-cellulose column. Therefore, when a mixture of normal 5SrRNA and FU-5SrRNA is eluted with an upwardly concave salt gradient of increasing sodium chloride concentration the FU-5SrRNA is more strongly retained on the column and elutes after the normal 5SrRNA. The resulting enriched FU-5SrRNA has been shown to exhibit about 83% replacement of the U base by 5-FU (6).

Most FU-5SrRNA enrichment experiments were performed with a 0.9 x 40 centimeter Whatman DE 32 column according to the procedure of Kaiser (6). The DEAE-cellulose was precycled as prescribed by the manufacturer (7). After the precycled material was poured into the column it was generally washed with 3 volumes of high salt buffer (pH 8.9). The high salt buffer contained 0.02 molar tris (pH 8.9), 0.01 molar magnesium chloride and 1 molar sodium chloride. Then it was equilibrated with 3

volumes of 0.02 molar tris buffer (pH 8.9) containing 0.3 molar sodium chloride and 0.01 molar magnesium chloride (low salt buffer). The 5SrRNA sample, dissolved in low salt buffer, was applied to the column and allowed to wash in with a small amount of the same buffer. The maximum amount of 5SrRNA that could be applied to the column was about 200 A_{260} units.

A schematic diagram of the gradient maker used for most enrichment experiments is shown in Figure 2.6. The diameter of the mixing reservoir was 5.7 centimeters while the smaller reservoir had a diameter of 3.0 centimeters. To the mixing reservoir 235 milliliters of the low salt buffer (0.3 molar sodium chloride) mentioned above and a stir bar were added. The smaller reservoir was filled with about 70 milliliters of the same buffer containing 0.7 molar sodium chloride. The two reservoirs were interconnected by means of polyethylene tubing inserted into their bases. The shape of the gradient was estimated according to the formula derived in Figure 2.6.

A Gilford microfractionator was used to collect the eluent and separation was monitored by measurement of the A_{260} either by an LKB Uvicord II connected to a Fisher Recordall Series 5000 recorder or as individual fractions on a Gilford 240 spectrometer. The A_{280}:A_{260} ratio was used as an indication of 5-FU enrichment since the FU-5SrRNA has an increased value for this ratio (approximately 0.55 as compared to 0.52) (6). A typical elution profile is shown in Figure 2.7.

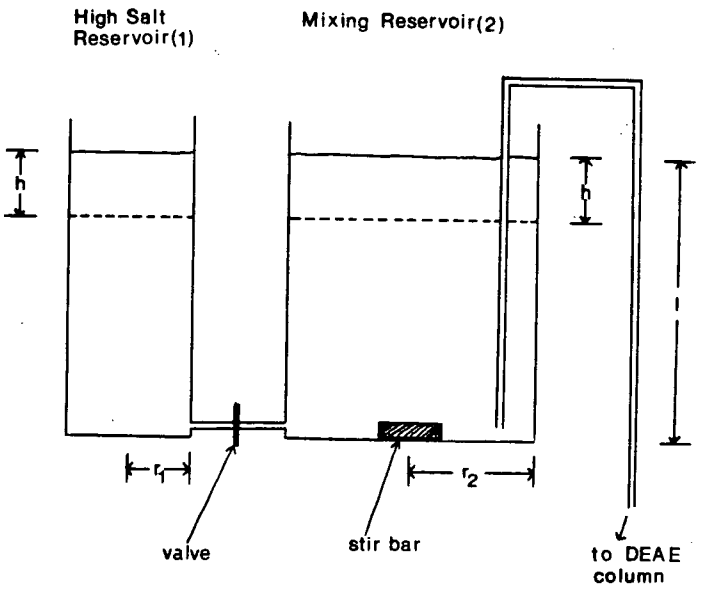

ℓ - the initial distance between the surface of the buffer solution and the bottom of the reservoir.
r_1 - radius of the high salt cyclindrical reservoir.
r_2 - radius of the cyclindrical mixing reservoir.
$C_1(i)$ - initial concentration of buffer in the high salt reservoir.
$C_2(i)$ - initial concentration of low salt buffer in the mixing reservoir.
V_{T2} - initial volume of low salt buffer in the mixing reservoir: $V_{T2} = \ell\Pi r_2^2$.
h - change in surface height of the buffer resulting from the flow of buffer in the high salt reservoir.
$V_1(h)$ - the volume of buffer in the high salt reservoir as a function of h: $V_1(h) = h\Pi r_1^2$.
$V_2(h)$ - the volume of buffer in the low salt reservoir as a function of h: $V_2(h) = h\Pi r_2^2$.

From the above parameters the salt concentration of the buffer in the mixing reservoir ($C_2(h)$) as a function of h is derived as follows:

$$C_2(h) = \frac{V_1(h)[C_1(i)] + [V_{T2} - V_2(h)][C_2(i)]}{[V_{T2} - V_2(h)]} \quad (1)$$

$$= \frac{V_1(h)}{[V_{T2} - V_2(h)]}[C_1(i)] + [C_2(i)] \quad (2)$$

Substituting the following equations into equation 2:

$$V_1(h) = h\Pi r_1^2 \quad (3)$$

$$V_2(h) = h\Pi r_2^2 \quad (4)$$

$$V_{T2} = \ell\Pi r_2^2 \quad (5)$$

one arrives at the final expression for $C_2(h)$. This is given by equation 6.

$$C_2(h) = \left[\frac{r_1}{r_2}\right]^2 \left[\frac{h}{\ell - h}\right][C_1(i)] + [C_2(i)] \quad (6)$$

Figure 2.6. A schematic side view of the cyclindrical reservoirs used to generate concave upward gradients of increasing salt concentration. Such gradients were used to separate N-5SrRNA from FU-5SrRNA on DEAE columns (see text). Also included is a derivation of the salt concentration of the mixing reservoir ($C_2(h)$) as a function of the change in surface height (h) which results from the flow of buffer to the DEAE column.

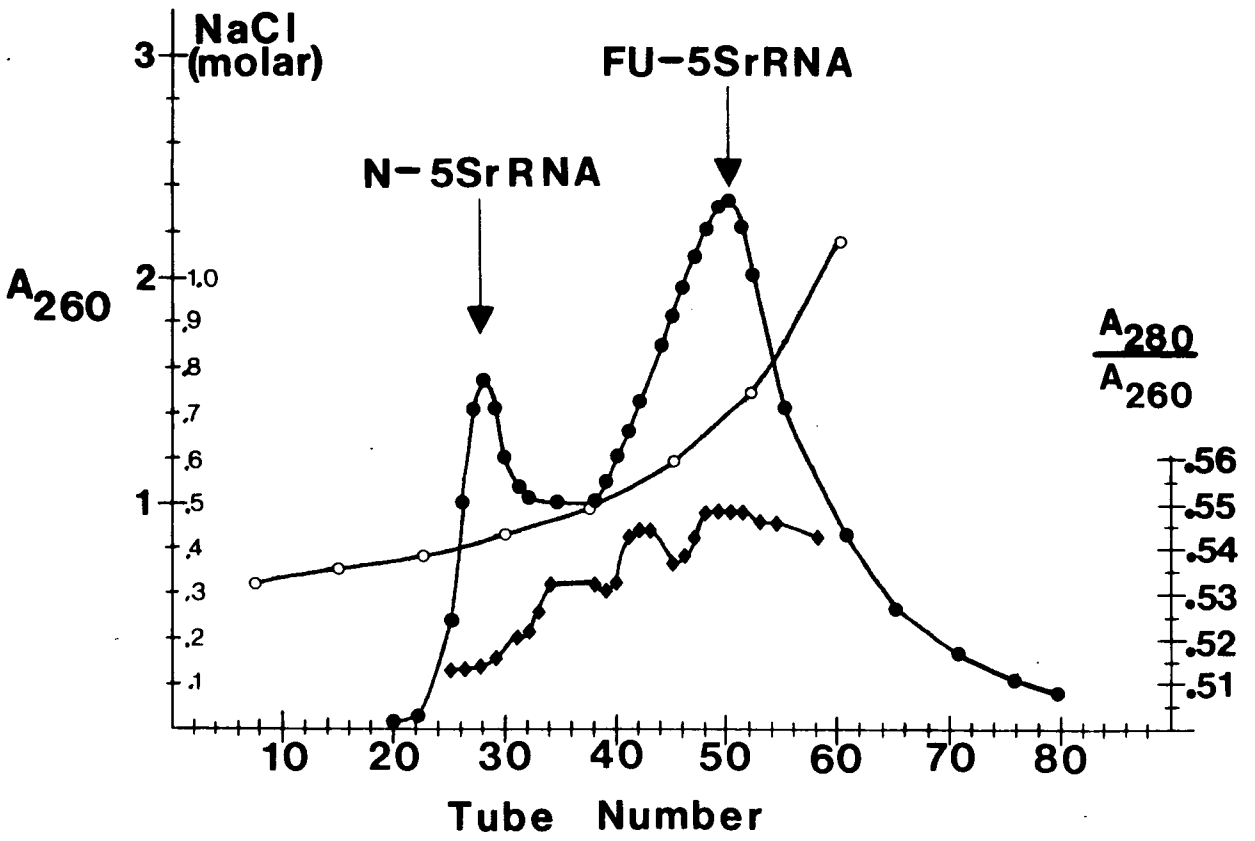

Figure 2.7. The separation of N-5SrRNA from FU-5SrRNA by DEAE-cellulose chromatography. The solid dots represent the elution profile of the RNA monitored by A_{260}. The solid diamonds indicate A_{280}:A_{260} ratios and the circles represent the estimated NaCl concentration calculated according to the equation shown in Figure 2.6. The column dimensions were 0.9 x 40 centimeters and the eluent per tube was about 3.4 milliliters.

The fraction corresponding to enriched FU-5SrRNA was precipitated with 95% ethanol cooled to -20 degrees centigrade after the addition of 0.1 volumes of 0.1 molar magnesium chloride. The precipitate was allowed to settle overnight at -20 degrees centigrade. Then after most of the solution was decanted it was centrifuged at 10,000 g for about 10 minutes. The enriched FU-5SrRNA pellet was then drained and dissolved in a minimal amount of deionized water. Desalting and freeze-drying of the sample was according to the procedure outlined in Step V of Section 2.3.

The purpose of this 5-fluorouracil enrichment procedure was to improve the ^{19}F-nmr signal to noise ratio by removing unfluorinated 5SrRNA. This reduced the acquisition time required to obtain FU-5SrRNA ^{19}F-nmr spectra. Both the broadness of the DEAE profile and the A_{280}/A_{260} ratios shown in Figure 2.7 suggest heterogeneity with respect to number of fluorouracils per molecule. However each of the fluorine resonances is really the sum of the fluorine label (or labels) from a specific region of each 5SrRNA molecule contained in the nmr sample tube. Incomplete fluorination of some of the FU-5SrRNA molecules will have some effect on the intensity but not the position or T_1 of resonances due to the absence of fluorine labels in specific molecules. Consequently heterogeneity with respect to 5-fluorouracil labeling in FU-5SrRNA should not affect the structural and conformational interpretation of the ^{19}F-nmr results.

2.5 Sample Purity by Polyacrylamide Gel Electrophoresis

The purity of 5SrRNA samples was periodically checked by polyacrylamide gel electrophoresis. A photograph of a sample gel is shown in Figure 2.8. As shown tRNA samples were run concurrently as standards to better discriminate the position of 5SrRNA. The band characterizing 5SrRNA is actually two closely positioned bands representing the A and B conformations of this RNA species (8). All samples indicated slight traces of tRNA contamination. The amount of contamination was smallest for samples obtained from the longer-narrower columns (2 x 190 centimeters instead of the 5 x 90 centimeters). The homogeneity of 5SrRNA from the longer columns was judged to be much greater than 95%. The electrophoresis procedure outlined below is divided into 4 steps (9).

Step I. Preparation of the Electrode Buffer

The electrode buffer consisted of 20 millimolar tris-acetate, pH 8.0, prepared with deionized water and containing 1 millimolar EDTA and 4 molar urea. Usually 1 liter of this buffer was sufficient for each experiment.

Step II. Preparation of Polyacrylamide Gel Slabs

First, 50 milliliters of acrylamide solution was prepared. This solution consisted of 10% acrylamide and 0.5% bisacrylamide prepared with the electrode buffer of step I. The solution was then mixed with 0.025 milliliters of N,N,N',N'-tetramethyethylene

diamine and 0.2 milliliters of freshly prepared 10% ammonium sulfate. This mixture was immediately placed in the slab making device and allowed to solidify. After solidification it was pre-run for about 3 hours with 20 milliamperes of current.

Step III. Preparation of RNA Samples for Electrophoresis

RNA samples were dissolved in a 20% sucrose solution prepared with the electrode buffer (step I) and containing 0.05% bromophenol blue. Usually a 1 milligram RNA per milliliter solution was prepared by mixing 0.1 milligrams of RNA with 0.1 milliliters of this solution. Then the solution was heated to 65 degrees centigrade for 1 minute. After pre-running of the polyacrylamide slab 10 microliters of this RNA solution was carefully applied to appropriate slots on the slab. Electrophoresis was carried out, at room temperature, for approximately 4 hours with a current of 15-20 milliamperes. The migration of the bromophenol blue dye to the end of the slab indicated completion.

Step IV. Preparation of the RNA Stain

The RNA staining solution consisted of 0.2% methylene blue in deionized water that contained 0.02 molar sodium acetate and 0.02 molar acetic acid. The gel slab was immersed for about 30 minutes in this solution and then washed overnight with cold tap water.

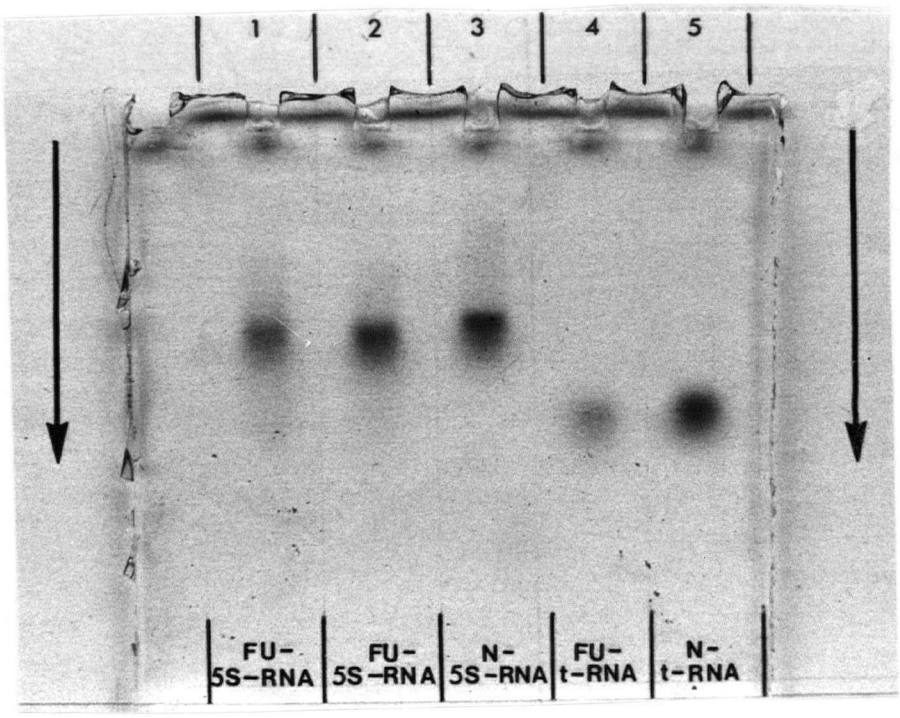

Figure 2.8. Sample purity was periodically checked by polyacrylamide gel electrophoresis. As indicated tRNA samples were run concurrently to better discriminate the position of 5SrRNA.

2.6 Verification of 5-FU Incorporation into E. coli RNA

The addition of 5-FU to media containing actively growing E. coli B cells caused cellular destruction and the cessation of cell division. This prompted concern about the extent of 5-FU incorporation into the bacteria's RNA. In order to determine whether 5-FU was being actively metabolized by the remaining E. coli B cells an experiment was devised using 5-FU labeled with carbon-14 at the 2-carbon position. Since small quantities of cells were employed the radioactivity in isolated tRNA was used to evaluate the degree of 5-FU incorporation.

One liter of sterilized media (see section 2.2) was inoculated with 10 milliliters of an E. coli B culture which had been growing overnight at room temperature on a shaker. After inoculation the flask was placed on a shaker, at ambient temperature, until turbidity measurements indicated early exponential growth ($A_{686} \simeq 0.3$). Then 25 milligrams of 5-FU was added. After about 5 minutes 20 microcuries of carbon-14 labeled 5-FU with a specific activity equal to 10.26 millicuries per millimole was added. The flask remained on the shaker for 3 hours. The cells were harvested by centrifugation (10,000 g for 10 minutes) and the yield was about one gram of cells (wet weight). The sRNA was isolated according to the procedure outlined in section 2.3, step II. The tRNA was separated from the rRNA on a small Sephadex G-100 column (about 0.5 x 40 centimeters). Fractions were collected with a Gilson microfractionator and the A_{260} was monitored on the Gilford 240 spectrometer.

Measurement of radioactivity was obtained on the departmental scintillation counter. Fractions of 1.5 milliliters each were collected on the microfractionator. Aliquots of 0.5 milliliters were accurately withdrawn from alternate fractions and placed in scintillation vials which contained 5 milliliters of Fisher Scintiverse scintillation fluid. Then the counts per minute for each vial was obtained on the scintillation counter. Previous to this experiment a standard curve was determined from samples of known disintegrations per minute (D.P.M.). This curve is shown in Figure 2.9. The D.P.M. for each sample was then determined from its counting efficiency obtained from Figure 2.9.

The Sephadex G-100 elution profile and corresponding D.P.M. measurements are recorded in Figure 2.10. The area under this curve, which corresponds to tRNA, represents 18.9 A_{260} units or 0.86 milligrams (3.44×10^{-5} millimoles) assuming that highly purified tRNA has an A_{260} of 7.45 per micromole phosphorus (or 22 A_{260} units per milligram tRNA) (10). The area underneath the radioactivity curve, associated with the tRNA elution profile, corresponds to about 93,108 D.P.M. or 4.19×10^{-8} curies. Given that the specific activity of the radioactively labeled 5-FU was 10.26 millicuries per millimole the radioactive 5-FU in 0.86 milligrams of tRNA (3.44×10^{-5} millimoles) was determined to be equal to 4.09×10^{-6} millimoles. Since 20 microcuries of labeled 5-FU (1.94×10^{-3} millimoles) and 25 milligrams of unlabeled 5-FU (0.2 millimoles) were added to the growing E. coli

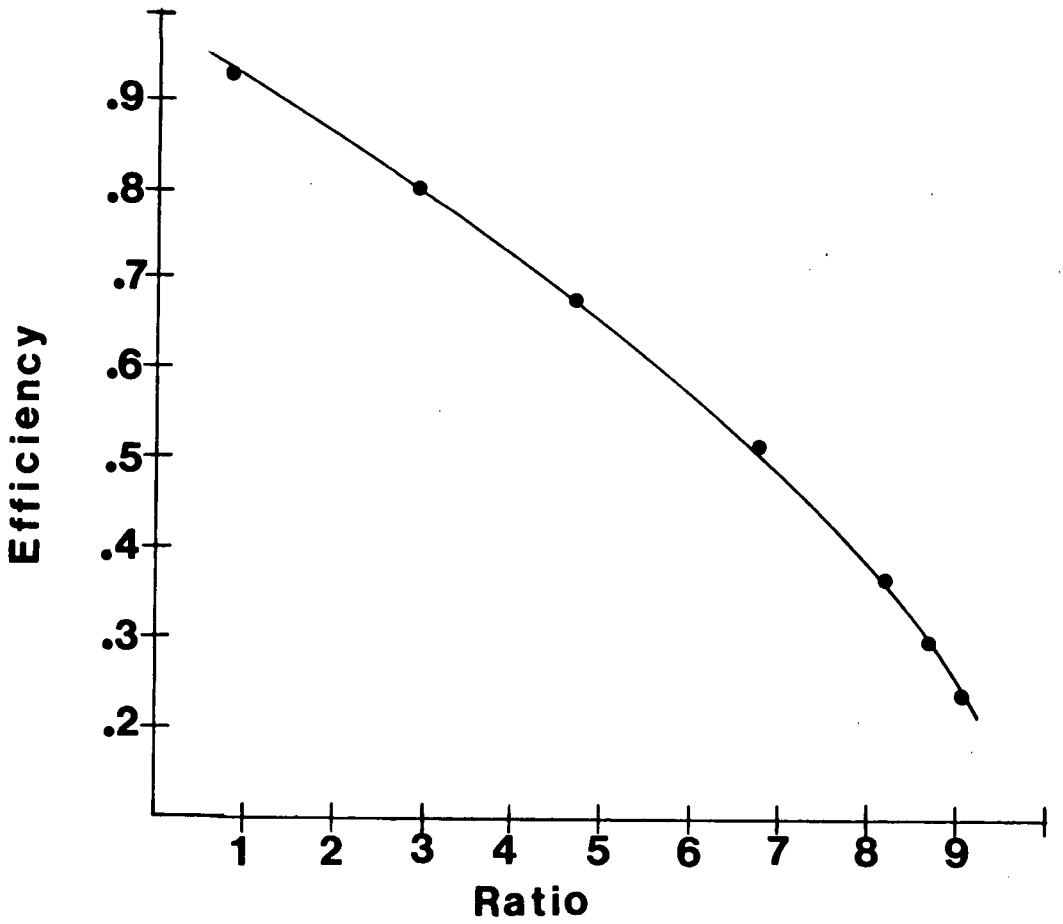

Figure 2.9. A calibration curve of counting efficiency versus channel-ratios for samples with known D.P.M. values. This curve was used to determine the D.P.M. values for unknowns by extrapolation of their counting efficiency from the channel-ratios of each sample using this curve.

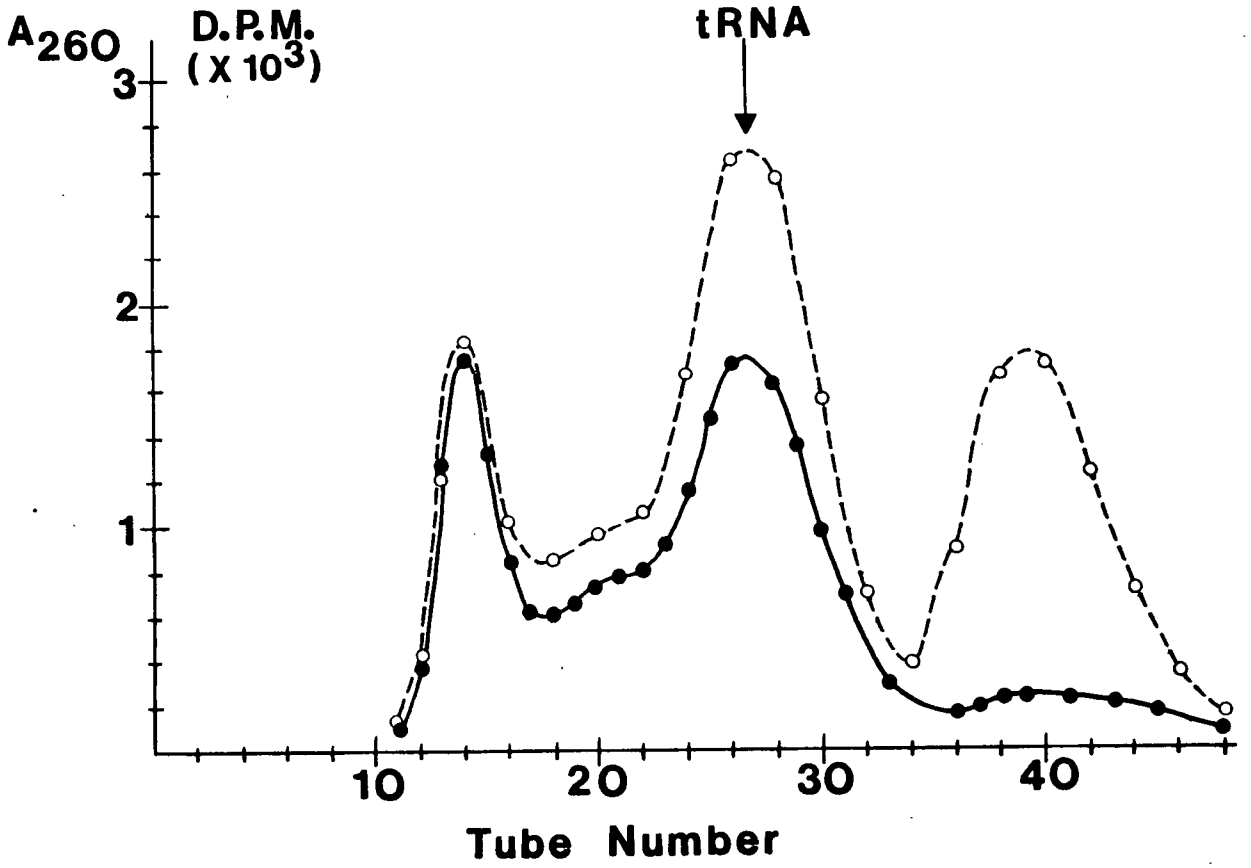

Figure 2.10. A Sephadex G-100 chromatography of sRNA which contains ^{14}C labeled 5-FU residues. The dimensions of the column were about 1.5 x 40 centimeters. The solid line connecting the solid dots indicates the A_{260} measurements of the eluent from individual fractions. Each tube contained 1.5 milliliters of eluent. For the radioactivity measurements (the dotted line connected by hollow circles) 0.5 milliliters of eluent were withdrawn from alternate fractions and placed in scintillation vials containing Fisher Scintiverse scintillation fluid. Channel-ratios for the samples were obtained on the departmental scintillation counter. Counting efficiencies were obtained from these ratios by extrapolation using Figure 2.9. From the efficiencies the D.P.M. values for the samples were computed.

B cells the ratio of labeled to unlabeled 5-FU was 102.6. Multiplication of this ratio by the number of millimoles of radioactive 5-FU (4.09×10^{-6} millimoles) gives the total number of millimoles of 5-FU in the 3.44×10^{-5} millimoles of tRNA. That is, there was 4.2×10^{-4} millimoles of 5-FU in 3.44×10^{-5} millimoles of tRNA. This corresponds to an average of approximately 12 5-FU residues per tRNA molecule.

The remaining fractions, corresponding to the tRNA in Figure 2.10, were pooled and 0.1 volumes of 0.1 molar magnesium chloride was added followed by 2.5 volumes of 95% ethanol precooled to -20 degrees centigrade. The precipitated tRNA consisted of a mixture of FU-tRNA and components containing little or no 5-FU. In order to improve ^{19}F-nmr signal to noise it was desirable to remove the unfluorinated components. An enrichment procedure of this type had been devised using DEAE-cellulose chromatography (see section 2.4).

Precycled Whatman DE 32 (microgranular) was poured into a 5 milliliter pipet which had a glass wool stopper at the bottom end. The column was washed with the buffer described in section 2.4 containing 1 molar sodium chloride. When the A_{260} reading was less than 0.05 it was equilibrated with 3 volumes of 0.325 molar sodium chloride in the same buffer. An apparatus similar to the one shown in Figure 2.6 was constructed to generate a concave upward sodium chloride gradient of increasing concentration. The mixing reservoir had a diameter of 1.8 centimeters. It was connected to a standard 10 milliliter graduated cyclinder

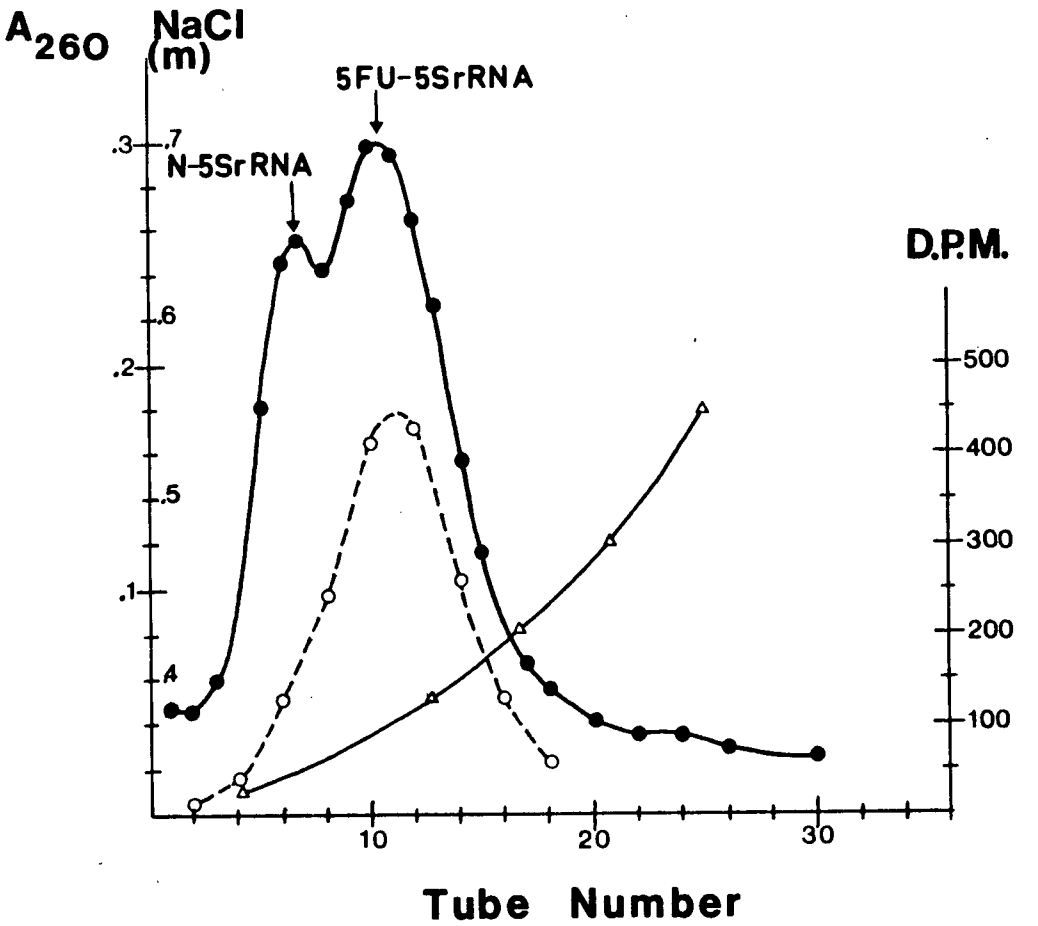

Figure 2.11. A DEAE-cellulose salt gradient of the tRNA fractionated in Figure 2.10. Each tube represents 1.5 milliliters of eluent. The line connecting the solid dots represents A_{260} values of the eluent while the dotted line connecting the hollow circles indicates the D.P.M. values for 0.5 milliliter aliquots. The estimated salt concentration is indicated by the line connecting the triangles.

(1 centimeter diameter) via a glass tube siphon. The mixing reservoir was filled with approximately 20 milliliters of the buffer described in section 2.4 and containing 0.325 molar sodium chloride. About 10 milliliters of the same buffer containing 0.6 molar sodium chloride was added to the graduated cyclinder. A portion of the tRNA pellet obtained from the preceding experiment was dissolved in a minimal amount of the low salt buffer and washed onto the equilibrated DEAE-cellulose column. Separation of normal tRNA from FU-tRNA is evident from the elution profile and the corresponding D.P.M. measurements which are given in Figure 2.11. They were obtained as previously described for Figure 2.10.

Evaluation of the areas underneath the A_{260} and D.P.M. curves of Figure 2.11 indicate that the enrichment technique was successful. The total radioactivity corresponds to 15,354 D.P.M. or 6.92×10^{-6} millicuries. With a specific activity of 10.26 millicuries per millimole of radioactive 5-FU this corresponds to 6.74×10^{-7} millimoles of radioactivity in 0.11 milligrams (4.22×10^{-6} millimoles) of tRNA. The total 5-FU incorporation is then equal to 6.92×10^{-5} millimoles. This corresponds to about 16 5-FU molecules per tRNA molecule.

This experiment provided evidence that 5-FU incorporation into the bacterial tRNA was extensive (averaging about 12 5-FU per molecule of tRNA). It also demonstrated that enrichment of the FU-tRNA was effective in removing the non-fluorinated component and increasing the average number of 5-FU residues per molecule.

2.7 ^{19}F-FT nmr Spectroscopy of FU-5SrRNA

Feasibility was initially demonstrated with unfractionated FU-tRNA. Samples were prepared from E. coli B cells grown according to the procedure given in section 2.2. The FU-tRNA was isolated as outlined in section 2.3 except that the tRNA fraction instead of the 5SrRNA fraction was collected and precipitated following Sephadex G-100 chromatography (see Figure 2.3). The final lyophilized product from step V of section 2.3 was dissolved in deuterium oxide (D_2O) and re-lyophilized. This was repeated a second time with D_2O to yield unfractionated FU-tRNA having 15 A_{260} units per milligram per milliliter. The sample was then dissolved in a D_2O buffer of 0.01 molar sodium cacodylate, 0.002 molar EDTA (disodium salt) and adjusted to pH 7 with sodium deuteroxide. The final sample concentration was approximately 11 milligrams per milliliter. The FT ^{19}F-nmr spectra of FU-tRNA, at 16 degrees centigrade and 72 degrees centigrade, are shown in figure 2.12. They were obtained on the departmental Varian XL 100 FT nmr spectrometer equipped with a Varian 620 L computer. Magnetic field strength was stabilized using an internal D_2O lock. The acquisition time was 0.2 seconds, with a sensitivity enhancement time constant of 0.1 seconds and a total time of 1.5 seconds between successive 90 degree pulses.

The first FT ^{19}F-nmr spectra of FU-5SrRNA were obtained on the same spectrometer mentioned above. Samples were prepared

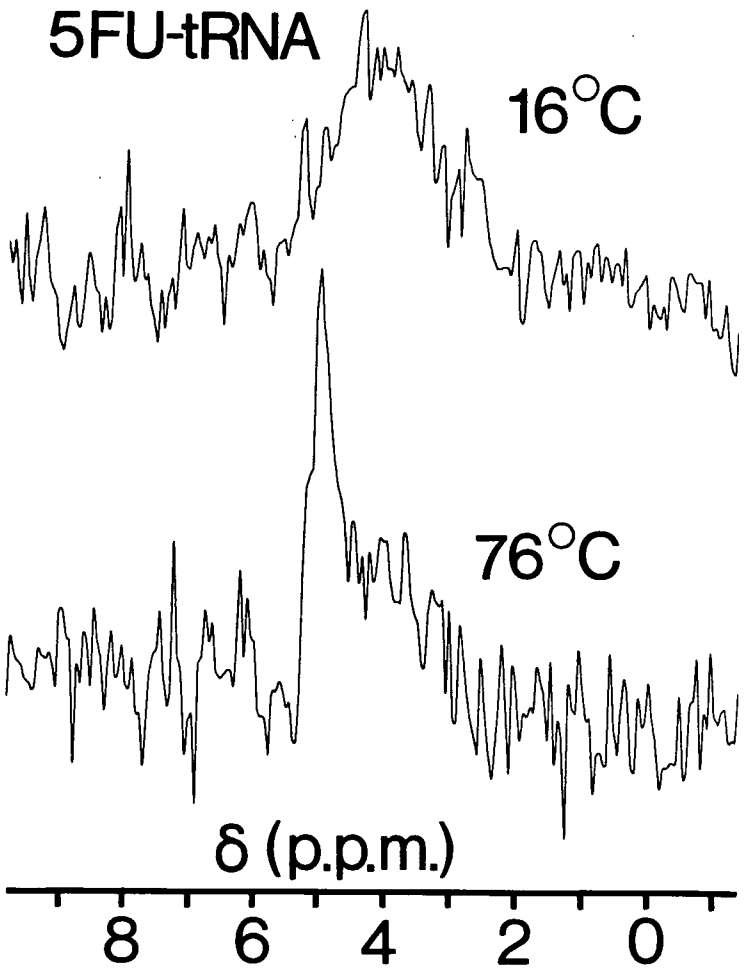

Figure 2.12. FT ^{19}F-nmr spectra of unfractionated native (16°C) and heat-denatured (76°C) 5-fluorouracil transfer-RNA. Total tRNA concentration is 0.627 O.D. (260 nm), or about 11 mg tRNA per ml, in a buffer of 0.01M cacodylate, 2mM EDTA (disodium salt), in D_2O with a pH meter reading of 7.55. Both spectra are plotted with 5 Hz/point, based on 4000 transients (16°C) or 1000 transients (76°C), with a sensitivity enhancement time constant of 0.1 sec. Chemical shift, δ, in parts per million, is referred to the chemical shift for free 5-fluorouracil at the same temperature in the same buffer. Heat denaturation of this sample was reversible.

from E. coli B cells grown according to the procedure given in section 2.1. Isolation and enrichment were according to the methods outlined in sections 2.3 and 2.4. The enriched FU-5SrRNA samples were lyophilized twice against D_2O and then dissolved in a D_2O buffer consisting of 0.02 molar sodium cacodylate (pH 7) containing 0.01 molar EDTA (dosodium salt) and 0.02 molar magnesium chloride. Sample concentration was obtained from A_{260} measurements where a 1 milligram per milliliter solution of FU-5SrRNA corresponded to 21 A_{260} units (11). The ^{19}F-nmr spectra of FU-5SrRNA, at 35 degrees centigrade and 72 degrees centigrade, are compared to monomeric 5-FU and 5-fluoro-deoxy-uridine monophosphate in Figure 2.13. When the sample at 72 degrees centigrade was returned to 35 degrees the spectrum was identical to the original 35 degree spectrum prior to heat denaturation. A spectrum was also obtained, at 35 degrees centigrade, for an FU-5SrRNA sample which contained no magnesium chloride. This is shown in Figure 2.14. The 35 degrees ^{19}F-nmr spectrum shown in Figure 2.13 is divided into 4 regions labeled a, b, c, and d. They are respectively centered about 6.6, 4.6, 3.6, and 2.1 p.p.m. relative to 5-FU. The entire chemical shift range that encompasses these 4 regions is about 8 p.p.m.. The spectrum of FU-5SrRNA in buffer containing no magnesium (Figure 2.14) indicates only two prominent peaks at 1.9 and 4.9 p.p.m..

A spin-lattice relaxation time (T_1), at 94.1 MHz, for the thermally denatured sample was obtained from the signal to

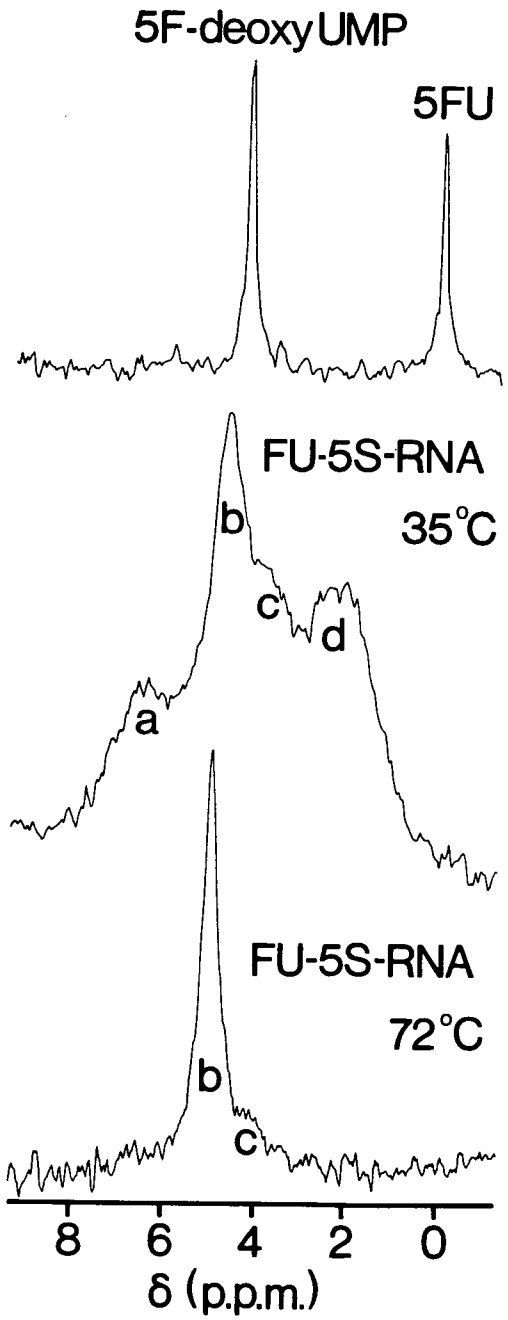

Figure 2.13. FT ^{19}F-nmr spectra of 5-fluorouracil (5-FU) in various molecules: (Top) Approximately equimolar mixture (each 0.0075 M) of FU and 5-fluoro-deoxy-UMP in 0.01 M Cacodylate D_2O buffer, pH 7. This sample was used to determine correct phase adjustment for this spectral range. (Middle) 3 x 10^{-4} M FU-5SrRNA at 35°C, 30,000 transients, 0.01 M Cacodylate buffer, pH meter reading 7.6 in D_2O. The four resolved groups of peaks are labeled from a to d. (Bottom) 3 x 10^{-4} M FU-5SrRNA at 72°C, 10,000 transients, 0.01 M Cacodylate buffer, pH meter reading 7.6 in D_2O. The dominant signal, labeled "b", corresponds to FU residues which are exposed to the external solution (see text). No proton decoupling was employed in any of the spectra. The buffer for the RNA sample also contained 20 millimolar magnesium chloride (13).

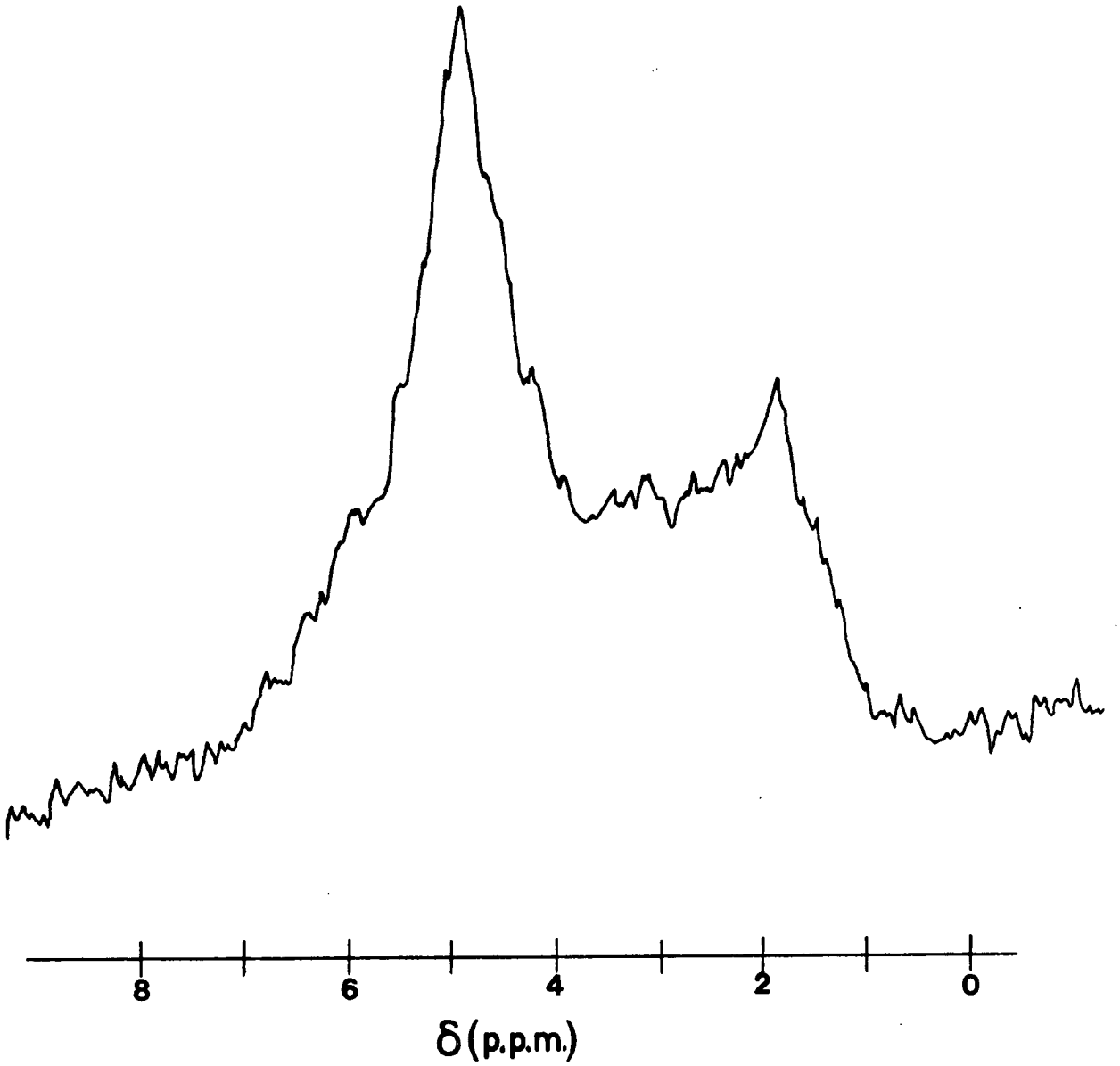

Figure 2.14. The FT ^{19}F-nmr spectrum of FU-5SrRNA in 0.02 molar sodium cacodylate D_2O buffer containing 0.01 molar EDTA. The absence of monovalent (Na^+) and divalent (Mg^{++}) has caused alterations in the spectrum. The spectral conditions are the same as those given in Figure 2.13.

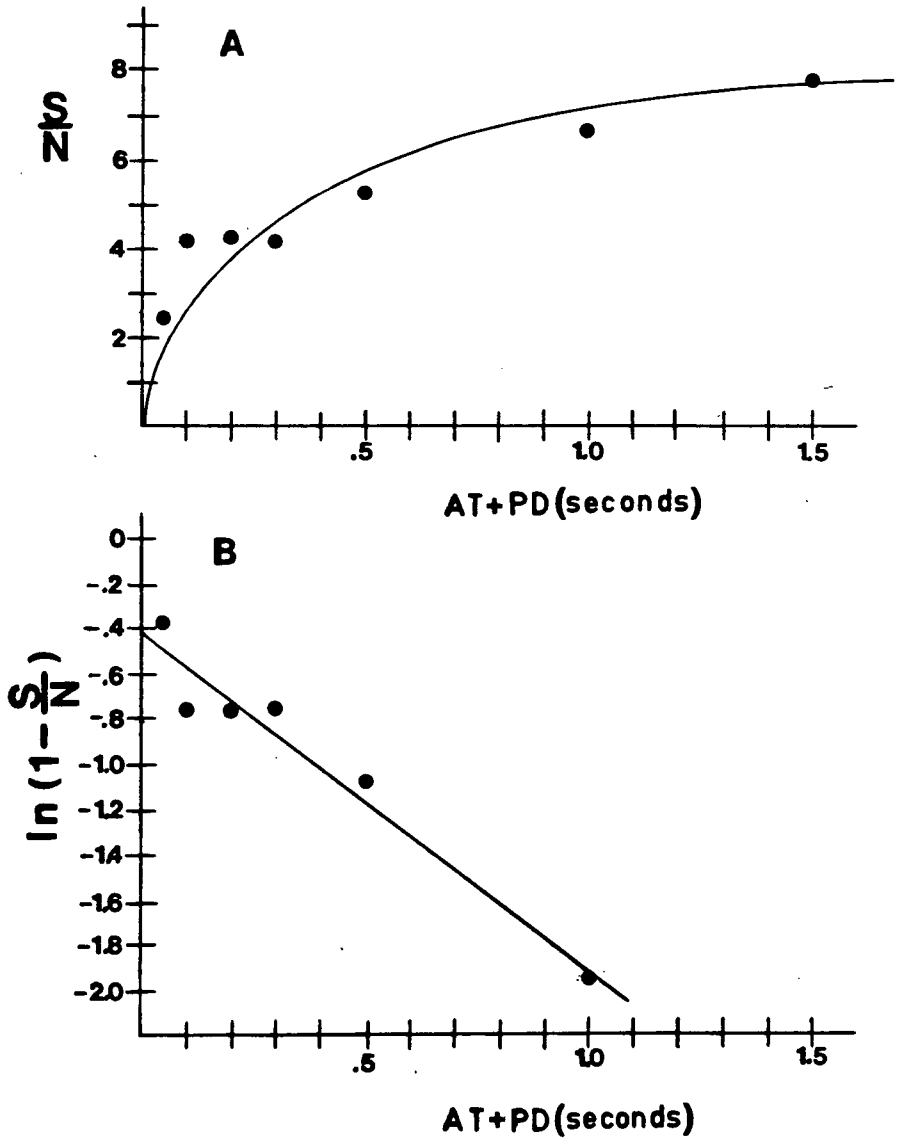

Figure 2.15. The T_1 determination of thermally denatured FU-5SrRNA (see Figure 2.13) employing a 90°, τ, 90° pulse technique. A constant number of transients (1000) were acquired for each data point. The reciprocal of the slope of B, equal to T_1, is 0.6 seconds with a standard deviation of about 12%. AT and PD are acquisition and pulse delay times respectively.

noise ratio of a constant number of transients (1000) at various pulse delays and acquisition times. The data is indicated by the two graphs shown in Figure 2.15. A linear regression of the data points in Figure 2.15(b) gives a best fit straight line with slope -1.51 and standard deviation of 0.17. The reciprocal of the slope, equal to T_1, is 0.6 seconds with a standard deviation of about 12%.

The ^{19}F-nmr spectra of FU-5SrRNA, at 254 MHz, were obtained on an HX270 Brüker FT nmr spectrometer at the University of Alberta Biochemistry Department in Edmonton. The assistance of Dr. Brian Sykes, whose earlier work on the fluorine labeled alkaline phosphatase enzyme led to formulation of this study (12-15), is greatly appreciated. The samples were prepared as above and dissolved in either a D_2O or an H_2O phosphate buffer (pH 7) that contained 0.01 molar phosphate, 0.01 molar magnesium chloride and 0.1 molar sodium chloride. The H_2O and D_2O spectra are shown in Figures 2.16 and 2.17 respectively. Also included in each of these figures is a spectrum in which a convolution difference technique has been employed to enhance the spectral resolution. The peak positions for the D_2O and H_2O spectra are tabulated in p.p.m. relative to 5-FU in Table 2.1. T_1 estimates of individual peaks were obtained from the graphs shown in Figure 2.18. This data was acquired from the signal to noise ratio of peak intensities obtained during a 180^{o}-τ-90^{o}-AT pulse sequence where τ was varied between 0.03 and 0.6 seconds. The T_1

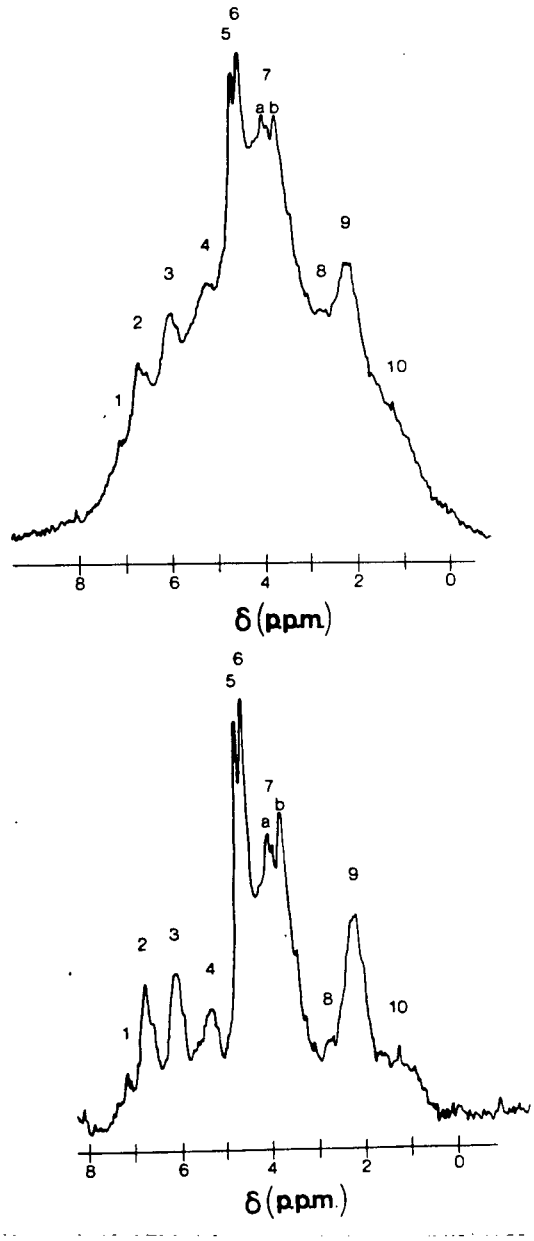

Figure 2.16. The FT ^{19}F-nmr spectrum of FU-5SrRNA in H_2O buffer (see text). This spectrum was obtained at 254 MHz on a Bruker WH-270 nmr spectrometer. The top spectrum was obtained from the Fourier transformation of the free induction decay accumulated from 38,000 time-domain transients (5 mm sample). Typical experimental parameters were: 8k time-domain data set, 5000 Hz spectral width, 0.5 sec relaxation delay, quadrature detection, 10 microsecond pulse width (approximately 90°), and signal to noise enhancement by exponential multiplication to give a line broadening of 5 hertz. The bottom spectrum is the convolution difference which improves the resolution of individual peaks.

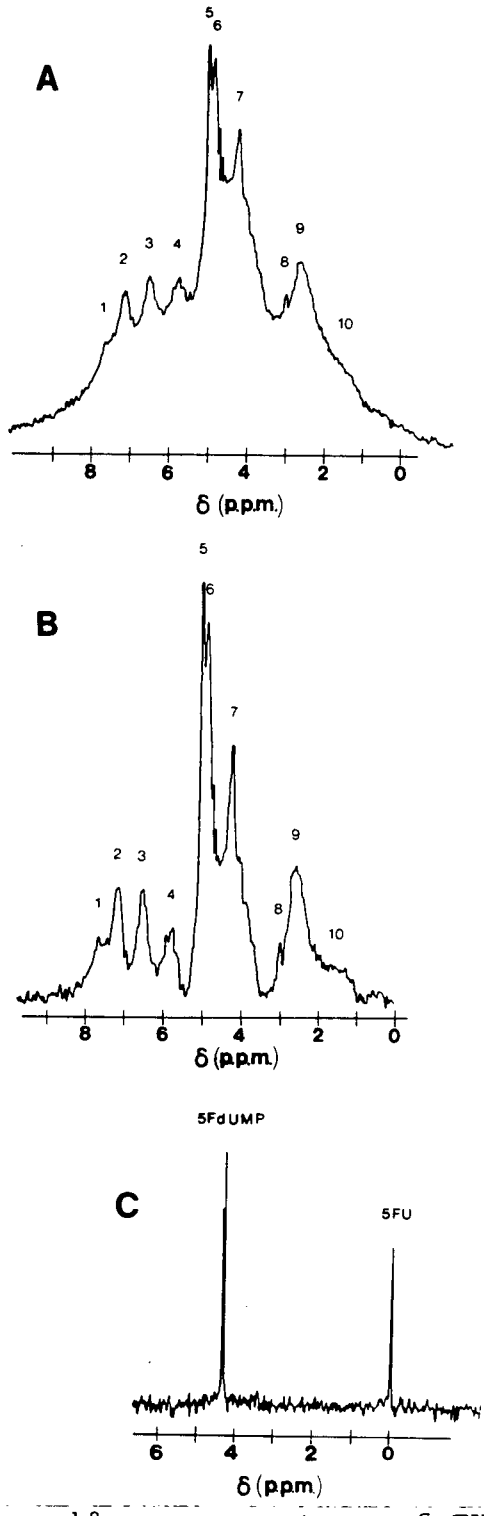

Figure 2.17. The FT ^{19}F-nmr spectrum of FU-5SrRNA in the D_2O buffer described in the text (A). The spectrometer and the spectral parameters are the same as indicated in Figure 1.16. A convolution difference technique was employed to improve the spectral resolution of the individual peaks (B). Spectrum C gives the relative positions of the 5-fluoro-2'-deoxyuridine monophosphate (5FdUMP) and 5-fluorouracil (5-FU).

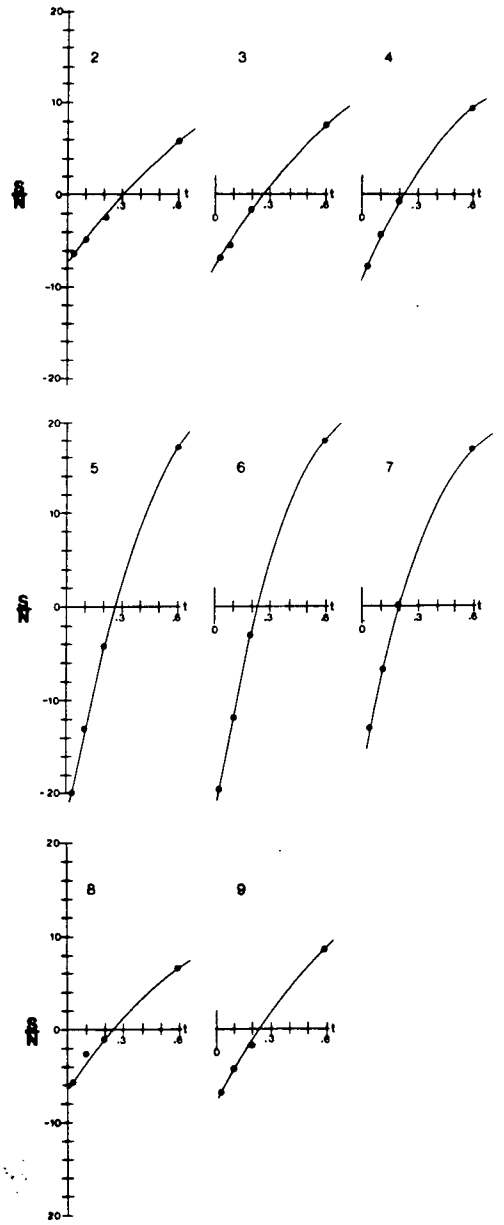

Figure 2.18. The T_1 determination of individual peaks of FU-5SrRNA (in D_2O buffer) at 254 MHz. A 180^0, τ, 90^0 pulse sequence was employed to collect 4 data points for each peak. In this figure signal-to-noise ratios (from 1000 transients) are plotted against time delay, t, in seconds. In order to determine T_1 values the data points were assumed to lie along an exponential.

Peak	D_2O p.p.m. from 5-FU	H_2O p.p.m. from 5-FU	Δ = p.p.m. (D_2O) - p.p.m. (H_2O)
1	7.64(?)	7.02(?)	0.62(?)
2	7.14	6.70	0.44
3	6.52	6.00	0.52
4	5.78	5.22	0.36
5	5.06	4.90	0.36
6	4.91	4.56	0.35
7	4.28	a) 4.00	a) 0.28
		b) 3.76	b) 0.52
8	3.00	2.7	0.3
9	2.64	2.20	0.44
10	1.56(?)	1.36(?)	0.4(?)

Table 2.3. The peak positions measured in p.p.m. relative to 5-FU for the H_2O and D_2O spectra of FU-5SrRNA obtained at 254 MHz. The 5-FU position in H_2O is shifted 0.2 p.p.m. downfield from the D_2O spectrum (14). This correction is included in the determination of the peak positions of the H_2O spectrum.

values were obtained from the x-intercept where $M_z = 0$ and $T_1 = \frac{t_0}{\ln 2}$. These values are given in Table 2.4.

The final experiment obtained on the Brüker HX270 involved a nuclear Overhauser enhancement study. This is shown in Figure 2.19. Broad band irradiation of the protons at 270 MHz reduces the peak intensity to zero except for a very slight amount of peak intensity as indicated.

The presence of monovalent cations stabilize the RNA structure by neutralizing the coulombic repulsion of the negatively charged phosphates. The result is a tighter and more efficient stacking of base pairs in helical regions. This is evident from

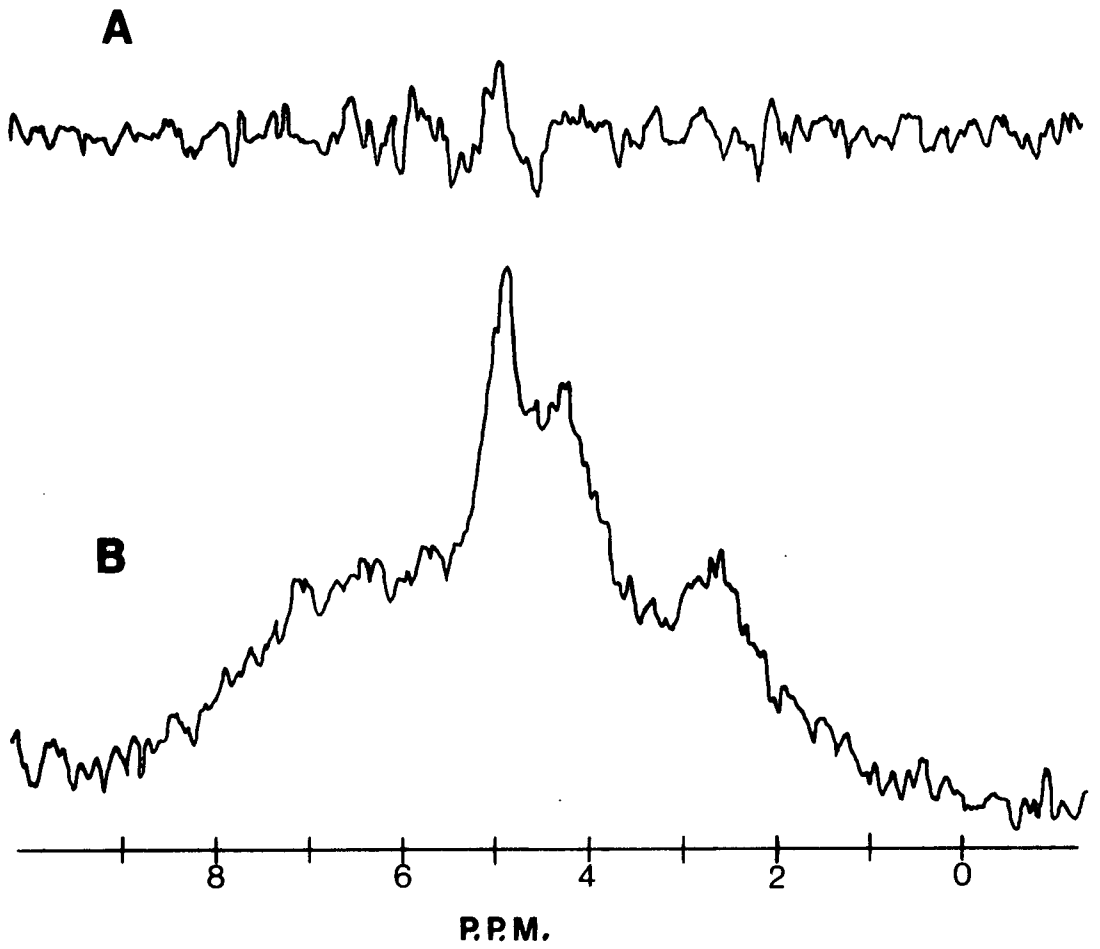

Figure 2.19. A nuclear Overhauser enhancement experiment of FU-5SrRNA (in D_2O buffer) at 254 MHz. The ^{19}F spectrum shown in A (from 1000 transients) was obtained immediately following broadband saturating irradiation of the corresponding ^{1}H-nmr spectrum. The decoupling oscillator was turned off during ^{19}F data acquisition. Spectrum B was obtained from 1000 transients for the same system, but in the absence of irradiation at the ^{1}H resonant frequencies.

	t_0	$T_1 = \frac{t_0}{\ln 2}$
2	0.3	0.43
3	0.27	0.40
4	0.23	0.33
5	0.27	0.39
6	0.23	0.33
7	0.20	0.29
8	0.24	0.35
9	0.24	0.35

Table 2.4. T_1 determinations for the individual peaks of the D_2O sample of FU-5SrRNA obtained at 254 MHz. T_1 values were estimated from t_0 values (x-intercept where $M_z=0$) of Figure 2.18.

a linear dependence of the transition temperature on the logarithm of the activity of the monovalent counterions (16). The divalent cation magnesium also appears to be important in stabilizing RNA structure. The 5SrRNA of E. coli has at least 4 strong magnesium binding sites (17). The 94 MHz spectrum of FU-5SrRNA was obtained in a buffer containing only the divalent cation magnesium (at a concentration of about 20 magnesium per FU-5SrRNA molecule). It is likely that the molecules in the 94 MHz sample exist in a somewhat less compact state than the FU-5SrRNA sample used for the 234 MHz study where 0.1 molar NaCl was also present. However, the overall rigidity of the molecule is not likely to be altered significantly since the sedimentation coefficient ($S_{20,w}$), obtained by ultra-centrifugation, is fairly insensitive to changing counterion concentration (18).

2.8 Laser Raman Spectroscopy of 5SrRNA and FU-5SrRNA

2.8.1 Introduction

Raman spectroscopy has been used extensively to interpret conformational properties of biological molecules. These interpretations are based largely on observed changes in the intensities of various Raman lines due to changing macromolecular conformation. The major purpose of the experiments shown in this section was to compare the conformations of normal 5SrRNA (N-5SrRNA) and FU-5SrRNA. The Raman spectra of an RNA molecule is the sum of the ring vibrations of the bases which compose it plus vibrational contributions from the ribophosphate backbone.

This section is divided into two parts. The first part (section 2.8.2) gives Raman spectra of aqueous solutions of uracil, 2-deoxyuridine, 2-deoxyuridine monophosphate, 5-FU, 5-fluoro-2-deoxyuridine, and 5-fluoro-2-deoxyuridine monophosphate. Spectra of polycrystalline uracil and polycrystalline 5-FU were also obtained. Comparison of all these spectra provided information about the effects of 5-fluoro- substitution upon the ring vibrations of the uracil base. Intensity changes due to 5-fluoro- substitution is a necessary consideration for the interpretation of the FU-5SrRNA spectra. In section 2.8.3 the Raman spectra of N-5SrRNA and FU-5SrRNA in aqueous buffer are given. Comparison of these spectra provided information about conformational differences and similarities between the two molecules.

2.8.2 Laser Raman spectra of 2-deoxyuridine 5-fluoro-2-deoxyuridine and related monomers

Aqueous (or D_2O) solutions of 50 millimolar 5-FU, 5-fluoro-2-deoxyuridine, 5-fluoro-2-deoxyuridine monophosphate, or 2-deoxyuridine were prepared with deionized water containing 50 millimolar sodium perchlorate. The sodium perchlorate was used as an internal frequency and intensity standard. The aqueous uracil sample was only 20 millimolar due to its lower solubility and contained no internal standard. The solutions were titrated to desired pH values with small aliquots of concentrated sodium hydroxide or concentrated hydrochloric acid. All pH measurements were obtained with a Radiometer pH meter 28, equipped with a Radiometer type GK 2322 C combined electrode. Raman samples were prepared by loading 20 microliter aliquots of solution at the desired pH into Kimax melting point capillary tubes (0.8-1.1 mm i.d.). For the polycrystalline spectra of uracil and 5-FU the powder was added to the same size capillary tubes.

Raman spectra of the above samples are presented in Figures 2.20 - 2.24. All spectra were obtained with a Spex Ramalog 4 laser Raman spectrometer system equipped with a Spectra-Physics Model 164 argon ion laser (5145 angstroms). Aqueous (and D_2O) samples were transversely illuminated with 600 milliwatts of laser power. A spectral slit width of 7-9 cm^{-1} with a scan speed of 0.2 wave numbers per second and a period of 10 seconds was employed for all solution spectra. The

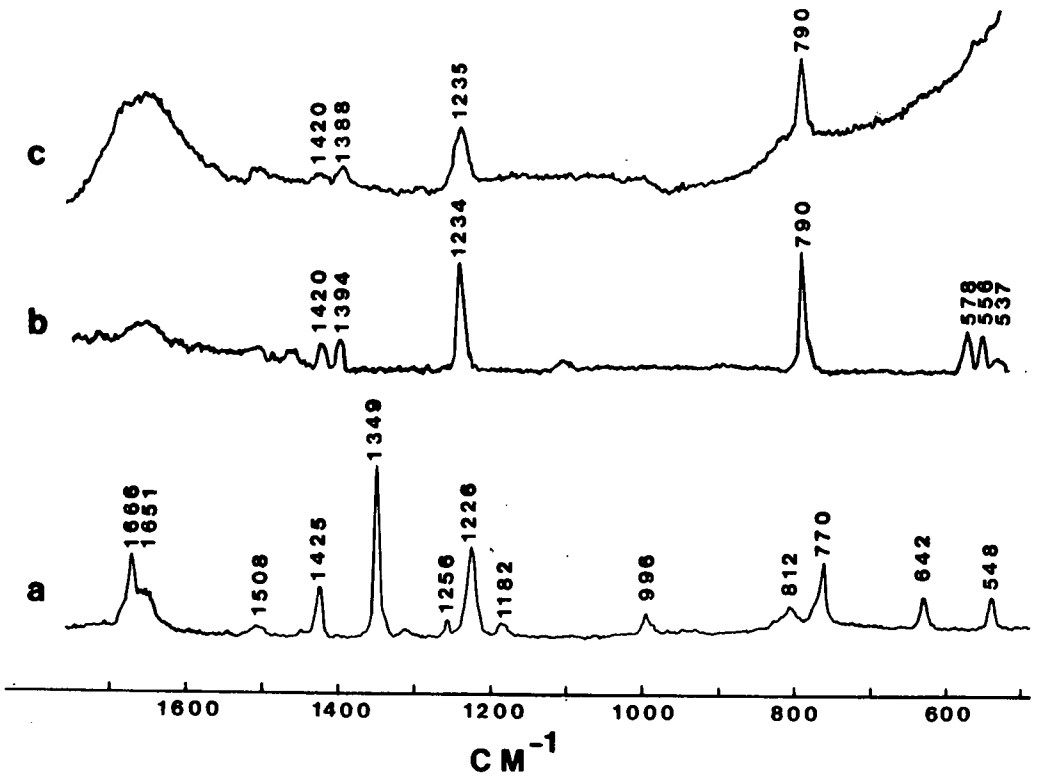

Figure 2.20. Laser Raman spectra of (a) polycrystalline 5FU , (b) polycrystalline U, and (c) 20 mM U (neutral form) in H_2O.

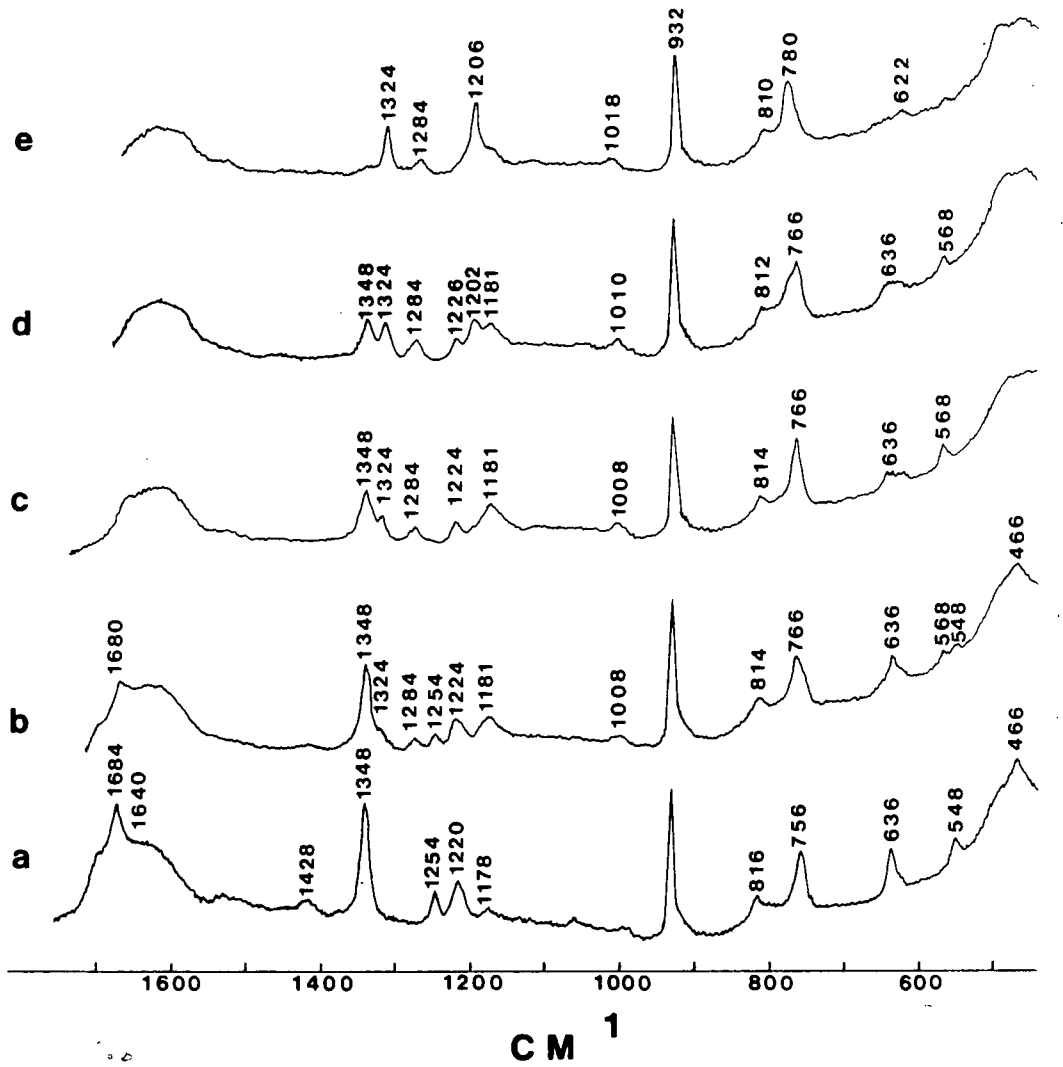

Figure 2.21. Laser Raman spectra of 50 mM 5FU with 50 mM $NaClO_4$ (932 cm^{-1} line) in H_2O at different pH.

(a) pH 4.8
(b) pH 8 (first ionization)
(c) pH 11.3
(d) pH 12.1
(e) pH 13 (second ionization)

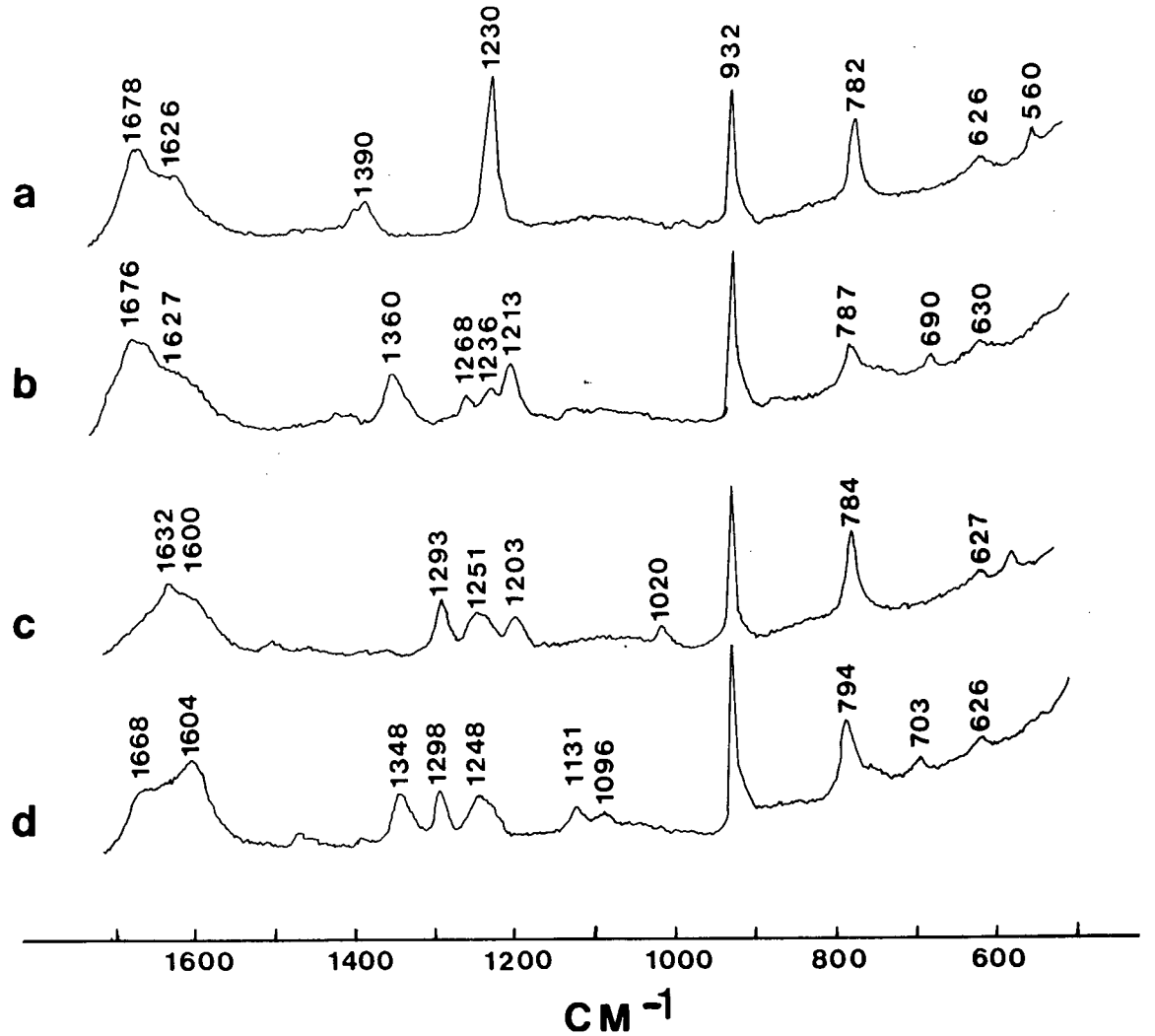

Figure 2.22. Laser Raman spectra of neutral and anionic forms of dUrd and 5FdUrd in H_2O containing 50 mM $NaClO_4$ (932 cm^{-1}).
(a) 50 mM dUrd, pH 5.6 (neutral form)
(b) 50 mM 5FdUrd, pH 4.8 (neutral form)
(c) 50 mM dUrd, pH 11 (anionic form)
(d) 50 mM 5FdUrd, pH 11 (anionic form)

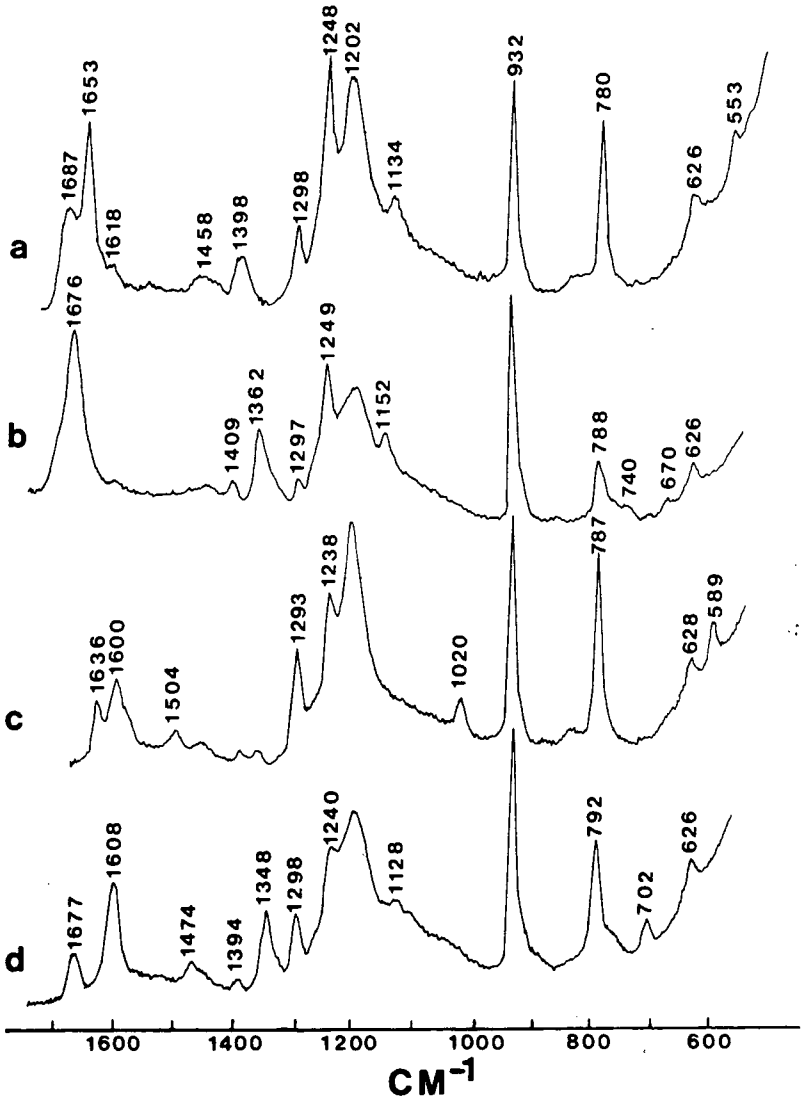

Figure 2.23. Laser Raman spectra of neutral and anionic forms of dUrd and 5FdUrd in D_2O containing 50 mM $NaClO_4$ (932 cm^{-1}).
(a) 50 mM dUrd, pH 6.2 (neutral form)
(b) 50 mM 5FdUrd, pH 5.8 (neutral form)
(c) 50 mM dUrd, pH 11.2 (anionic form)
(d) 50 mM 5FdUrd, pH 12.1 (anionic form)

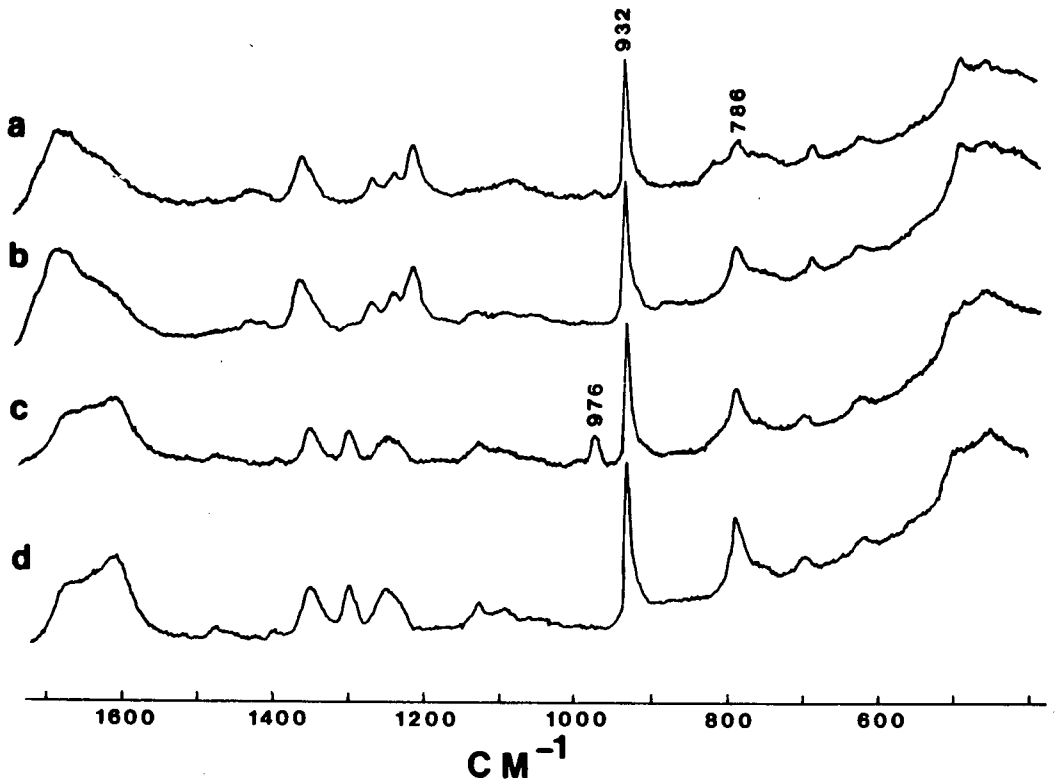

Figure 2.24. Laser Raman spectra of neutral and anionic forms of 5FdUrd and 5FdUMP in H_2O containing 50 mM $NaClO_4$ (932 cm^{-1}).
(a) 47.5 mM 5FdUMP, pH 6 (neutral form)
(b) 50 mM 5FdUrd, pH 5.6 (neutral form)
(c) 47.5 mM 5FdUMP, pH 11.6 (anionic form)
(d) 50 mM 5FdUrd, pH 11 (anionic form)

positions of all Raman lines (except aqueous U) were measured relative to the 932 wave number line of the sodium perchlorate internal standard. Spectra of polycrystalline uracil and 5-FU were obtained with 50 milliwatts laser power, spectral slit width of approximately 6 wave numbers, scan speed of 2 wave numbers per second, and a period of 2.5 seconds. Uncertainties of ± 2 wave numbers are assigned to sharp peaks. Interpretation of these spectra are given in Chapter 3.

2.8.3 Laser Raman spectra of normal 5SrRNA and FU-5SrRNA

The RNA samples were prepared from normal and 5-FU treated E. coli B cells according to the procedure outlined in section 2.3 using 2 x 190 centimeter Sephadex G-100 or G-75 columns. Samples from 5-FU treated cells were also subjected to the procedure given in section 2.4 to remove unfluorinated 5SrRNA. Dialysis of normal 5SrRNA samples was carried out two times against 2 millimolar magnesium chloride in deionized water, once against deionized water and then lyophilized. Dialysis of the FU-5SrRNA sample did not produce resolvable spectra. Hence Raman spectra of FU-5SrRNA were obtained without dialysis against magnesium.

Samples were prepared from freeze-dried normal or 5-FU containing 5SrRNA. The aqueous buffer consisted of 0.01 molar phosphate adjusted to pH 7, 0.1 molar sodium chloride, and 0.01 molar magnesium chloride. Between 0.5 milligrams and 0.7 milligrams of normal or 5-FU containing 5SrRNA was

dissolved in 10 microliters of this buffer. Using a 10 microliter hypodermic syringe samples were placed in Kimax capillary tubes (size 0.8-1.10 millimeter i.d.) and centrifuged at 10,000 g for about 10 minutes. Samples were then transversally illuminated with a Spectra-Physics Model 164 argon ion laser (5145 angstroms). Spectra were obtained with a Spex Ramalog 4 laser Raman spectrometer system using a spectral slit width of 0.5 wave numbers. A scan speed of 0.5 wave numbers per second with a period of 10 seconds and a gain of 1×10^4 pc counts per second was employed.

Raman spectra of the RNA samples are given in Figures 2.25 and 2.26. Figure 2.25 compares normal 5SrRNA before and after dialysis. In Figure 2.26 the Raman spectrum of normal 5SrRNA and FU-5SrRNA are compared. The intensities of the Raman lines of polynucleotides are generally normalized to the 1100 wave number line which is due to the symmetric stretching mode of the PO_2^- groups that compose the ribophosphate backbone of these molecules. This line is independent of conformation provided ionic strength is not drastically altered (19). Hence normalization of the other Raman lines to the 1100 wave number line provides a concentration independent measure of line intensities. In Table 2.3 the normalized intensities of the major lines shown in Figures 2.25 and 2.26 are given. The intensity values represent the average of at least 5 spectra and reproducibility of sharp well resolved lines were within 5%. The baseline for the 1100 wave number line was obtained

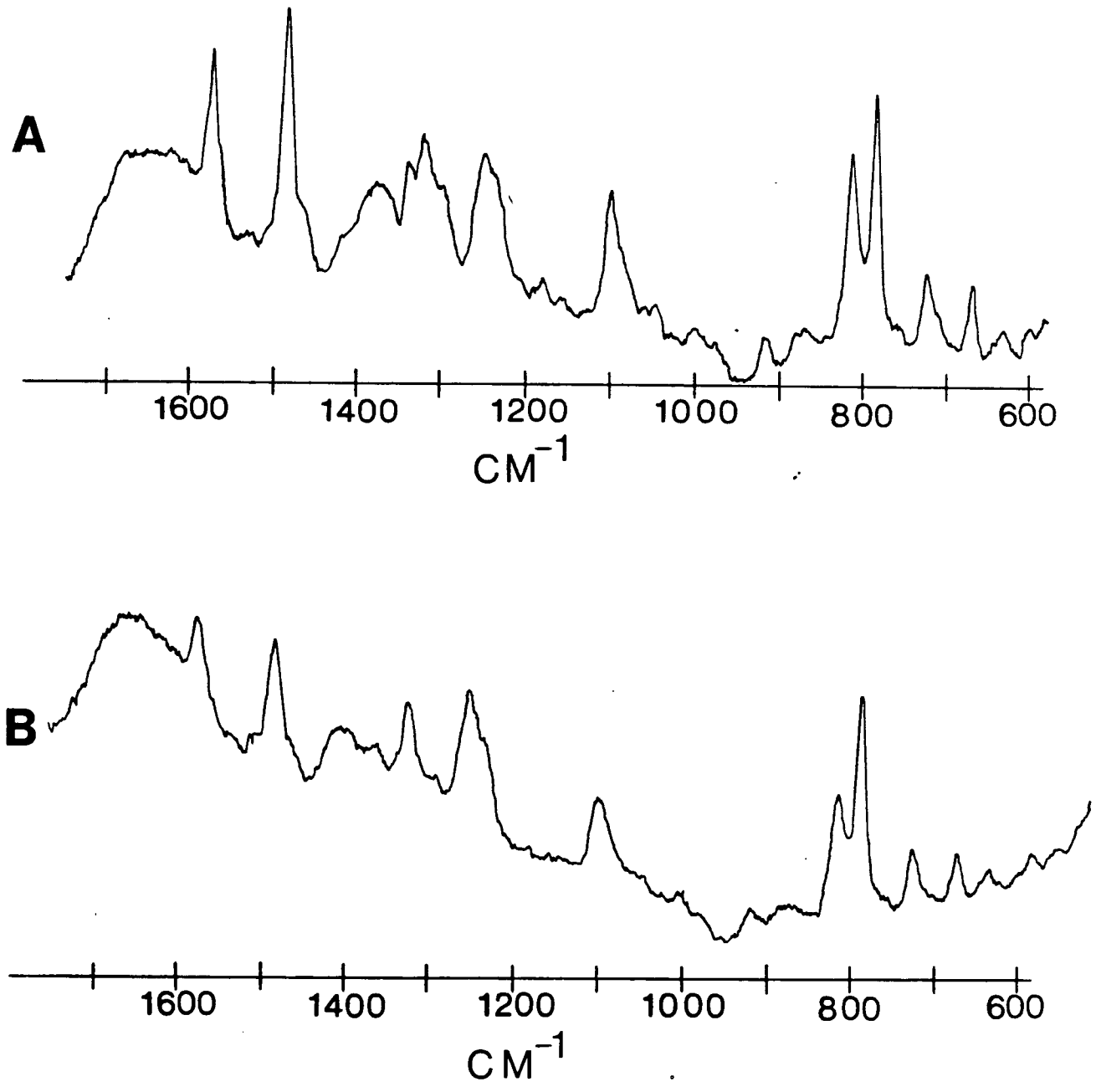

Figure 2.25. Raman spectra of aqueous samples of N-5SrRNA before (B) and after dialysis (A). Methods for sample and buffer preparation are outlined in section 2.8.3.

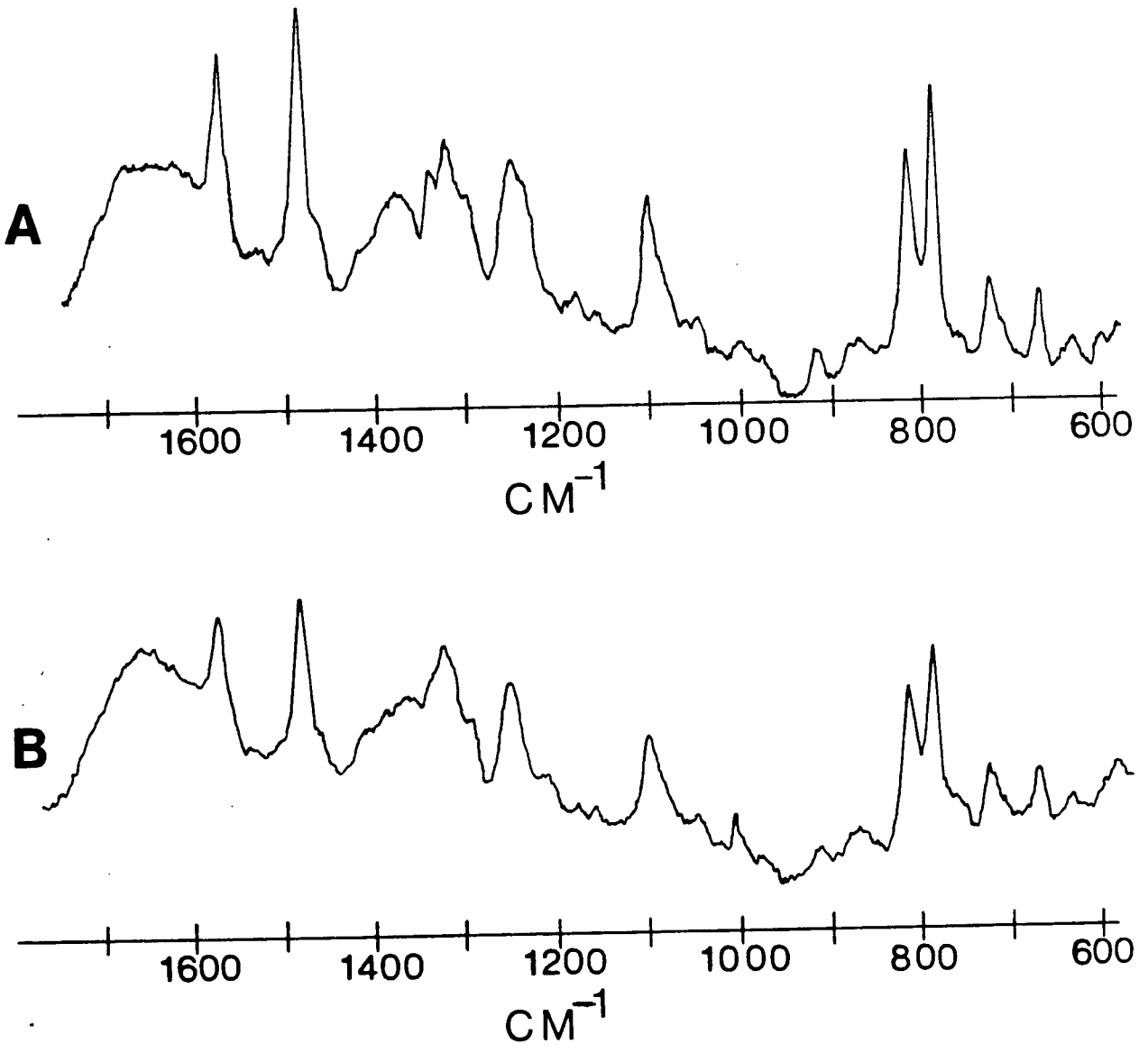

Figure 2.26. Raman spectra of aqueous samples of N-5SrRNA (A) after dialysis and FU-5SrRNA (B). Methods for sample and buffer preparation are outlined in section 2.8.3.

Frequency (cm^{-1})	Origin	N-5SrRNA (before dialysis)	N-5SrRNA (after dialysis)	FU-5SrRNA
670	G	0.59	0.66	0.70
725	A	0.80	0.65	0.74
785	C,U	2.96	2.21	2.10
814	-OPO-	1.65	1.65	1.73
1100	PO_2^-	1.00	1.00	1.00
1242	U,C,A	1.96	1.17	1.16
1300	A,C		0.85	0.55
1321	G	1.53	1.31	1.36
1338	A		1.04	1.10
1485	A,G	1.89	2.21	2.06
1575	A,G	2.04	1.94	2.03

Table 2.5. Line intensities of the spectra shown in Figures 2.25 and 2.26. All intensities have been normalized to the 1100 wave number line of the PO_2^- group.

by constructing a line between points at 1120 and 1060 wave numbers on the Raman spectrum. The baseline for the 814, 785, 725 and 670 wave number lines were made by joining the points at 840 and 650 wave numbers. Intensities of the Raman lines between 1210 and 1440 wave numbers were obtained by construction of a baseline between these two points on a Raman spectrum. Finally, for the lines at 1485 and 1575 wave numbers a baseline was constructed between the points at 1440 and 1800 wave numbers. The actual intensities of all these Raman lines were obtained by the construction of a vertical line from the peak maximum to its corresponding baseline and measuring the lengths of these lines to the nearest 0.1 centimeters.

REFERENCES: CHAPTER 2

1. M. Demerec and E. Cahn, J. Bacteriol. 65, 27 (1953).

2. T. Schleich and J. Goldstein, J. Mol. Biol. 15, 136 (1966).

3. In Sephadex, Gel Filtration in Theory and Practice, Appelbergs Boktryakeri, Uppsala, 1971; pages 31-49.

4. Reference 3; pages 24-26 and page 31.

5. I.I. Kaiser, Biochemistry 8, 231 (1969).

6. I.I. Kaiser, Biochemistry 9, 569 (1970).

7. In Whatman Laboratory Manual of Advanced Ion-Exchange Celluloses, Whatman Ltd., Maidstone; pages 8-9.

8. J. Hindley, J. Mol. Biol. 30, 125 (1967).

9. G.M. Rubin, J. Biol. Chem. 248, 3860 (1973).

10. In Graduate Laboratory Manual Department of Biochemistry Faculty of Medicine, U.B.C., page 77.

11. M. Litt, Bichem. Biophys. Res. Commun. 32, 506 (1968).

12. B.D. Sykes, H.I. Weingarten, and M.J. Schlesinger, Proc. Nat. Acad. Sci. USA 71, 469 (1974).

13. W.E. Hull and B.D. Sykes, J. Mol. Biol. 98, 121 (1975).

14. W.E. Hull and B.D. Sykes, Biochemistry 13, 3431 (1974).

15. W.E. Hull and B.D. Sykes, Biochemistry 15, 1535 (1976).

16. V.A. Bloomfield, D.M. Crothers, and I. Tinoco in Physical Chemistry of Nucleic Acids, Harper & Row, Publishers, New York, 1974; page 332.

17. B. Appel, V.A. Erdmann, J. Stulz and T. Ackerman, Nuc. Acid. Res. 7, 1043 (1979).

18. H. Boedtker and G. Kelling, Biochem. Biophys. Res. Comm. 29, 758 (1967).

19. M.C. Chen. R. Giege, R.C. Lord, and A. Rich, Biochemistry 17, 3134 (1978).

CHAPTER 3

FLUORINE NUCLEAR MAGNETIC RESONANCE SPECTROSCOPY OF E. COLI FU-5SrRNA

While unpaired electrons (usually artificial nitroxide) spin-labels have been used for more than 10 years as probes of macromolecular structure, the introduction of artificial nuclear spin-labels has so far been limited to ^{13}C enrichment of specific carbons in proteins (1-2) and nucleic acids (3-4), and to fluorine-labeling of a number of enzymes (5-7). This work represents the first ^{19}F-nmr study of a fluorine labeled nucleic acid, FU-5SrRNA.

The specific advantages of fluorine as a nuclear spin-label in RNA are manifold. First, of the four major bases only uracil is replaced by 5-FU. This means that only about 20 of the 120 bases in 5SrRNA contribute to the ^{19}F-nmr spectrum. Therefore greater simplification in spectral assignment and analysis is obtained. Second, the replacement of uracil by 5-FU does not significantly alter the function of 5SrRNA (as judged by binding to ribosomes) (8) or the tRNA (as judged by amino acid acceptor function (9), optical spectrum (9) or heat-denaturation profile (10)) from E. coli. Third, since ^{19}F-nmr chemical shifts are much more widely dispersed than proton shifts, one can expect to monitor relatively small changes in

the environments of various individual fluorouridylates simultaneously (5). Fourth, compared to ^{13}C (even when nonselectively (3) or selectively (4) enriched or ^{15}N or ^{31}P nmr from native tRNA (11-12), the fluorine label gives much stronger nmr signals. The spectra shown in Figure 2.13, at 94.1 MHz were obtained from about 10,000 to 30,000 transients for FU-5SrRNA concentrations of less than 3×10^{-4} molar, while comparable ^{13}C or ^{31}P spectra would require of the order of 1,000,000 transients using either much higher RNA concentration or much larger sample volume. Finally, the 5-FU label is cheaper than commercially available ^{13}C-enriched nucleic acid bases by a factor of about 1000.

The 94.1 MHz spectra of FU-5SrRNA, at 35 degrees centigrade and at 72 degrees centigrade, are presented in Figure 2.13 (13). Each of these spectra represents the superposition of the ^{19}F-nmr signals from about 20 labeled bases. Nevertheless, at least four distinct groups of peaks are resolved at 35 degrees centigrade, and the heat-denatured species (72 degrees centigrade) is sufficiently unfolded such that virtually all the fluorine nuclei have a common chemical shift (a sharp signal at about 5 p.p.m. downfield from free 5-FU), which implies a common chemical environment for most of the 5-FU residues in denatured FU-5SrRNA. Moreover, the denatured spectrum is centered near the resonant frequency of free 5F-deoxyuridine monophosphate, indicating that this chemical shift corresponds to an environment in which the fluorine-lable is exposed to

solution. Comparing the relative intensity of the FU-5SrRNA for the 35 and 72 degrees spectra, at this frequency, it is possible to estimate that approximately 25-35% of the 5-FU residues in the native FU-5SrRNA structure are exposed to solution. A 90^{o}, τ, 90^{o} pulse sequence method was employed to determine the spin-lattice relaxation time (T_1) for the heat denatured (72 degrees centigrade) spectra. The method is shown in Figure 2.15. From the data a T_1 of 0.6 seconds was obtained. Finally, the heat denaturation was reversible since the low temperature spectrum appeared to be identical before and after heating to 72 degrees centigrade.

Increased magnetic field strength improved the resolution of the four regions which were designated to the 94.1 MHz spectrum shown in Figure 2.13. At 254 MHz (Figure 2.16 and 2.17) the "a" region, which was only a pronounced shoulder at 94.1 MHz, consists of a slight shoulder and three well defined peaks. The "b" region, believed to be due to 5-FU residues exposed to the surface, appears as two closely spaced narrow peaks. The "c" region, a shoulder at 94.1 MHz, is a sharp well defined peak at 254 MHz. Finally, the "d" region appears as two peaks and a slight shoulder. Together the 254 MHz spectrum of FU-5SrRNA consists of eight well defined peaks and two shoulders; a marked improvement in resolution over the 94.1 MHz spectrum. The peak positions, in p.p.m. relative to 5-FU, are shown in Table 2.3 for samples prepared in H_2O and D_2O buffer.

In Table 2.1 the peak positions for FU-5SrRNA in D_2O and H_2O buffer are given. For the spectrum of FU-5SrRNA in D_2O buffer the chemical shifts are in p.p.m. relative to 5-FU in D_2O. In H_2O 5-FU is shifted downfield by about 0.2 p.p.m. (15). The chemical shift values of the H_2O sample of FU-5SrRNA are relative to this new zero position for 5-FU. The Δ term in Table 2.3 is the difference between these D_2O and H_2O chemical shifts. The smallest Δ values are an indication of the greatest solvent effect since the 0.2 p.p.m. correction for the H_2O sample will cancel out shifts of exposed 5-FU residues which experience the greatest solvent effect. Resonances 4, 5, 6, and 7a have the smallest Δ values; the region associated with the peak position of 5 fluoro-2'-deoxyuridine monophosphate.

Individual peaks were sufficiently resolved for an estimation of T_1 values. A 180°, τ, 90° pulse sequence method was employed where τ was the delay time following a 180° pulse (14). This pulse sequence is illustrated in Figure 3.1. The 180° pulse inverts the magnetization (M_z) along the Z' axis of a coordinate system which rotates at the Larmor precession frequency. During a time delay, τ, the inverted M_z component will decay by various relaxation processes in an effort to return to the equilibrium value (M_o). Relaxation of M_z is given by the familiar Bloch equation:

$$\frac{dM_z}{dt} = - \frac{M_z - M_o}{T_1} \qquad (1)$$

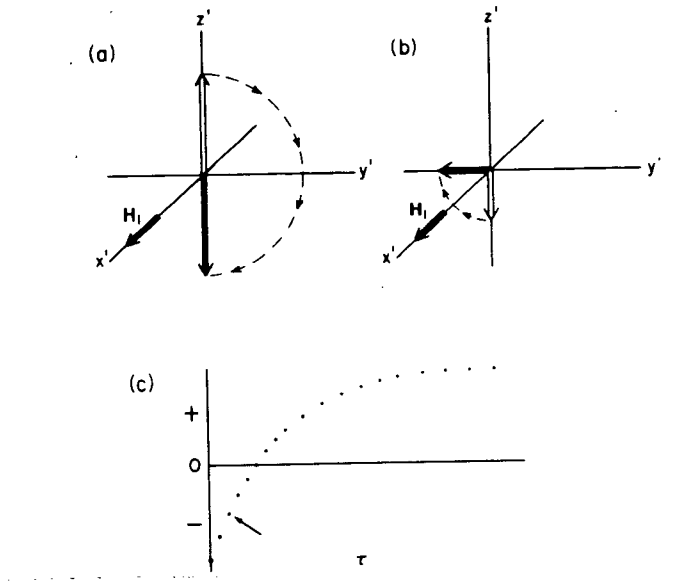

Figure 3.1. Determination of T_1 by 180^0, τ, 90^0 sequences. (a) M is inverted by a 180^0 pulse at time 0. (b) After a time τ a 90^0 pulse rotates M to the y' (or -y') axis. (c) The initial amplitude of the FID after the 90^0 pulse, which is proportional to the value of M at time τ, is plotted as a function of τ. Note that each point results from a separate 180^0, τ, 90^0 sequence. The point corresponding to (b) is indicated by the arrow (14).

Immediately after the pulse, at t=0, $M_z=-M_o$. Integration of equation (1) gives:

$$M_z = M_o(1-2e^{-t/T_1}) \qquad (2).$$

Equation (2) implies that a plot of peak intensity (signal to noise ratio) versus τ will increase exponentially from $-M_o$ with increasing τ for a 180^o, τ, 90^o pulse sequence. The point of intersection with the x-intercept, where $M_z=0$ and $t=t_o$ provides a ready estimation of T_1. This is given in equation (3):

$$T_1 = \frac{t_o}{\ln 2} = 1.4427t_o \qquad (3).$$

Plots of intensity versus τ of four different values of τ were presented in Figure 2.18 for peaks 2-9. It was assumed that the four data points for each peak lie along exponential curves and T_1 values were determined according to the method described above. Estimated T_1 values for peaks 2-9 are given in Table 3.1.

Peak	Estimated T_1 (seconds)
2	0.43
3	0.40
4	0.33
5	0.39
6	0.33
7	0.29
8	0.35
9	0.35

Table 3.1. The estimated T_1 values for the 254 MHz ^{19}F-nmr spectrum of FU-5SrRNA in D_2O buffer. A 180^o, τ, 90^o pulse sequence method was employed to obtain these results.

The most important T_1 relaxation mechanism for molecules in solution is due to magnetic interactions between fluorine and neighboring nuclei which have magnetic dipoles. In this study fluorine relaxation is expected to be largely due to neighboring protons. As the RNA molecule tumbles the local magnetic field of the protons located near fluorine nuclei generate time dependent fluctuations which interact with the fluorine's local magnetic field. Only fluctuations which are at the natural precession frequency of the fluroine nucleus will cause relaxation. This so-called dipole-dipole relaxation can be due to protons which are a part of the 5-FU moiety (intramolecular) or protons from other portions of nucleic acid which are proximal to the fluorine nucleus (inter molecular). If this relaxation is entirely intramolecular then about 95% will be caused by the nearest neighbor proton (15). There is a negative sixth power dependence of dipole-dipole relaxation on the distance between contributing nuclei. This will be shown shortly. Given the carbon-hydrogen bond length and bond angle for a typical vinylic proton the distance between the 6-carbon proton and the fluorine atom has been estimated from the X-ray crystal structure of 5-FU (16-17). This is shown to be 2.58 angstroms in Figure 3.2.

Hull et. al. (15) and Doddrell et. al. (19) have expressed dipole-dipole relaxation times of a spin i (^{19}F) relaxed by spins j (^{1}H) in terms of the following equations:

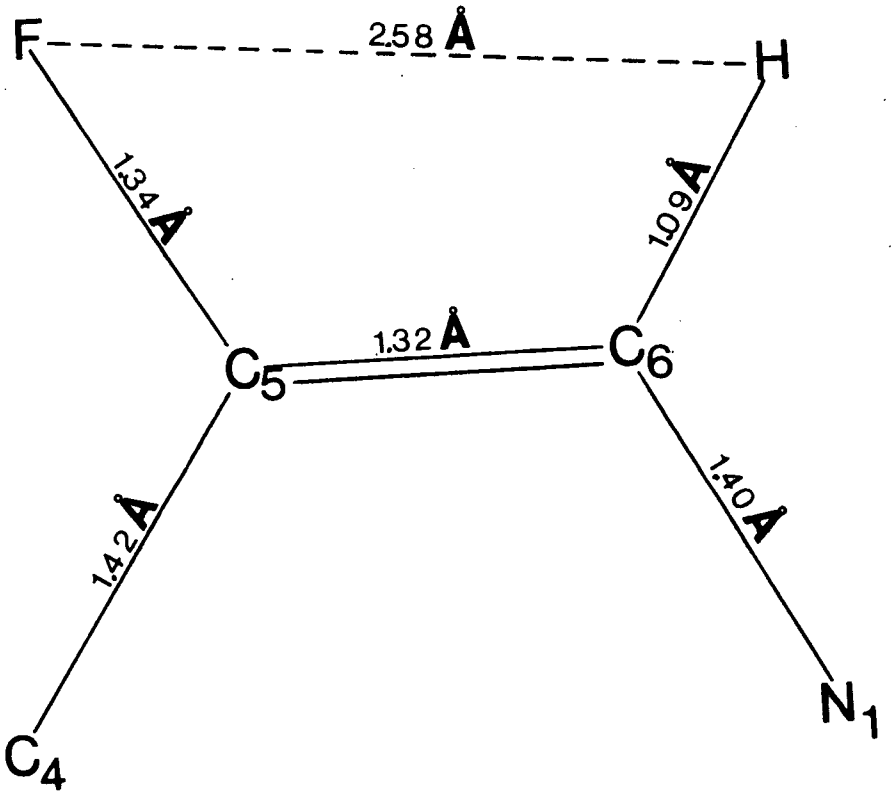

Figure 3.2. The intramolecular distance between fluorine and the nearest proton for 5-fluorouracil. The carbon-carbon and carbon-fluorine bond distances and bond angles are based on the available X-ray crystal structures of 5-FU (16-17). For the vinylic proton (bonded to C_6) the bond angle, $C_5{=}C_6{-}H$, and bond distance, $C_6{-}H$, were assumed to be the same as for ethylene (18).

$$\frac{1}{T_{1i}} = K \left(\sum_j r_{ij}^{-6}\right) F_1 \qquad (4)$$

$$\frac{1}{T_{2i}} = \frac{K}{2} \left(\sum_j r_{ij}^{-6}\right) F_2 \qquad (5)$$

where,

$$K = \left(\frac{1}{10}\right) \gamma_i^2 \gamma_j^2 \hbar^2 = 5.0449 \times 10^{10} \frac{(\text{angstroms})^6}{(\text{seconds})^2} \qquad (6)$$

since $\gamma_i = 2.5176 \times 10^4$ radians/second·gauss (7)

$\gamma_j = 2.6753 \times 10^4$ radians/second·gauss (8)

and $\hbar^2 = 1.05443 \times 10^{-27}$ erg·seconds. (9)

The functions F_1 and F_2 in terms of spectral density functions (J) are given by:

$$F_1 = J(\omega_i-\omega_j) + 3J(\omega_i) + 6J(\omega_i+\omega_j) \quad (10)$$

and

$$F_2 \cong F_1 + 4J(0) + 6J(\omega_j) \quad (11)$$

where ω_i and ω_j are the resonance frequencies, in radians per second, of fluorine (i) and protons (j) at a given magnetic field strength. These values are given in Table 3.2 for the three most commonly employed magnetic field strengths. The J

Field Strength (KG)	^{19}F Resonance Frequency (MHz)	^{19}F Resonance Frequency, ω_i (radians/second)	^{1}H Resonance Frequency (MHz)	^{1}H Resonance Frequency, ω_j (radians/second)
23.5	94.1	5.91×10^8	100	6.28×10^8
63.4	254.0	1.6×10^9	270	1.7×10^9
84.6	338.7	2.13×10^9	360	2.26×10^9

Table 3.2. The resonance frequency of the proton and the fluorine nucleus at the three most commonly employed magnetic field strengths.

terms in equations 10 and 11 are spectral density functions for isotropic motion and are of the form shown in equation 12,

$$J(\omega) = \frac{\tau_c}{1+\omega^2\tau_c^2} \quad (12)$$

where τ_c is the overall molecular correlation time. Equations 4 and 5 may be rearranged into the following form:

$$T_1 \sum_j r_{ij}^{-6} = 1/KF_1 \qquad (13)$$

$$T_2 \sum_j r_{ij}^{-6} = 2/KF_2 \qquad (14)$$

Plots of equations 13 and 14 for the resonance frequencies of fluorine and hydrogen, shown in Table 3.2, are given in Figures 3.3-3.5.

Figures 3.3-3.5 indicate that fluorine T_1 and T_2 values are equal for fast motion. However as the molecular tumbling rate slows down (larger τ_c) T_1 and T_2 diverge. The T_2 time continues to decrease while T_1 reaches an absolute minimum and then begins to increase again. The minimum T_1 value, corresponding T_2 values, the τ_c associated with divergence of T_1 and T_2, and τ_c associated with a minimum T_1 are summarized for Figures 3.3-3.5 in Table 3.3. These values assume that relaxation is due only to the 6-carbon proton of the 5-FU base which is 2.58 angstroms from fluorine.

The estimated T_1 values for the individual fluorine peaks, at 254 MHz, are given in Table 3.1. The accuracy of these results were hindered by the broadness of the peaks and their relatively close proximity to each other. Therefore large uncertainties (about 30%) must be associated with these values. The tabulated values for T_1 range between 0.29 and 0.43 seconds;

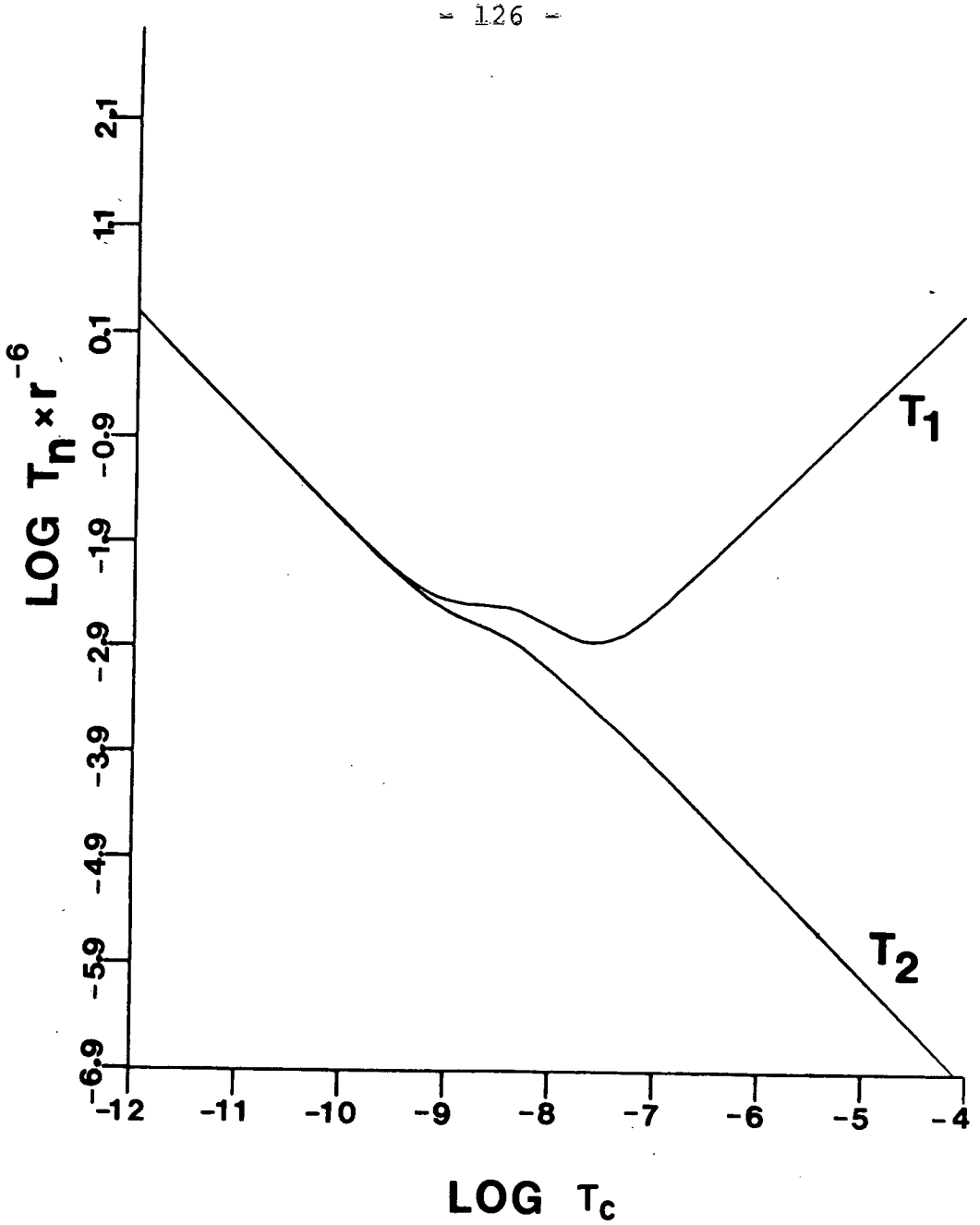

Figure 3.3. Log plots of $T_1 \times r^{-6}$ and $T_2 \times r^{-6}$ versus the log of the overall molecular time (τ_c) at 94.1 MHz. These values are obtained from equations 13 and 14. The calculations assume that the two relaxation times are exclusively dipolar and due only to the nearest neighbor proton located 2.58 angstroms (r) away from the fluorine.

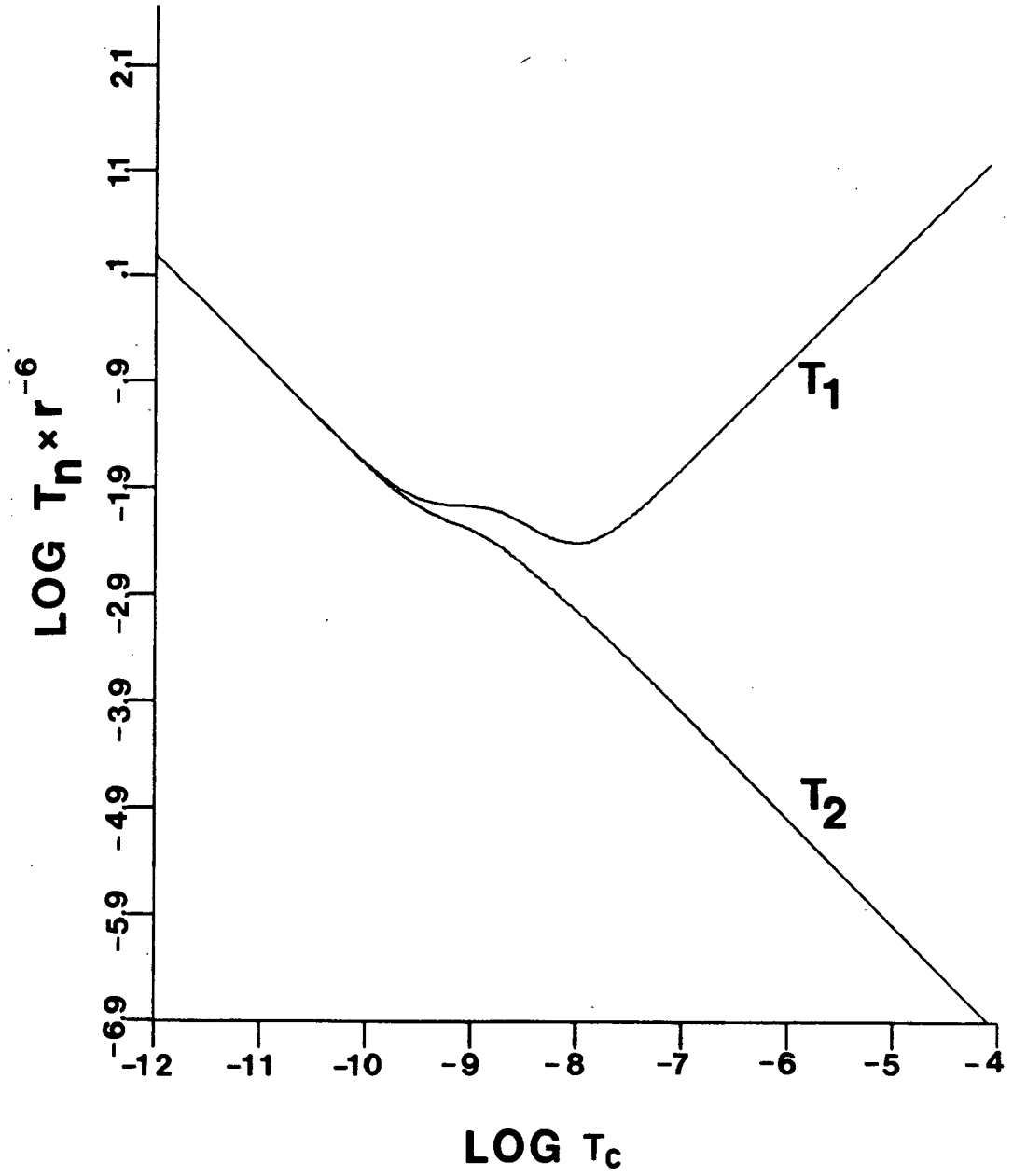

Figure 3.4. Log plots of $T_1 \times r^{-6}$ and $T_2 \times r^{-6}$ versus log τ_c calculated at 254 MHz using equations 13 and 14.

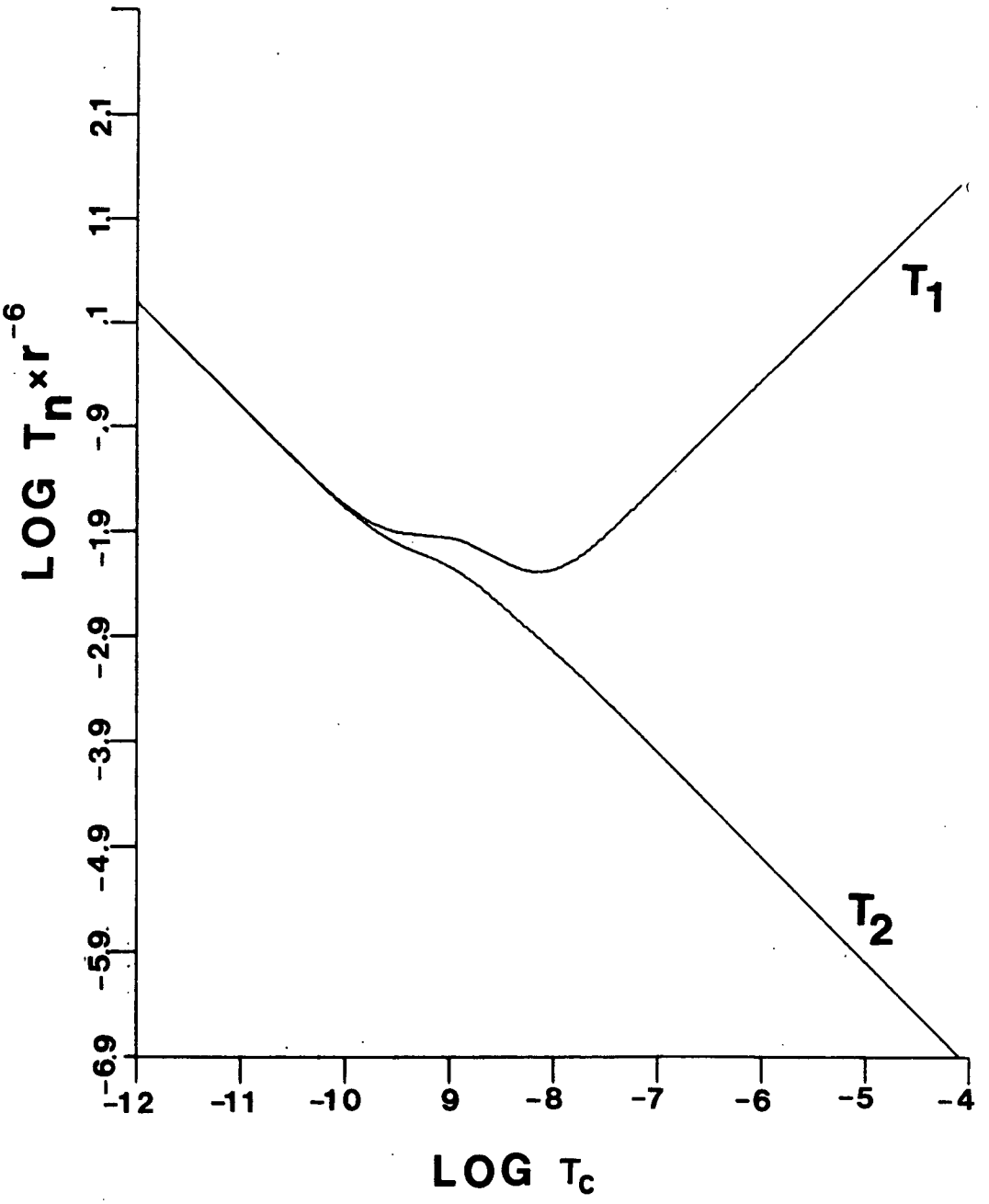

Figure 3.5. Log plot of $T_1 \times r^{-6}$ and $T_2 \times r^{-6}$ versus log τ_c calculated at 338.7 MHz using equations 13 and 14.

Field Strength (KG)	T_1 (seconds)	T_2 (seconds)	τ_c at minimum T_1	$T_1 \neq T_2$
23.5	0.44	0.11	2.5×10^{-8}	$\tau_c > 5 \times 10^{-10}$
63.4	1.19	0.27	1×10^{-8}	$\tau_c > 2.5 \times 10^{-10}$
84.6	1.59	0.34	7.9×10^{-9}	$\tau_c > 1.5 \times 10^{-10}$

Table 3.3. Minimum T_1 values, corresponding T_2 values, the τ_c associated with divergence of T_1 and T_2, and τ_c associated with the minimum T_1 for Figures 3.2-3.4. These values assume dipolar relaxation via the 6-carbon proton of 5-FU. T_1 and T_2 are proportional to magnetic field strength. The τ_c value associated with minimum T_1 and the divergence of T_1 and T_2 are also field dependent.

substantially less than the predicted minimum value of 1.19 seconds (see Figure 3.3) due exclusively to intramolecular dipole-dipole relaxation via the proton nearest to the fluorine nuclei of 5-FU. The short time scale for these T_1 values implies a relatively rigid solution structure for FU-5SrRNA. A τ_c value of 1×10^{-8}, which corresponds to a minimum T_1 is a reasonable value for the tumbling of a macromolecule the size of 5SrRNA. The inherent stability of base pairing and base stacking interactions in RNA molecules suggest that in FU-5SrRNA the 5-FU bases are rigidly situated and internal rotation, which would increase both T_1 and T_2 (15), is highly improbable. This is verified by a nuclear Overhauser enhancement (N.O.E.) experiment to be discussed shortly.

Another source of T_1 relaxation of fluorine is chemical shift anisotropy. The presence of an applied field causes the

electronic cloud about the fluorine nucleus to circulate. Since fluorine is not spherically symmetric (like the proton) a secondary magnetic field is generated at the nucleus. As a molecule tumbles time dependent oscillating components of this field will be generated which are perpendicular to the applied field and contribute to relaxation. Hull and Sykes have concluded that this mechanism does not contribute significantly to T_1 relaxation in their study of the fluorotyrosine labeled alkaline phosphatase enzyme system at 94 MHz or 235 MHz (20). However they have shown that T_2 relaxation is significantly affected by fluorine's chemical shift anisotropy and this effect increases in proportion to increased magnetic field strength. Therefore at high magnetic field strength spectral resolution is hindered despite improved frequency separation of peaks since there is also a proportionate increase in line width.

The accurate measurement of T_2 relaxation times are not possible for the FU-5SrRNA spectra due to the extensive overlapping of peaks. In Figures 2.16 and 2.17 estimated line widths, at half amplitude, are in the neighborhood of at least 200 hertz. Line widths associated with the surface environment (peaks 5 and 6) appear to be somewhat narrower. If the line shapes of these peaks are assumed to be Lorentzian and line widths at half amplitude equal to $2/T_2$ rad sec^{-1} (21) then the T_2 values of the individual peaks are all less than 10 milliseconds.

The above discussion of T_1 and T_2 relaxation times must be taken with considerable caution. The 254 megahertz spectrum reveals only 8 well resolved peaks. In E. coli 5SrRNA there are 20 uracils and our FU-5SrRNA is expected to exhibit at least 85% replacement (9). This means that the individual peaks referred to in the above discussion are more appropriately considered as regions. Each region is likely to be the superposition of more than one fluorine. Therefore line widths and T_1 relaxation times of these regions are likely to be the net effects of more than one fluorine.

An N.O.E. experiment provided the most definitive information about the 5-FU labels in FU-5SrRNA. The proton resonances were saturated with a strong 270 MHz frequency signal (the Larmor frequency of the proton) and the ^{19}F-nmr spectrum obtained with a weaker radio frequency signal at the Larmor frequency of fluorine (254 MHz). As shown in Figure 2.19 there is almost complete loss of the ^{19}F-nmr spectrum under the condition of proton saturation. This is expected for a molecule the size of 5SrRNA assuming spin-lattice relaxation exclusively due to a dipole-dipole mechanism (22). In order to understand this conclusion it is necessary to first consider relaxation of a two spin system (23).

The energy level diagram for a system consisting of two nuclear spins, I and S, is shown in Figure 3.6. The spins can be aligned against the static magnetic field, indicated by the α subscript, or in the direction of the static field (the β

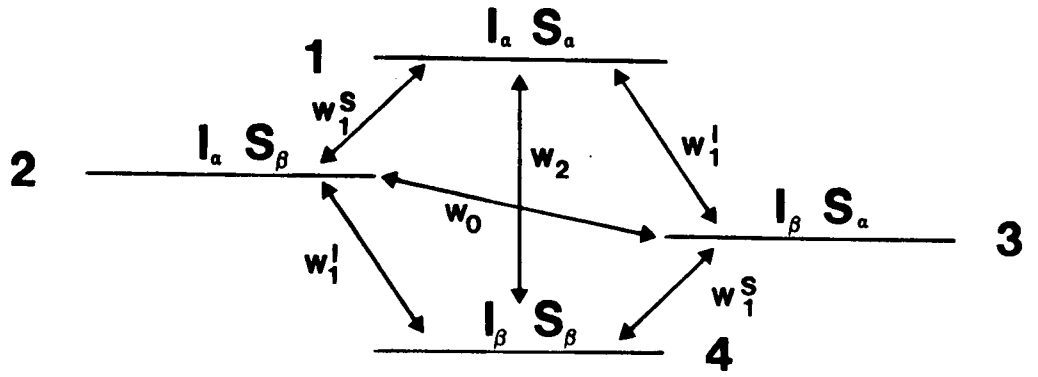

Figure 3.6. An energy level diagram of a system consisting of two nuclear spins, I and S. The subscripts, α and β, refer respectively to alignment of the spins opposed to and in the direction of the applied magnetic field. The W terms represent relative transition probabilities between specified energy levels (see text).

subscript), with the latter being the energetically more favorable situation. The four possible transition probabilities needed to describe T_1 relaxation during an N.O.E. experiment are indicated in Figure 3.6. W_1^S and W_1^I represent respectively the rates for single quantum transitions of an S spin, given that I remains unchanged, and for an I spin with the S spin remaining unchainged. The superscript indicates the spin undergoing the quantum transition. The transition probability, W_0, is for both spins I and S undergoing transitions of the type $I_\alpha S_\beta \longrightarrow I_\beta S_\alpha$ or $I_\beta S_\alpha \longrightarrow I_\alpha S_\beta$. Lastly, W_2 is the likelihood that two spins aligned in the same direction will relax at the same time. That is, transitions of the type $I_\alpha S_\alpha \longrightarrow I_\beta S_\beta$ or $I_\beta S_\beta \longrightarrow I_\alpha S_\alpha$. Noggle and Schirmer have shown that for a two spin system where S = I = ½ the fractional enhancement of the integrated intensity of the I spin, given that the S spin is saturated, is described by equation 15 (24).

$$f_I(S) = \frac{W_2 - W_0}{2W_1^I + W_0 + W_2} \qquad (15)$$

The numerator, $W_2 - W_0$ is called the cross relaxation term. It is transitions associated with W_2 and W_0 that cause the N.O.E. effect. The effect of saturating the S spins on the energy level diagram shown in Figure 3.5 is to equalize the spin populations of levels 1 and 2 as well as 3 and 4. This results in a change in the populations of all the energy levels from their equilibrium values prior to saturation. Consequently the system

will attempt to re-establish the equilibrium populations in these levels. Neither W_1^S or W_1^I transitions cause net changes in the populations of these levels. However, W_2 attempts to re-establish the equilibrium population by increasing the population of energy level 4 through a corresponding decrease in energy level 1. This process will facilitate an increase in the absorption intensity of the I spins. W_0 will redistribute the populations between energy levels 2 and 3 which at equilibrium are equal. It effects a decrease in the population of energy level 3 and an increase in the population of energy level 2. Its net effect is to decrease the intensity of the nmr resonance of the I spins. Hence W_0 and W_2 transitions have opposing effects under the condition of saturation of one of the spins.

Solomon has derived expressions for the transition probabilities associated with Figure 3.6 assuming that the resonance frequencies of the two spins, ω_I and ω_S are not equal (25). They are given by equations 16-19.

$$W_0 = \frac{h^2\gamma_I^2\gamma_S^2}{10b^6} \frac{\tau_c}{1 + (\omega_I-\omega_S)^2\tau_c^2} = K_1 \frac{\tau_c}{1 + (\omega_I-\omega_S)^2\tau_c^2} \qquad (16)$$

$$W_1^I = \frac{3h^2\gamma_I^2\gamma_S^2}{20b^6} \frac{\tau_c}{1 + \omega_I^2\tau_c^2} = K_2 \frac{\tau_c}{1 + \omega_I^2\tau_c^2} \qquad (17)$$

$$W_1^S = \frac{3h^2\gamma_I^2\gamma_S^2}{20b^6} \frac{\tau_c}{1 + \omega_S^2\tau_c^2} = K_2 \frac{\tau_c}{1 + \omega_S^2\tau_c^2} \qquad (18)$$

$$W_2 = \frac{3h^2\gamma_I^2\gamma_S^2}{5b^6} \frac{\tau_c}{1 + (\omega_I+\omega_S)^2\tau_c^2} = K_3 \frac{\tau_c}{1 + (\omega_I+\omega_S)^2\tau_c^2} \qquad (19)$$

For a two spin system of ^{19}F (I) and ^{1}H (S) nuclei in 5-FU γ_F and γ_H are their gyromagnetic ratios. They are, respectively, 25,179 radians/seconds·gauss and 26,753 radians/seconds·gauss. The ω_I and ω_S terms are equal to $2\Pi \cdot 254 \times 10^6$ cycles/second and $2\Pi \cdot 270 \times 10^6$ cycles/second respectively. The b expression is the internuclear distance between fluorine and the nearest neighbor proton (2.58 angstroms) of 5-FU. The molecules correlation time is τ_c and $\hbar$ is Planck's constant (in units of ergs per second) divided by 2Π. Given the above parameters K_1, K_2, and K_3 can be computed. They are:

$$K_1 = 1.6331 \times 10^8/\text{seconds}^2$$
$$K_2 = 2.4497 \times 10^8/\text{seconds}^2$$
$$K_3 = 9.7987 \times 10^8/\text{seconds}^2$$

As shown by equations 16-19 transition probabilities are governed by the molecular correlation time, τ_c. In Figure 3.7 these transition probabilities are plotted against τ_c. For slow rotation ($\tau_c > 7.1 \times 10^{-10}$) $W_0 > W_2$ and according to equation 15 the fractional enhancement, $f_I(S)$, is then negative. That is, since W_0 transitions dominate for slow molecular motion the nmr spectrum due to I (^{19}F) will decrease with saturation of the S (^{1}H) spins. For fast tumbling ($\tau_c < 7.1 \times 10^{-10}$ seconds) $W_2 > W_0$ and transitions of the type $I_\alpha S_\alpha \longrightarrow I_\beta S_\beta$ will

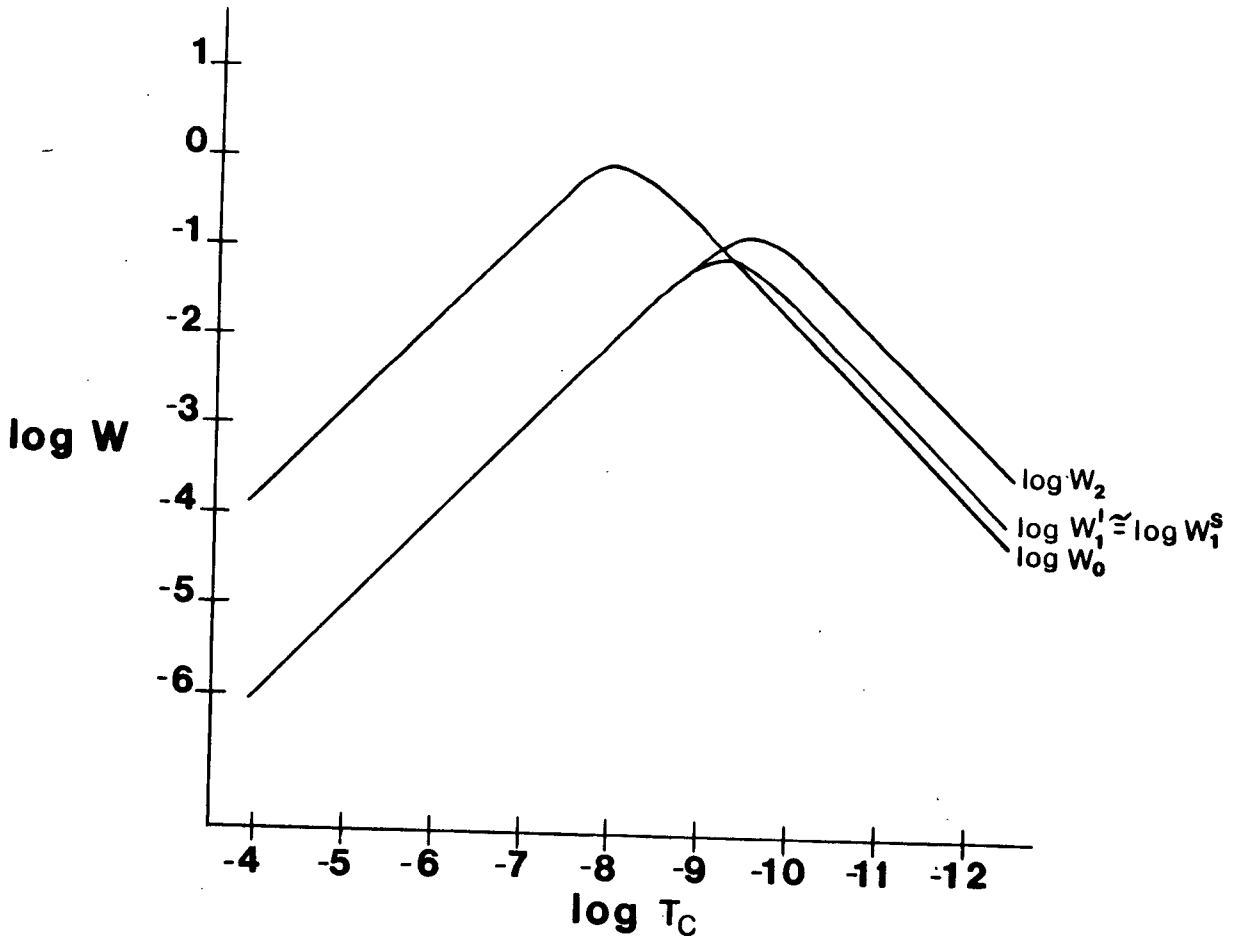

Figure 3.7. Log-log plot of transition rates versus rotational correlation time for the system of Figure 3.6, in which I is F-5 and S is H-6 of 5-fluorouracil. Fluorine relaxation is taken as pure dipolar between F-5 and H-6, resulting from isotropic rotational diffusion.

dominate. This will result in positive enhancement; an increase in the signal due to the I spins when the S spins are saturated.

Substitution of equations 16-19 into equation 15 provides the following expression for the fractional N.O.E. of unlike spins (5):

$$\frac{\text{area (with } ^1\text{H irradiation)} - \text{area (without } ^1\text{H irradiation)}}{\text{area (without } ^1\text{H irradiation)}} = \frac{\gamma_H}{\gamma_F} \frac{5 + 5\omega_I^2\tau^2 + 6(\omega_I-\omega_S)^2\tau^2 - (\omega_I+\omega_S)^2\tau^2 + 6\omega_I^2(\omega_I-\omega_S)^2\tau^4 - \omega_I^2(\omega_I+\omega_S)^2\tau^4}{10 + 7\omega_I^2\tau^2 + 4(\omega_I+\omega_S)^2\tau^2 + 9(\omega_I-\omega_S)^2\tau^2 + 6\omega_I^2(\omega_I-\omega_S)^2\tau^4 + \omega_I^2(\omega_I+\omega_S)^2\tau^4 + 3(\omega_I-\omega_S)^2(\omega_I+\omega_S)^2\tau^4} \quad (20)$$

The graph of equation 20 as a function of correlation time is shown in Figure 3.8 assuming an ^{19}F resonance frequency of 254 megahertz and proton saturation with 270 megahertz. When $\tau_c > 1 \times 10^{-8}$ (slow molecular rotation) then $f_I(S) = -1$, which corresponds to a complete loss of the ^{19}F signal intensity.

The observed collapse of the FT ^{19}F-nmr spectrum shown in Figure 2.19 when the protons are irradiated at their resonance frequency confirms a fractional N.O.E. value for all the ^{19}F resonances of $f_I(S) = -1$. This implies that cross relaxation via W_0 dominates and that the FU labels are slowly tumbling at a correlation time given by $\tau_c > 1 \times 10^{-8}$ sec. This circumstance would be required if the 5FU labels were rigidly situated (immobile) in the 5FU-5SrRNA molecule and tumbling at its correlation time.

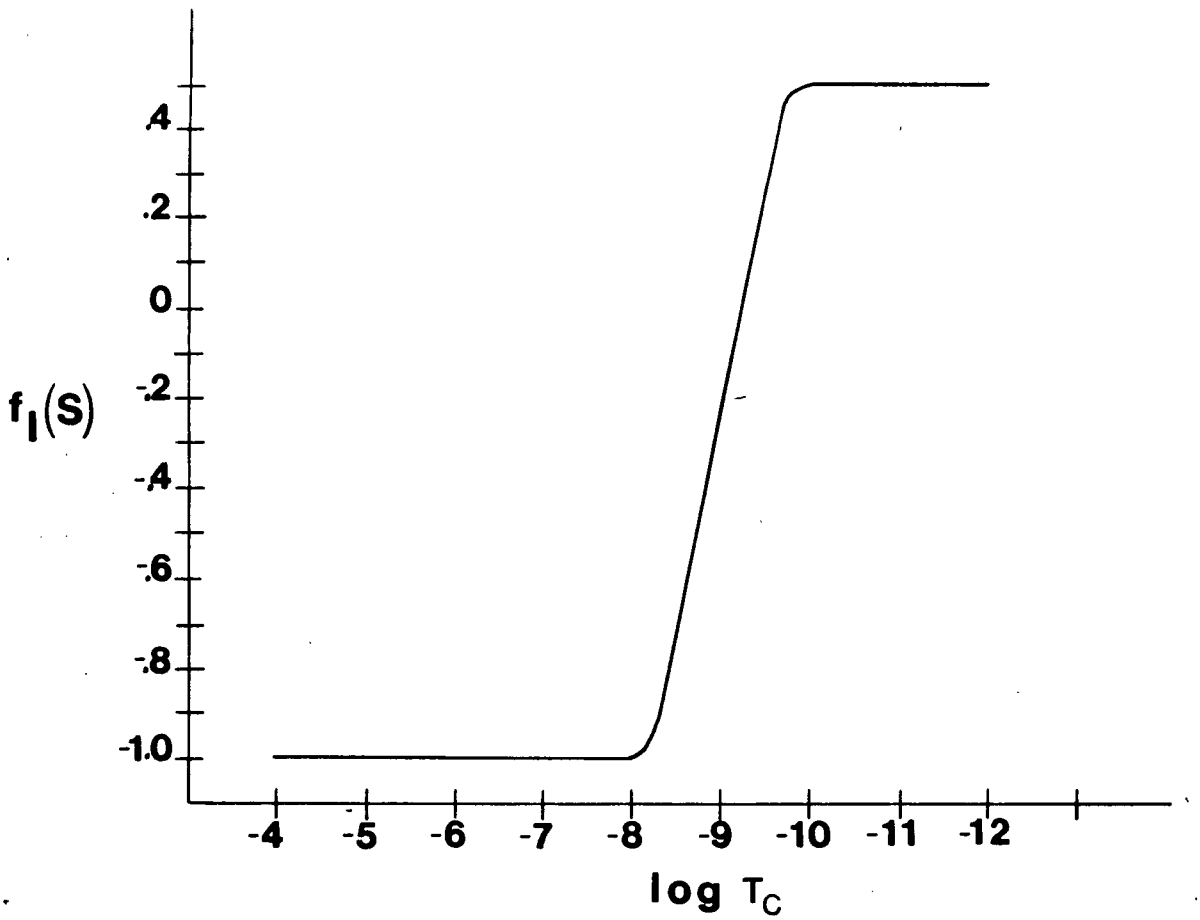

Figure 3.8. Fluorine-proton fractional nuclear Overhauser enhancement factor, $f_I(S)$, versus rotational correlation time (log scale) for 5-fluorouracil, computed from the transition rates of Figure 3.7.

If FU-5SrRNA were a rigid sphere, its τ_{rot} calculated from the Stokes-Einstein equation (26),

$$\tau_{rot} = \frac{4\Pi hR^3}{3kT} \qquad (21)$$

in which h is viscosity, k is Boltzmann's constant, T is absolute temperature, and R is the macromolecular radius (computed from a molecular weight of 40,000), would be about 10 nsec, assuming no water of hydration. A rigid FU-5SrRNA should therefore exhibit $f_I(S) = -1$ as shown in Figure 3.8. This corresponds to complete nulling of the ^{19}F signal on irradiation of the H-6 proton. According to Figure 3.8 there is a marked variation of $f_I(S)$ with τ_{rot} in this motional region. This means that even a small increase in local flexibility at the labeled site should lead to a large increase in $f_I(S)$ and incomplete nulling (or even an increase) of the ^{19}F peak on proton irradiation. Thus, the instrumental and molecular parameters of the FU-5SrRNA Overhauser experiment happen to fall in a range such that the N.O.E. experiment is optimally tuned to detect local flexibility at the labeled uracils of FU-5SrRNA.

In conclusion, the 254 MHz ^{19}F-nmr spectra of FU-5SrRNA (Figures 2.16 and 2.17) indicate at least 10 different chemical shifts which corresponds to 10 distinct chemical environments. This is an improvement in resolution when compared to the 94.1 MHz spectrum (Figure 2.13) where only 4 groups of peaks are observed. In Figures 2.16 and 2.17 peaks 5 and 6 have the same chemical shift as the single peak obtained on heat denaturation;

thus, this part of the spectrum probably corresponds to FU residues exposed to solution. In support of this view, it may be noted that peaks 5 and 6 are much narrower than peaks shifted to either side, and therefore correspond to residues that are more rotationally labile than the shifted and presumably "buried" peaks. Furthermore, T_1 measurements indicate that virtually all the observed peaks have relatively short T_1 (0.3 - 0.4 seconds), in agreement with the minimum T_1 calculated to occur for τ_{rot} = 10 nsec which corresponds to a rigid solution structure. The ^{19}F-^{1}H N.O.E. experimental results (Figure 2.19) are particularly striking. It is clear that virtually the entire ^{19}F spectrum is completely nulled on ^{1}H irradiation, definitively confirming (see Figure 3.8) that essentially all the fluorinated uracil residues have rotational correlation times approaching 10 nsec or longer. Furthermore, demonstration of the full Overhauser nulling of the ^{19}F resonances ($f_I(S) = -1$) confirms that T_1-relaxation is pure dipolar, as assumed in the theoretical calculations (5). [Strictly speaking, the $f_I(S) = -1$ result can also occur in the presence of very rapid internal motion (5). However, such rapid motion would have the additional effect of narrowing the ^{19}F resonances to line widths, less than are observed. Thus, we may safely conclude that the τ_{rot} values are in fact very long (10 nsec or greater) rather than very short.]

REFERENCES: CHAPTER 3

1. M.W. Hankapiller, S.H. Smallcombe, and J.D. Richards, Biochemistry 12, 4732 (1973).

2. I.M. Chaiken, M.H. Freedman, J.R. Lyerla, and J.S. Cohen, J. Biol. Chem. 248, 884 (1973).

3. P.F. Agris, F.G. Fujiwara, C.F. Schmidt, and R.N. Loeppky, Nucleic Acids Res. 2, 1503 (1975).

4. W.D. Hamill, D.M. Grant, W.J. Horton, R. Lundquist, and S. Dickman, J. Am. Chem. Soc. 98, 1276 (1976).

5. W.E. Hull and B.D. Sykes, J. Mol. Biol. 98, 121 (1975).

6. J. Bode, M. Blumenstein, and M.A. Faftery, Biochemistry 14, 1153 (1975).

7. D.T. Browne and J.D. Otvos, Biochem. Biophys. Res. Comm. 68, 907 (1976).

8. J.L. Johnson, K.R. Yamamoto, P.O. Weislogel, and J.L. Horowitz, Biochemistry 8, 1901 (1969).

9. I. Kaiser, Biochemistry 9, 569 (1969).

10. J. Horowitz, C.-N. Ou, M. Ishaq, J. Ofengand, and J. Bierbaum, J. Mol. Biol. 88, 301 (1974).

11. D. Gust, R.B. Moon, and J.D. Roberts, Proc. Nat. Acad. Sci., U.S.A. 72, 4696 (1975).

12. M. Gueron and R.G. Shulman, Proc. Nat. Acad. Sci., U.S.A. 72, 3482 (1975).

13. A.G. Marshall and J.L. Smith, J. Am. Chem. Soc. 99, 635 (1977).

14. T.C. Farrar and E.D. Becker, in Pulse and Fourier Transform NMR, Academic Press, New York, 1971; pages 20-22.

15. W.E. Hull and B.D. Sykes, Biochemistry 13, 3431 (1974).

16. L. Fallon, Acta. Cryst. B59, 2549 (1973).

17. D. Veot and A. Rich, J. Am. Chem. Soc. 91, 3069 (1969).

18. N. Allinger, in Organic Chemistry, Worth Publishers, New York, 1971; page 133.

19. D. Doddrell, V. Glushko, and A. Allerhand, J. Chem. Phys. 56, 3683 (1972).

20. W.E. Hull and B.D. Sykes, J. Mol. Biol. 98, 121 (1975).

21. A. Carrington and A.D. McLachlan, in Introduction to Magnetic Resonance, Harper & Row, New York, 1967; pages 9-10.

22. P. Balaram, A. Bothner-By, and J. Dadok, J. Am. Chem. Soc. 94, 4015 (1972).

23. J.H. Noggle and R.E. Schirmer, in The Nuclear Overhauser Effect, Academic Press, New York, 1971.

24. Reference 23; page 16.

25. I. Solomon, Phys. Rev. 99, 559 (1955).

26. A.G. Marshall, in Biophysical Chem., Wiley, New York, 1971; page 719.

CHAPTER 4

LASER RAMAN SPECTROSCOPY OF N-5SrRNA AND FU-5SrRNA

4.1 Introduction

Molecules are dynamic entities which undergo continuous nuclear and electronic motion. Besides overall translational motion, the nuclear movement can be described in terms of three specific types of motion; rotation of the molecule as a whole, molecular vibrations between chemically bonded nuclei in the molecule, and the spins of individual nuclei. Associated with the electrons are orbital motion about the nucleus and spin. The rotational and vibrational components of nuclear motion and the orbital motion of the electrons are described in quantum mechanical terms as energy eigenvalues which together represent the total internal energy of a given molecule. In the last chapter nuclear spin and molecular rotation were considered. Raman spectroscopy provides a method for obtaining vibrational energies (and in some cases rotational energies) of chemically bonded nuclei in molecules.

Rigorous theoretical interpretation of Raman spectra is only applicable for small molecules of high symmetry, where group theory can be employed to determine the number and the kinds of energy levels associated with the molecules' normal vibrational modes. Most molecules of biological interest are

large and asymmetric. A 5SrRNA molecule consists of 3,987 atoms which corresponds to 11,955 (3N-6) vibrational degrees of freedom. Even the rigorous interpretation of the ring vibrations of the purines and pyrimidines is unfeasible. Still, much useful information can be otbained by employing an empirical approach. Stretching and bending modes of specific molecular groupings occur at characteristic frequencies. In RNA molecules these so-called "group frequencies" are due to the characteristic ring vibrations of the purine and pyrimidine bases and the ribophosphate backbone. They are outlined in Table 2.3. The intensities of many of these Raman lines are affected by RNA conformation. These empirical observations are based on observed changes in Raman intensities of model compounds of purine and pyrimidine polyribonucleotides (1) and tRNA in both native and denatured forms (2-4).

This chapter presents Raman spectra of N-5SrRNA and FU-5SrRNA (Section 4.3). The comparison of the intensities of various Raman lines was used to evaluate the effects of 5-FU incorporation on 5SrRNA conformation. A necessary consideration of this study was the effect of 5-fluoro- substitution on the ring vibrations of the uracil base since alterations in the intensity of the ring vibrations of this base could be misinterpreted as changes in FU-5SrRNA conformation as compared to N-5SrRNA. This latter aspect is considered in section 4.2.

4.2 Laser Raman Study of 5-FU, 5-Fluoro-2'-deoxyuridine, and 5-Fluoro-2'-deoxyuridine Monophosphate

To date, X-ray (5,6), ^{13}C-nmr (7), ^{19}F-nmr (8), and infrared spectroscopy (9,10) have been used to examine the effects of fluorination on the structural and chemical properties of the uracil base. In order to evaluate the effect of 5-fluoro-substitution on the vibrational properties of the uracil bases, laser Raman spectra of polycrystalline U and 5-FU, 5-FU in H_2O, 5-fluoro-2'-deoxyuridine (5-FdUrd) in H_2O and D_2O, and 5-fluoro-2'-deoxyuridine monophosphate (5-FdUMP) in H_2O were obtained for comparison to normal 2'-deoxyuridine (dUrd) in H_2O and D_2O.

A generalized structure for U, dUrd, 5-FU, 5-FdUrd, and 5-FdUMP is shown in Figure 4.1. U and 5-FU each possess dissociable protons at N-1 and N-3.

4.2.1 Uracil and 5-Fluorouracil

Laser Raman spectra of polycrystalline (powder) samples of 5-FU and U were presented in Figures 2.20a and 2.20b. Peaks associated with C-N stretching vibrations (1226 cm^{-1} for 5-FU; 1234 cm^{-1} for U), and with ring breathing motions (770 cm^{-1} for 5-FU; 790 cm^{-1} for U) are similar in appearance for both compounds. The carbonyl stretching region (1600-1700 cm^{-1}) is different for 5-FU than for U; the differences are more pronounced and more easily interpreted for the corresponding nucleosides discussed in section 4.2.2.

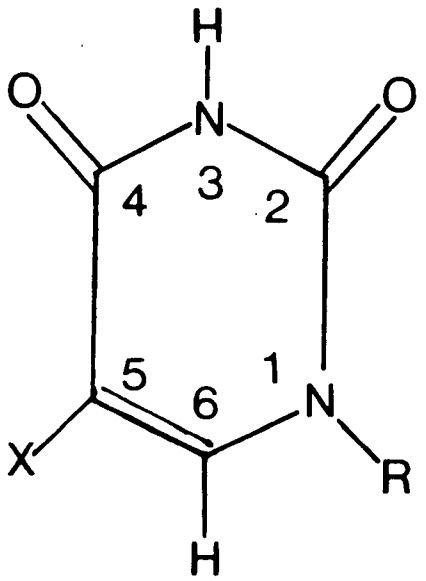

X = H; R = H	Uracil
X = H; R = 2'-deoxyribose	dUrd
X = F; R = H	5FU
X = F; R = 2'-deoxyribose	FdUrd
X = F; R = 2'-deoxyribose-5'-monophosphate	FdUMP

Figure 4.1. A Generalized structure for U, dUrd, 5-FU, 5-FdUrd, and 5-FdUMP.

The most striking difference between these Raman spectra is the presence of an intense peak at 1349 cm^{-1} for 5-FU, which is absent in the U spectrum. This peak may be assigned to a C-F stretching vibration on this basis, and because C-F stretching frequencies have previously been observed for model compounds in this region (11).

Finally, a comparison of Figures 2.20b and 2.20c indicates a close resemblance between the spectra of polycrystalline U and neutral U in H_2O.

Infra-red and ultraviolet spectroscopic measurements show that the first ionization for uracil occurs preferentially at N-3 rather than at N-1. 5-Fluorination lowers this first pK_a by 1.3 pH units (from 9.45 to 8.15) and also increases the preference for N-3 ionization; 6-fluorination increases the proportion of N-1 ionization (10). Figure 2.21 shows Raman spectra of 5-FU in H_2O at several pH values. As the pH is increased above neutrality, Raman spectral changes coincide with the first and second deprotonation steps (pK_a = 8.15, 13) (9). Changes at pH $\geq$ 10 do not occur for the corresponding nucleosides, because in those cases the N-1 position is substituted with 2-deoxyribose (see Figure 4.1).

4.2.2. 2'-Deoxyuridine and 5-Fluoro-2'-deoxyuridine

A comparison of the Raman spectra for 5-FU in Figure 2.21 with those for 5-FdUrd in Figure 2.22 indicates that the introduction of the sugar moiety, which itself shows no observable Raman vibrations in this frequency range, alters substantially the vibrational properties of the 5-FU base. The effects of 5-fluorination on Raman properties of the dUrd nucleoside are evident from a comparison of the Raman spectra of dUrd and 5-FdUrd in H_2O and D_2O shown in Figures 2.22 and 2.23, respectively; in all cases, the Raman vibrations from the base are confined to a spectral range between 500 and 1750 cm^{-1}. Lord and Thomas (12) have made reliable assignments for several Raman

lines in aqueous (and D_2O) solutions of uridine, providing a basis for the present analysis of 2'-deoxyuridine and its 5-fluorinated derivative.

Double Bond Stretching Region: H_2O

In uridine, the spectral region between 1550 and 1750 cm^{-1} consists principally of vibrational contributions from two carbonyls and the C-5:C-6 double bond, with a small contribution (in H_2O only) from a deformation mode of the acidic N-3 proton (12). In H_2O it is not possible to resolve the individual carbonyls nor the C-5:C-6 double bond stretching vibrations.

For dUrd in H_2O, the neutral form (Figure 2.22a) exhibits an intense peak at 1678 cm^{-1} with a pronounced shoulder at 1626 cm^{-1}. Lord and Thomas (12) have established that the 1676 cm^{-1} peak is predominantly due to carbonyl stretching, and the 1626 cm^{-1} shoulder to C-5:C-6 double bond stretching vibrations. On deprotonation of the base at N-3 (Figure 2.22c), these two peaks are replaced by lines at approximately 1632 cm^{-1} and 1600 cm^{-1}.

For 5-FdUrd in H_2O, the neutral form (Figure 2.22b) shows a strong broader peak centered at 1676 cm^{-1} with a less intense shoulder at approximately 1627 cm^{-1}. In contrast to dUrd, deprotonation (Figure 2.22d) of 5-FdUrd causes most of the intensity to shift to approximately 1604 cm^{-1}, leaving the remaining intensity at approximately 1668 cm^{-1} (near the original peak maximum before deprotonation).

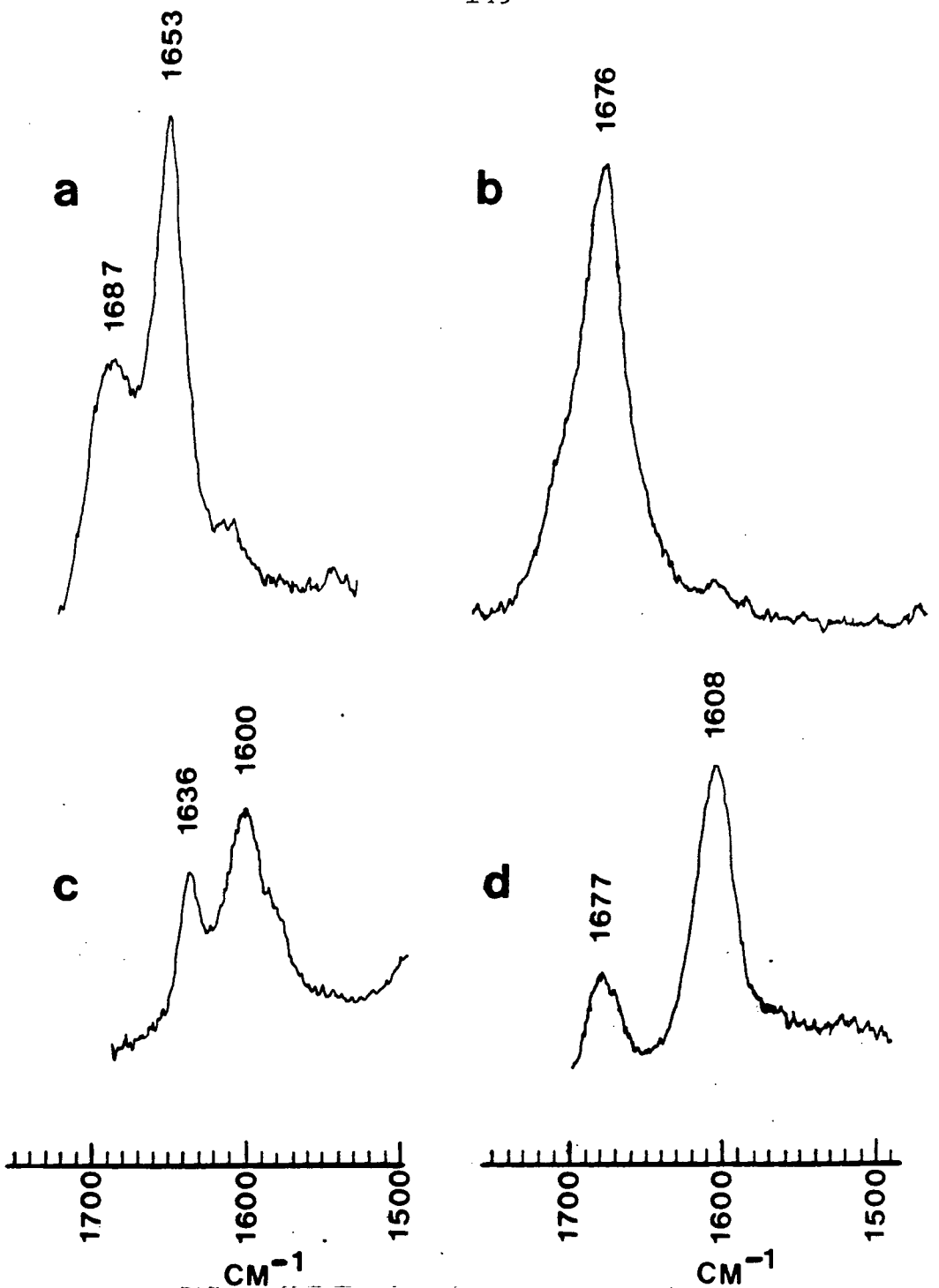

Figure 4.2. Laser Raman carbonyl stretching region for 50 millimolar D_2O solutions of:

(a) neutral dUrd (pH meter reading 5.8),
(b) neutral 5FdUrd (pH meter reading 5.8),
(c) anionic dUrd (pH meter 11.2),
(d) anionic 5FdUrd (pH meter 11.1).

These spectra were obtained as described in section 2.8.2.

Double Bond Stretching Region: D_2O

The much improved resolution for the 1600-1700 cm^{-1} region in D_2O permits a more definitive analysis in terms of the principle resonance structures for neutral and anionic dUrd and 5-FdUrd. The Raman carbonyl stretching region of dUrd and 5-FdUrd (in D_2O) are shown in Figure 4.2. The principle resonance structures for the neutral and anionic forms of these molecules are shown in Figure 4.3.

For neutral dUrd, the Raman spectrum of the carbonyl region (Figure 4.2a) shows two vibrationally nonequivalent carbonyls, with C_2=O at 1687 cm^{-1} and C_4=O at 1653 cm^{-1}, assigned by analogy to Urd (16,17). The lower frequency for the C-4 carbonyl favors resonance contributions from Ia and Ib, consistent with a lower ionization potential (by 1 e.v.) for the lone electron pair of O-4 compared to O-2 (13). Furthermore, structure Ia is favored over Ib, because X-ray diffraction shows that the C_5-C_6 bond is shorter (1.34 angstroms) than the C_4-C_5 bond (1.44 angstroms) (14).

For neutral 5-FdUrd, the Raman spectrum (Figure 4.2b) shows two vibrationally equivalent carbonyls at 1676 cm^{-1}. The C_4=O frequency has presumably increased relative to the C_2=O frequency, compared to dUrd, because α-fluoro- substitution is known to shift Raman carbonyl stretching to higher frequency in model compounds (15). X-ray bond lengths (1.33 angstroms for C_5-C_6 and 1.44 angstroms for C_4-C_5 in 5-FdUrd) (6) disfavor

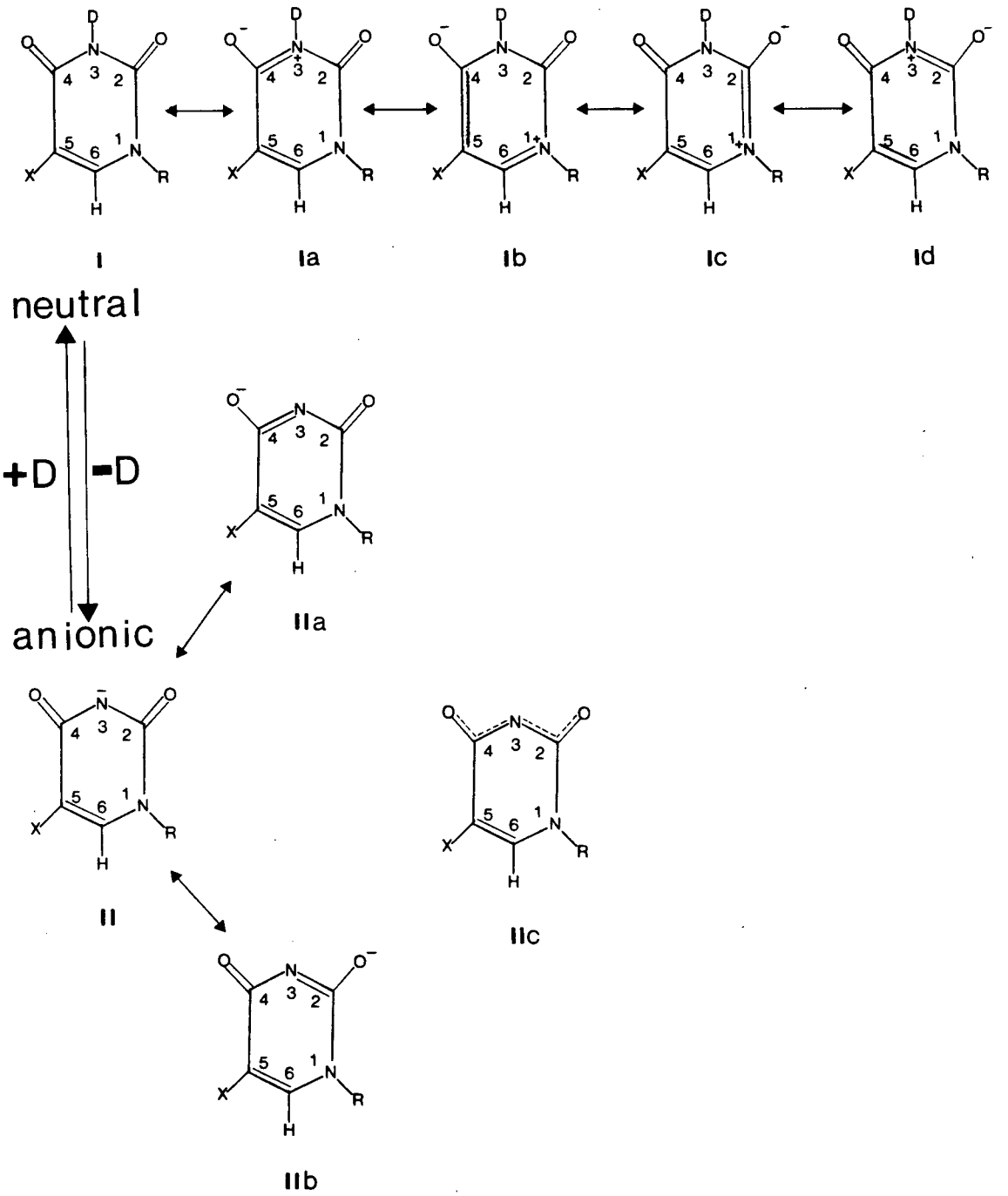

Figure 4.3. The principle resonance structures for neutral and anionic forms of dUrd (R = 2'-deoxyuridine, X = ^{1}H) and 5FdUrd (R = 2'-deoxyuridine and X = ^{19}F).

structure Ib. Thus, the Raman equivalence of C_2=O and C_4=O in Figure 4.2b requires increased contributions from structures Ic and Id relative to Ia in 5-FdUrd compared to dUrd.

For dUrd, both Raman carbonyl frequencies shift by the same amount (53 and 51 cm^{-1}) on deprotonation (Figures 4.2a and 4.2c), suggesting comparable contributions from IIa and IIb in the anion (perhaps better represented as IIc). On the other hand, the (equivalent) Raman carbonyl frequencies for neutral 5-FdUrd become nonequivalent (1677 and 1608 cm^{-1}) on deprotonation (Figures 4.2b and 4.2d). This nonequivalence almost certainly favors structure IIa over IIb or IIc in the 5-FdUrd anion, because the C_4=O is closer to the site of fluorination than is C_2=O; thus, the C_4=O would be expected to experience the larger Raman shift on deprotonation. In this respect, it may be noted that the ^{13}C-nmr chemical shift of C-4 moves much farther downfield on fluorination (by 147.5 Hz at 22.62 MHz) than does C-2 (43.0 Hz) (7).

Finally, since fluorine substitution increases the frequency of a double bond stretch (11), the 1676 cm^{-1} envelope for neutral 5-FdUrd (Figure 4.2b) may include a contribution from the C_5-C_6 double bond stretch.

Vibrations below 1400 cm^{-1}: dUrd and 5-FdUrd in H_2O and D_2O

The most intense Raman line for neutral dUrd in H_2O is located at 1230 cm^{-1} (Figure 2.22a). This line, which is weak in infra-red spectra, may be assigned, by analogy to uridine

(12), as originating predominantly from a concerted carbon-nitrogen stretching of the uracil ring (16), with probable major contribution from vibrations of the two C-N bonds associated with the protonated N-3. This interpretation is consistent with the observed sensitivity of this peak to pH and deuteration (Figures 2.22a, 2.22c; 2.23a, 2.23c). For 5-FdUrd in H_2O, the same spectral region shows an intense peak 1213 cm^{-1} and two smaller peaks at 1236 cm^{-1} and 1268 cm^{-1}, and these peaks are again sensitive to pH and deuteration (Figures 2.22b, 2.22d; 2.23b, 2.23d).

Neutral dUrd gives a moderately intense peak at 1390 cm^{-1} in H_2O (1398 cm^{-1} in D_2O), which disappears on N-3 deprotonation. Neutral 5-FdUrd does not show comparable Raman-active vibrations near this frequency (the peak near 1360 cm^{-1} has a different origin -- see below).

The intense line located between 780 and 794 cm^{-1}, assigned to a ring-breathing type of motion, is relatively insensitive to deprotonation, deuteration, or fluorination of dUrd (Figures 2.22 and 2.23). Similarly, the weak line at 626-630 cm^{-1} also appears insensitive to deprotonation, deuteration, or fluorination of dUrd. There is a line at 560 cm^{-1} in H_2O for dUrd (and at 690 cm^{-1} for 5-FdUrd) which shifts to higher frequency (by 27 cm^{-1} for dUrd and by 13 cm^{-1} for 5-FdUrd) on deprotonation, and a similar effect is seen in D_2O (Figures 2.23).

Finally there is one prominent peak for 5-FdUrd (1360 cm^{-1} at neutral pH in H_2O; 1348 cm^{-1} on deprotonation in H_2O) in Figures 2.22b and 2.22d, which is relatively unaffected by deuteration (Figure 2.23b; 2.23d). We tentatively assign this peak to a C-F stretch, since there is no corresponding peak for the unfluorinated dUrd, and because C-F stretching frequencies have been observed for other compounds in this region (11).

4.2.3 5-Fluoro-2'-deoxyuridine (5-FdUrd) and 5-Fluoro-2'-deoxyuridine-5'-monophosphate (5-FdUMP)

The laser Raman spectra of 5-FdUrd and 5-FdUMP, shown in Figure 2.24, exhibit no major changes in the Raman vibrations due to the 5'-phosphate group. The 976 cm^{-1} line, at pH > 7, indicated in Figure 2.24c is due to a symmetric stretching vibration of the PO_3^{-2} group (17). The only other detectable alteration which may be due to the phosphate group is a broadening of the spectral envelope for the concerted ring vibration at 786 cm^{-1}, shown in Figure 2.24a.

4.2.4 Concluding Remarks

To summarize this section, the new Raman data indicate that one important effect of 5-fluorination on the neutral form of 2'-deoxyuridine is to make the two carbonyls more equivalent by increasing the $C_4{=}O$ stretching frequency relative to the $C_2{=}O$ stretch, and the effect of 5-fluorination on the anionic form is to favor structures with more charge density at $C_4{=}O$ relative to $C_2{=}O$ than in unfluorinated 2'-deoxyuridine. All

peaks observed in solutions of neutral 5-FU, 5-FUrd, and 5-FUMP are also present for the polycrystalline forms of each species. A new prominent pH-sensitive peak at 1360 cm^{-1} (5-FUrd, H_2O, neutral pH), insensitive to deuteration at N-3, is tentatively assigned to a C-F stretch. Other major peaks have been assigned by analogy to previously analyzed spectra of uridine (12).

A major consideration of this study was to evaluate the effects of 5-fluoro- substitution on the peak intensities of the uracil base ring vibrations. This was applied to the interpretation of the FU-5SrRNA Raman spectrum. The 782 cm^{-1} and 1230 cm^{-1} lines of dUrd in H_2O are reduced by at least 40% and 87% respectively due to 5-fluoro- substitution (Figure 2.22a and 2.22b). These two Raman lines will be considered in the interpretation of the FU-5SrRNA Raman spectrum shown in section 4.3.

4.3 Laser Raman Spectroscopy of N-5SrRNA and FU-5SrRNA

As previously mentioned changes in the intensities of various Raman lines of an RNA spectrum are an indication of conformational change. Most of the Raman lines due to the purine and pyrimidine bases are hypochromic (3). That is, they decrease in intensity with an increase in the stacking efficiency of the bases. This observed hypochromicity is often difficult to interpret because of extensive overlap from the vibrational contributions of different bases. This is especially true of the spectral region between 1200-1600 cm^{-1} (3). A line at 725 cm^{-1} is due exclusively to adenine residues. This line is hypochromic since a decrease in its intensity corresponds to more efficient stacking of these residues (18-21). Conversely, the 670 cm^{-1} line which is due exclusively to guanine is reverse hypochromic (22,23) since increased stacking interactions cause an increase in its intensity. Another line of diagnostic utility is the 814 cm^{-1} line which has been assigned to the symmetric stretching of ordered phosphodiester bonds of the ribophosphate backbone (18-21). An increase in the intensity of this line is indicative of increased regularity of the phosphate backbone. Together the above three Raman lines are particularly useful because they are each due to a single vibrational component.

Since they are not complicated from overlapping contributions of different origins the 670 cm^{-1}, 725 cm^{-1}, and 814 cm^{-1}

Raman lines are the most useful indicators of RNA conformation. In yeast $tRNA^{Phe}$ the 670 cm^{-1} line undergoes almost a 3 fold decrease when the guanine bases go from a completely stacked configuration to an unstacked form (22,23). Conversely, the 725 cm^{-1} line increases about 12% when the partially stacked adenine residues become unstacked (3). The 814 cm^{-1} line is a measure of the helical order of the ribophosphate backbone (18-21). Its intensity is influenced by the geometry of the C-O-P-O-C linkages and an increase in intensity implies greater helical order.

A comparison of the Raman spectra of N-5SrRNA before and after dialysis are shown in Figure 2.25. This shows that conformational changes have taken place. In Table 2.3 the peak intensities, normalized to the invariant 1100 cm^{-1} line, are given. The observed increase in the intensity of the 670 cm^{-1} line by about 12% is an indication of more efficient stacking of the G bases due to dialysis against magnesium. Similarly, A stacking is improved since there is a decrease of about 19% after dialysis. Both samples exhibit comparable regularity in their ribophosphate backbone as evident from identical intensity values for the 814 cm^{-1} line. The 785 cm^{-1} line decreases by almost 25%. This line is due to the combined effects of cytosine and uridine residues and reduces in intensity with improved stacking interactions of these residues. Consequently, the substantial reduction is an indication of more efficient

stacking of cytosine and/or uridine bases. The Raman lines above 1200 cm^{-1} are also sensitive to stacking interactions and decrease with improved stacking (3). However, the overlapping of the vibrational contributions from different bases hinder interpretation. Clearly, alterations in stacking interactions due to dialysis against magnesium are apparent in the spectral region between 1200 cm^{-1} and 1600 cm^{-1} (see Table 2.5).

The Raman spectra of the dialysed sample of N-5SrRNA and that obtained by Chen et. al. are comparable. Differences in tabulated intensity values are attributable to their selection of different baselines. Measurement of the relative intensities of the 814 cm^{-1}, 785 cm^{-1}, 725 cm^{-1}, and 670 cm^{-1} lines using baselines consistent with this work gives values of 1.60, 2.32, 0.68 and 0.72 respectively; these agree favorably with those values shown in Table 2.5.

The Raman spectra of the dialysed sample of N-5SrRNA and FU-5SrRNA are similar. These spectra are shown in Figure 2.26 and intensities of Raman lines, relative to the 1100 cm^{-1} line, are given in Table 2.5. The intensities of the 670 cm^{-1} lines, due to guanine residues, are almost identical; an indication of comparable stacking of this residue. Some destacking of adenine residues is apparent since the 725 cm^{-1} line increases for the 5-FU containing sample. The intensity of the 814 cm^{-1} line is slightly greater for FU-5SrRNA which may indicate a slightly more ordered ribophosphate backbone.

The Raman spectra of dUrd and 5-FdUrd shown in Figure 2.22 indicate reduction in the intensities of both the 1234 cm^{-1} and 787 cm^{-1} lines of uridine due to 5-fluoro-substitution. In the case of the 1234 cm^{-1} line the reduction is approximately 87%. The 787 cm^{-1} line is reduced by about 40%. These reductions are expected to affect the 785 cm^{-1} and 1242 cm^{-1} lines in proportion to the relative number of 5-FU residues in FU-5SrRNA. 5SrRNA has 20 uracil residues and 36 cytosine residues. The uridine residues contribute about 25% of the 785 cm^{-1} line intensity (see Figure 2.22a) while the cytidine residues contribute approximately 75% (24). Assuming that there is 100% replacement of uridine by 5-fluorouridine and that cytidine, uridine, and 5-fluorouridine maximum intensities fall at the same Raman frequency (785 cm^{-1}) then a reduction in the uridine contribution by about 60% would be expected (see Figures 2.22a and 2.22b). In N-5SrRNA the intensity of the 785 cm^{-1} line is 2.21. This means that for N-5SrRNA 0.55 is due to uridine (25%) and 1.66 is from cytidine (75%). In an FU-5SrRNA sample, where all the uridines are replaced by 5-fluorouridine, the 5-fluorouridine contribution to the 785 cm^{-1} line will be 60% less than for normal uridine or equal to 0.22. This gives a total intensity for the FU-5SrRNA sample of approximately 0.22 + 1.66 = 1.88; a reduction of about 15%. A reduction of 15% represents the absolute maximum decrease in intensity for the 785 cm^{-1} line since it assumes 100% replacement of uridine

by 5-fluorouridine. The expected 5-fluorouridine incorporation was about 85% (25). Assuming 85% replacement by 5-fluorouridine, a reduction in intensity of the 785 cm^{-1} line of about 12% would be expected. In Table 2.3 the relative intensities for the 785 cm^{-1} lines of N-5SrRNA and FU-5SrRNA are 2.21 and 2.10 respectively. This corresponds to a 5% reduction due to 5-fluorouridine substitution. Deviation from the expected value of about 12% reduction could be due to less extensive incorporation than expected or hypochromic effects due to stacking interactions between 5-FU and neighboring bases.

For the 1242 cm^{-1} line uridine residues contribute about 26% (Figure 2.22a), cytidine residues about 69% (24), and adenine residues about 5% (26). In N-5SrRNA the peak intensity of the 1242 cm^{-1} line is 1.23 of which 26% (0.32) is due to uridine. A reduction of 87% reduces the uridine contribution to 0.04. This gives an expected line intensity for the FU-5SrRNA sample of 0.95 or a reduction when compared to N-5SrRNA of about 23%. The 1242 cm^{-1} lines of N-5SrRNA and FU-5SrRNA have the same intensities. In the above argument it was assumed that the maximum peak intensities for uridine, adenine, and 5-fluoroadinine occured at the same frequency (1242 cm^{-1}). Actually the 1242 cm^{-1} line is really a superposition of the 1234 cm^{-1} uridine line and a 1251 cm^{-1} line due to adenine and cytidine (3). Comparison of line widths at half the intensity of the 1242 cm^{-1} line indicate that for N-5SrRNA it is much larger;

40 cm^{-1} as compared to 24 cm^{-1} for FU-5SrRNA. This is attributed to replacement of uridine by 5-fluorouridine.

Other small changes in the spectral region between 1200-1600 cm^{-1} are evident. These differences must be attributed to alterations in conformation resulting from 5-fluorouridine incorporation but interpretation is hindered by extensive overlapping of vibrational contributions from various bases (3).

Three major conclusions can be obtained from the comparison of the Raman spectra of N-5SrRNA and FU-5SrRNA. First, the total base stacking is largely unaffected by 5-FU substitution and therefore the conformation of the two molecules must be fairly similar. Second, the amount of G-stacking is unaffected by substitution confirming a similar conformation. Lastly, minor differences in the spectra of FU-5SrRNA and N-5SrRNA are that the backbone order for the FU species is slightly greater and the adenine and uridine stacking are slightly less in FU-5SrRNA. The increase in backbone order may be a result of increased strength of bonding of adenine-uridine pairs due to the presence of the electronegative fluorine group (27). The decrease in adenine and uridine stacking is likely a result of decreased stacking efficiency for adenine:5-fluorouridine pairs. The presence of the fluorine may prevent efficient overlap of the adenine:5-fluorouridine base pair electron clouds with neighboring base pairs.

The laser Raman spectrum of FU-5SrRNA was obtained without dialysis of the sample against magnesium. The spectrum's high degree of order, comparable to N-5SrRNA after dialysis, is attributed to the 5-fluorouracil residues. The dialysis against magnesium is believed to renature N-5SrRNA (28). The dialysis of the FU-5SrRNA sample resulted in unacceptably high fluorescence background which prevented the obtainment of a spectrum.

The above results suggest that 5-FU substitution in 5SrRNA is expected to cause minimal perturbation of structure and conclusions resulting from a study of FU-5SrRNA structure should be applicable to N-5SrRNA.

REFERENCES: CHAPTER 4

1. G.J. Thomas and K.A. Hartman, Biochim. Biophys. Acta. 312, (1973).

2. G.J. Thomas, M.C. Chen, and K.A. Hartman, Biochim. Biophys. Acta. 324, 37.

3. M.C. Chen, R. Giegé, R.C. Lord, and A. Rich, Biochemistry 14, 4385 (1975).

4. K.A. Hartman, R.C. Lord, and G.J. Thomas in Physico-Chemical Properties of Nucleic Acids, J. Duchesne, Ed., Academic Press, London, Vol. 1 (1973); page 1.

5. L. Fallon, Acta. Cryst. B29, 2549 (1973).

6. D.R. Harris and W.M. Macintyre, Biophys. J. 4, 203 (1964).

7. A.R. Tarpley and J.H. Goldstein, J. Am. Chem. Soc. 93, 3573 (1971).

8. R.J. Cushley, I. Wempen, and J.J. Fox, J. Am. Chem. Soc. 90, 709 (1968).

9. I. Wempen and J.J. Fox, J. Am. Chem. Soc. 86, 2474 (1964).

10. K.L. Wierzchowski, E. Litonska, and D. Shogan, J. Am. Chem. Soc. 87, 4621 (1965).

11. F.U. Dollish, W.A. Fateley, and F.F. Bentley, in Characteristic Raman Frequencies of Organic Compounds, John Wiley & Sons, Inc., New York (1974); pages 67-68.

12. R.C. Lord and G.J. Thomas, Spectrachim. Acta. 231, 2551 (1967).

13. A. Padua, P.R. LeBreton, R.J. Dinerstein, and J.N.A. Ridyard, Biochem. Biophys. Res. Comm. 60, 1262 (1974).

14. A. Rahman and H.R. Wilson, Acta. Cryst. B28, 2260 (1972).

15. L.J. Bellamy, in The Infra-red Spectra of Complex Molecules, Chapman and Hall, London; pages 1570159.

16. Y. Nishimura, H. Haruyama, K. Nomura, A.Y. Hirakawa, and M. Tsuboi, Bull. Chem. Soc. Japan 52, 1340 (1979).

17. Reference 4, Vol. 2; pages 111-124.

18. W.L. Peticolas, in Advances in Raman Spectroscopy, J.P. Mathieu, ed., Heyden & Son, New York (1972); pages 285-295.

19. G.J. Thomas, in Vibrational Spectra and Structure, J.R. Durig, ed., Elesevier, New York (1975); pages 239-315.

20. G.J. Thomas and K.A. Hartman, Biochim. Biophys. Acta. 312, 311 (1973).

21. M.C. Chen and G.J. Thomas, Biopolymers 13, 615 (1974).

22. J.E. Ladner, A. Jack, J.D. Robertus, R.S. Borwn, D. Rhodes, B.F.C. Clark, and A. Klug, Proc. Nat. Acad. Sci. USA 72, 4414 (1975).

23. S.H. Kim, F.L. Suddath, G.J. Quigley, A. McPherson, J.L. Sussman, A.H.J. Wang, N.C. Seeman, and A. Rich, Science 185, 435 (1974).

24. T. O'Connor, C. Johnson, and W.M. Scovell, Biochim. Biophys. Acta. 447, 484 (1976).

25. I. Kaiser, Biochemistry 9, 569 (1970).

26. T. O'Connor, C. Johnson, and W.M. Scovell, Biochim. Biophys. Acta. 447, 495 (1976).

27. L. Pauling, in The Nature of the Hydrogen Bond, Cornell University Press, New York (1972); page 452.

28. M. Aubert, J.F. Scott, M. Reynier, and R. Monier, Proc. Nat. Acad. Sci. USA 61, 292 (1968).

CHAPTER 5

CONCLUDING REMARKS

From this study it can be concluded that ^{19}F-nmr spectroscopy and laser Raman spectroscopy can be used to interpret conformational properties of 5SrRNA (or FU-5SrRNA). The major advantage of both these physical techniques is that they provide information about molecular conformation in an aqueous environment. This is apparent from spectral changes which result when conditions of the molecular environment are altered.

The ^{19}F-nmr spectra of FU-5SrRNA presented in this work indicate a number of important features. The spectrum at 254 MHz consists of 8 distinct peaks and 2 shoulders with a chemical shift range of approximately 8 p.p.m.. Together they represent fluorine resonances from about 20 5-fluorouracil residues. The most exposed residues are assigned on the basis of the resonant frequency of the 5-fluoro-2'-deoxyuridine monophosphate monomer and the heat denatureation of FU-5SrRNA. The remaining fluorine peaks (about 70% of the total) are believed to be due to buried 5-fluorouracil residues. The T_1 values for the individual peaks are also determined; all are short (between 0.3 - 0.4 seconds), an indication of a rigid molecular structure. This is in contrast to the T_1 value of the 5-fluoro-2'-deoxyuridine monomer which is approximately 5 seconds. Comparison of theoretical and experimental ^{19}F-^{1}H nuclear Overhauser enhancements

demonstrates definitively that virtually all the labeled uracils are bound rigidly to the macromolecular frame with a rotational correlation time of about 10 nsec or longer. Since these uracil residues are widely distributed throughout the nucleotide sequence, it may be concluded that the entire FU-5SrRNA solution structure is highly rigid. This latter experiment also confirms that T_1 relaxation is purely dipolar since almost full Overhauser nulling is observed.

From the laser Raman spectroscopy data two important conclusions can be ascertained. First, 5-fluoro- substitution alters certain vibrational properties of the uracil base. The intensities of the 782 cm^{-1} and 1230 cm^{-1} lines of 2'-deoxyuridine in H_2O (neutral form) are reduced by at least 40% and 87%, respectively, due to 5-fluoro- substitution. A new prominent pH- sensitive peak at 1360 cm^{-1} (5-fluoro-2'-deoxyuridine, H_2O, neutral pH), insensitive to deuteration at N-3, is tentatively assigned to a C-F stretch. An additional effect of 5-fluorination on the neutral form of 2'-deoxyuridine is to cause an increase in the $C_4{=}O$ stretching frequency relative to the $C_2{=}O$ stretch. The effect of 5-fluorination on the anionic form is to favor more charge density at $C_4{=}O$ relative to $C_2{=}O$. Second, from comparison of N-5SrRNA spectra with those of FU-5SrRNA it seems evident that 5-fluorouracil substitution in 5SrRNA causes only minimal perturbation of structure and, thus, conclusions resulting from a study of FU-5SrRNA structure should be applicable to N-5SrRNA.

Recent infrared spectroscopy of native E. coli 5SrRNA indicates that all of its 20 uracils are base paired (6). Four of the uracils were shown to be tertiary and the remaining 16 secondary. In the numerous proposed structures of E. coli 5SrRNA the number of base pairs involving uracil range from 4 to 14. The comparison of the infrared spectrum of E. coli 5SrRNA at 52 ^{o}C, where tertiary base pairs are presumed disrupted, with computer simulated spectra of various proposed secondary structures of 5SrRNA are shown in Figures 5.1 - 5.4. These results indicate that only models in Figures 5.1e, 5.2b, 5.3c, 5.3f, and 5.4b have simulated spectra similar to the experimentally obtained spectrum at 52 ^{o}C. In Figure 5.5 simulated spectra for models where tertiary interactions are proposed were compared with the IR spectrum of E. coli 5SrRNA at 20 ^{o}C. Only the simulated spectrum in Figure 5.5a fits the experimental spectrum. In all cases for both the 52 ^{o}C and 20 ^{o}C spectra the proposed models which best fit the experimental spectrum have the most extensive A-U base pairs. The ^{19}F-nmr study tends to corroborate these results. At least 70% of the 5-fluorouracil residues were shown to experience secondary or tertiary effects. This fits well with models proposed by Cantor (7) and Luoma and Marshall (10 A-U and 6 G-U pairs) (4).

In conclusion, virtually all previously proposed secondary structural models for prokaryotic 5SrRNA (1-2) have a large

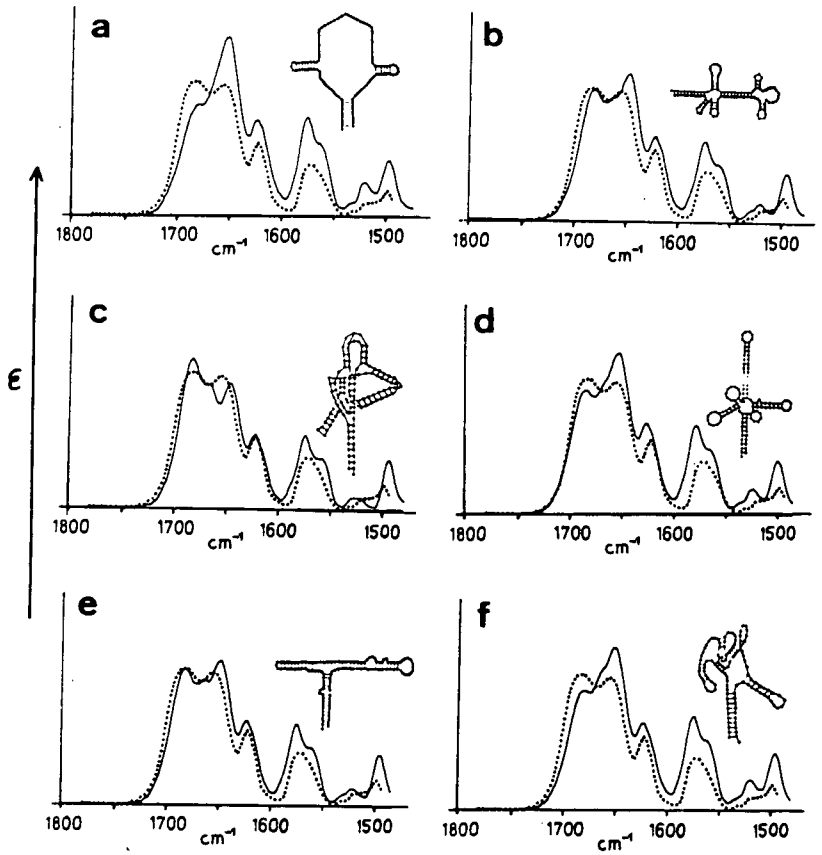

Figure 5.1. Simulated infrared spectra for E. coli 5SrRNA structural models (—) in comparison to the experimental spectrum recorded at 52°C (...)(6).

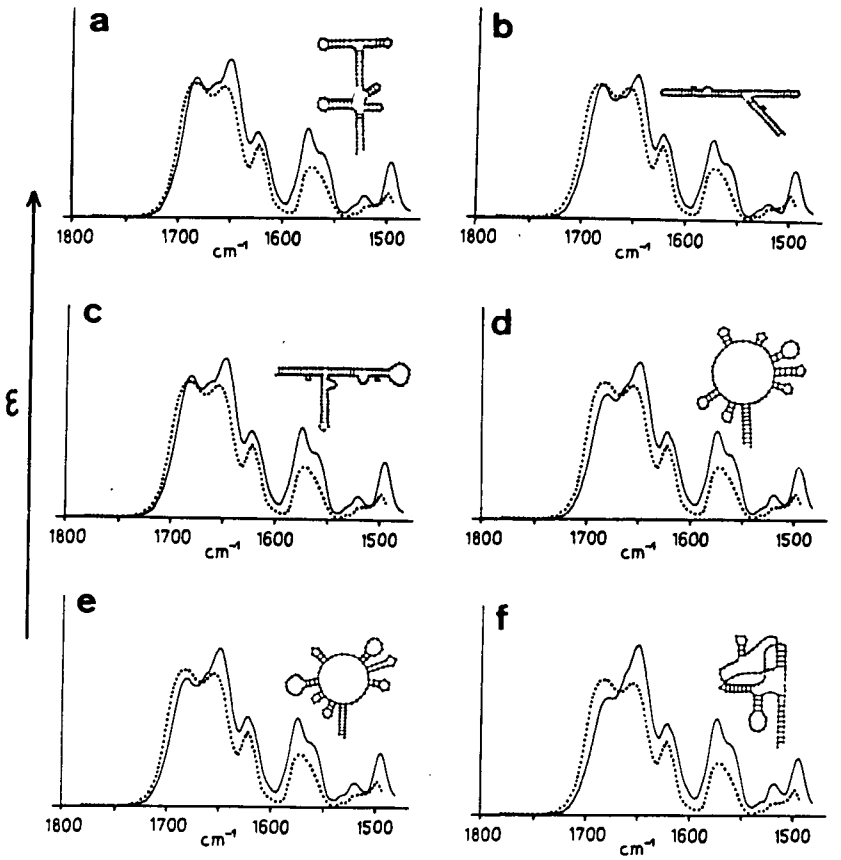

Figure 5.2. Simulated infrared spectra for E. coli 5SrRNA structural models (—) in comparison to the experimental spectrum recorded at 52°C (...)(6).

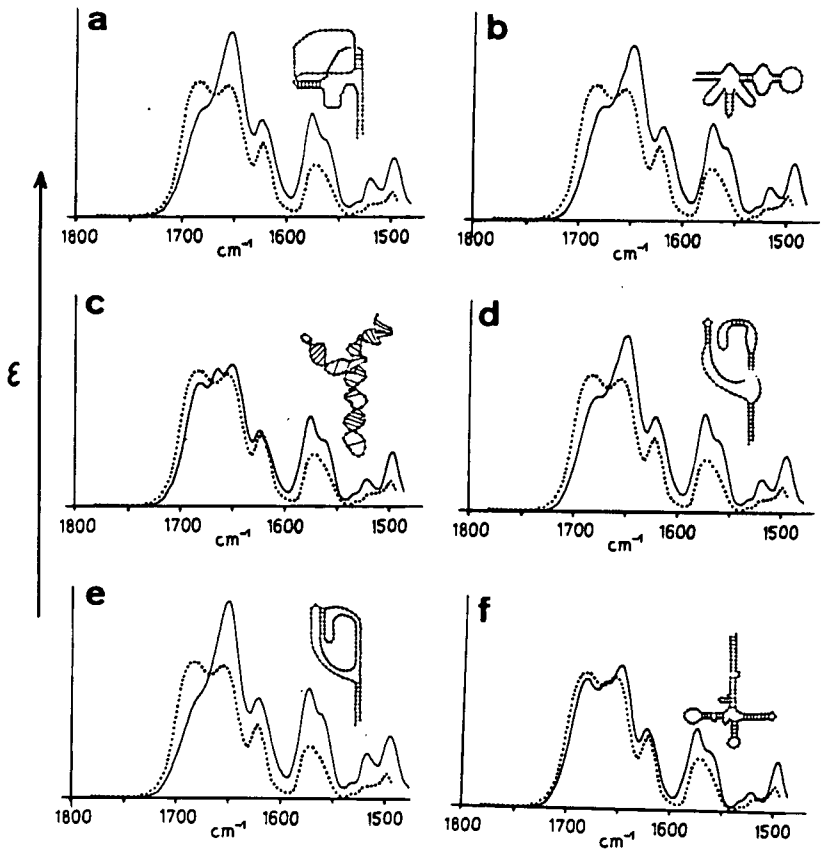

Figure 5.3. Simulated infrared spectra for E. coli 5SrRNA structural models (—) in comparison to the experimental spectrum recorded at 52°C (...)(6).

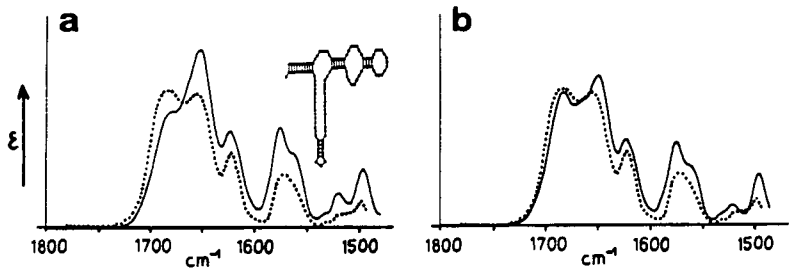

Figure 5.4. Simulated infrared spectra for E. coli 5SrRNA structural models (—) in comparison to the experimental spectrum recorded at 52°C (...)(6).

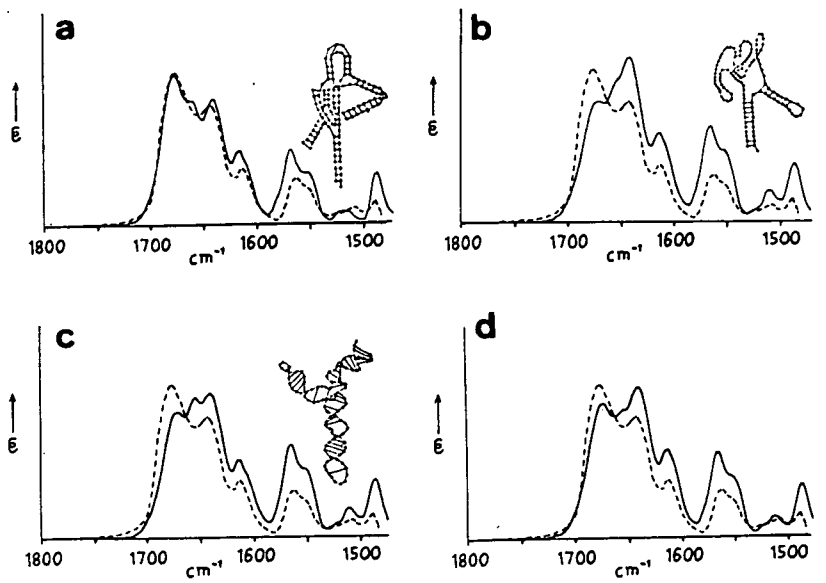

Figure 5.5. Simulated infrared spectra for those E. coli 5SrRNA structural models in which tertiary interactions have been proposed (—) in comparison to the experimental spectrum recorded at 20°C (---)(6).

fraction (usually more than half) of the uracil residues left unpaired. In contrast, the present theoretical and experimental ^{19}F-nmr and ^{19}F-^{1}H nuclear Overhauser enhancement results convincingly demonstrate that essentially all fluorouracil residues in E. coli 5SrRNA are bound firmly to a rigid macromolecular frame in solution. These results are consistent with Raman data (3) showing a high degree of overall base-pairing and RNA A-helix content in native E. coli 5SrRNA. Both the Raman and ^{19}F-nmr data support the most recently proposed "cloverleaf" secondary structure for prokaryotic 5SrRNA (4-5).

REFERENCES: CHAPTER 5

1. V.A. Erdman, Prog. Nucleic Acid Res. 18, 45 (1976).

2. V.A. Erdman, B. Appel, M. Digweed, D. Kluwe, S. Lorenz, A. Luck, A. Schreiber, and L. Schuster, in The Genetic and Evolutionary Aspects of Transcriptional and Translational Apparatus, Kondansha Scientific, Tokyo, 1979.

3. M.C. Chen, R. Giege, R.C. Lord, and A. Rich, Biochemistry 17, 3134 (1978).

4. G.A. Luoma and A.G. Marshall, Proc. Natl. Acad. Sci. U.S.A. 75, 4901 (1978).

5. G.A. Luoma and A.G. Marshall, J. Mol. Biol. 125, 95 (1978).

6. B. Appel, V.A. Erdman, J. Stulz, and Th. Ackermann, Nuc. Acid. Res. 7, 1043 (1979).

7. C.R. Cantor, Nature 216, 513 (1967).